# Geochemical and isotopic tracing of salinity loads into the Ramsar listed Verlorenvlei freshwater estuarine lake, Western Cape, South Africa

by

Nthabeliseni Thendo Sigidi

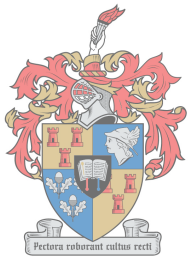


Thesis presented in fulfilment of the requirements for the degree of Master of Science in Geology, Department of Eath Science, at the Faculty of Science at Stellenbosch University



Supervisor: Dr Jodie Miller

Co-supervisor: Dr Cathy Clarke

March 2018

## DECLARATION

By submitting this thesis electronically, I declare that the entirety of the work contained therein is my own, original work, that I am the sole author thereof (save to the extent explicitly otherwise stated), that reproduction and publication thereof by Stellenbosch University will not infringe any third party rights and that I have not previously in its entirety or in part submitted it for obtaining any qualification.

March 2018

## ACKNOWLEDGEMENTS

I would like to first thank God for the strength and guidance throughout my thesis. I would like to express my deepest gratitude to my supervisor Dr Jodie Miller for the opportunity to study, her patience, encouragement and her guidance throughout my MSc and my co-supervisor Dr Cathy Clarke for her input and help into my study. I would also like to thank the National Research Foundation (NRF) for financial assistance and the Water Research Commission (WRC) of South Africa, funding the project. Thank you to Mike Butler from iThemba LABS in Johannesburg for the analyses of stable isotopes, and tritium, Petrus Le Roux from the University of Cape Town, for strontium isotope analysis, Riana Rossouw and Matt Gordon from the University of Stellenbosch CAF labs. Elna De Necker (Institute of Groundwater Studies) from Free State University for my major ion analyses. Thank you to the farm owners for their hospitality and willingness to help. I would like to thank Thendo Netsidzivhe and Cedrick Mukharhi for their constant support, Anya Eilers and Alice Petronia, for their assistance in the field as well as data compilation. Special thanks to Grace Maponya for her patience in helping me with ARC GIS, and Andrew Watson for his continuous assistance throughout this project. Finally, I would like to thank my family for their perpetual support throughout my MSc.

## ABSTRACT

The Verlorenvlei estuarine lake is a natural, semi-fresh lake along the West Coast of South Africa. The lake is situated in a semi-arid region, and is subject to high evaporation rates of up to 2400mm, and average rainfall of less than 300mm/per year. The lake is also an important host for diversified species of flora and fauna. Due to normal functions of the lake, variation in salinity of the lake is due to several factors. These include: (1) ingress and mixing with sea water; (2) floods, droughts and evaporation due to climate change and (3) salt transported into the lake from terrestrial sources. For the long term health and management of the lake, it is required to understand the role of terrestrial salinity and transport processes into the lake. Therefore, the study focuses on four main tributaries which are the Krom Antonies, Hol, Bergvallei, and the Kruismans. These four tributaries join at the Verloren confluence and thereafter form a single river system called the Verloren River. The Verloren River and its tributaries drain on predominantly fine- grained rocks of the Malmesbury group (contain high concentration of salts) and of the Table Mountain Group. The geology of this area has an important bearing on the composition of the water that enters the lake. To understand the origin and processes of salinity for surface water and shallow groundwater to the Verloren River, analysis of coupled major ion hydrochemistry and environmental isotopes ($\delta^{18}O$, $\delta^{2}H$, $^{87}Sr/^{86}Sr$ and $^{3}H$) has been undertaken. To fully evaluate the contribution from each tributary, the TDS values in both the surface and shallow groundwater are quantified, the daily overall discharge (surface runoff, interflow and baseflow) in each tributary has been established. Interaction with the aquifer matrix, evaporation, and precipitation-dissolution control the hydrochemistry of surface water and shallow groundwater. Due to the dominance of Na and Cl ions surface water and shallow groundwater can be characterised as Na-Cl water type. The presence of Mg and Ca ions in surface water and shallow groundwater corresponds to dissolution of dolomite limestones. The decrease in $Ca^{2+}$ and increase in $Na^{+}$, is a result of cation exchange processes and weathering of feldspars and micas. High sulphate concentrations correspond to dissolution of gypsum and nitrate concentrations can be related to the use of fertilisers. Evaporation for surface water and shallow groundwater in the Hol, Bergvallei and Kruismans is a dominant source for salt concentration, therefore increasing Na and Cl ions in water. The use of strontium isotopes indicates mixing between the Hol and the Bergvallei as source of observed salinity and water composition for surface and shallow groundwater in the Verloren confluence. The results show that the Hol contributes the least salt load (5.3%), followed by the Krom Antonies (6.2%), then the Bergvallei (35.0%) and the Kruismans contribute the most salt load (53.5%), into the Verloren confluence.


Keywords: salinity; surface water and shallow groundwater chemistry; salt load; Verlorenvlei estuarine lake

# TABLE OF CONTENTS

## LIST OF FIGURES

## LIST OF TABLES

# 1. GENERAL INTRODUCTION

## 1.1 Introduction

Salinisation of shallow groundwater and surface water resources has become a long-term global process that degrades water quality and threatens future water exploitation (Wang et al., 2012; Vengosh et al., 1999). Salinisation limits the use of water for domestic, agricultural and industrial applications and threatens the biodiversity of flora and fauna in major and important estuarine lakes. Areas that are most affected by salinisation are located in arid and semi-arid regions (Haung & Pang, 2012; Richter & Kreitler 1993; Philips et al., 2003; Williams, 1999). Studies conducted in arid and semi-arid regions show that surface water in rivers or lakes and groundwater salinisation can result from either point sources (e.g., leakage of industrial and domestic waste water) or nonpoint sources (e.g., agriculture return flows or irrigation with sewage effluent) derived directly from anthropogenic contamination. Salinisation can also result from natural processes such as seawater intrusion, evaporation, mineral dissolution and rock-water interactions (Kumar, 2011; Zaidi et al., 2015; Vengosh et al., 1999). Therefore, it is critical to have a detailed understanding of the sources and mechanisms by which salts are transferred into, or concentrated within, different water bodies for the management of salinisation of surface and shallow groundwater. Critical to managing salinisation of surface water and shallow groundwater is a detailed understanding of the sources and mechanisms by which salts are transferred into, or concentrated within, different water bodies. According to Sami (1992), not only is salinisation linked to natural or anthropogenic sources, salinisation is also associated with climate change. Therefore, studies have to relook on climate change and its impact on salinisation as it becomes more pronounced and given expectations concerning the nature of climate change, it is likely that its importance will increase even further following extensions of dryland areas.

Climate change is a phenomenon that has been well-documented globally and has a direct impact on meteorological variables such as air temperature, the distribution of precipitation, and evaporation rates (Seun & Lai, 2013; Warner, et al., 2013). A semi-arid country like South Africa is particularly vulnerable to climate change because less than 9% of annual rainfall ends up in rivers and nationally only 5% reaches aquifer systems as recharge (Ziervogel et al., 2014). Furthermore, changing precipitation patterns are most directly observed through the higher frequency of flood and drought events in South Africa (Ziervogel et al., 2014) in recent years. Consequently, floods and droughts having a strong impact on modifying water quality through dilution or concentration of dissolved salts (Delpla et al., 2009).

Under future climate scenarios considered by the Long Term Adaptation Scenarios (LTAS), South Africa's mean annual temperatures have increased by at least 1.5 times the observed global average of 0.65°C over the past 5 decades (Ziervogel et al., 2014). Therefore, changes in mean ambient air temperature directly influence the mean ambient surface water temperature, which in turn drives chemical reactions such as dissolution and evaporation resulting in an increase in dissolved species (Delpla et al., 2009). Salinity either as natural, anthropogenic or climate change related influences may exacerbate the stresses on water resources and ecosystems in estuarine lake systems more (Suen & Lai, 2013).

South Africa is defined as a semi-arid country (Pitman, 2011), with a number of river basins, particularly on the west coast, that have been affected by salinization (Flugel,1995; Clercq et al., 2010). South Africa also has several estuarine lakes, one of the largest in Africa being the St Lucia estuarine lake located in the Province of Kwazulu–Natal. Lake St Lucia underwent major changes over 5 years (2002-2007) as a result of drought, high evaporation rates and human interventions, leading to high levels of salinity, resulting in it becoming a hypersaline lake (Cyrus, at al., 2011). The Verlorenvlei estuarine lake is a natural, semi-fresh lake along the west coast of South Africa and its significant biodiversity has resulted in it being RAMSAR listed. Like the St Lucia wetlands, the Verlorenvlei lake is situated in a semi-arid region, and is subject to high evaporation rates of up to 2400mm/year (Meadows et al 1996), with average rainfall of less than 300mm/year. It is also associated with inflows of surface and shallow groundwater salt loads from upper tributaries and human interferences through construction of bridges, agricultural activities. These factors contribute to the lake's vulnerability to salinisation, which impacts on the long term health of the lake. Currently, the Verlorenvlei estuarine lake is at risk of becoming hypersaline like the St Lucia estuarine lake through severe drought and evaporation due to climate change, significantly threatening the flora and fauna of the lake (Cyrus, et al., 2011). Therefore, conservation and management measures need to be implemented for the lake.

**Figure 1***: Picture of the Verlorenvlei lake taken during summer.*

This study focuses on four major tributaries that join at the Verloren confluence to form a single river system called the Verloren River, the latter feeding the Verlorenvlei lake. The tributaries are the Krom Antonies, Hol, Kruismans and the Bergvallei. These tributaries contribute variable amounts of salt into the Verloren River and thereafter the Verloren River transports the salt loads to the lake. Sinclair et al. (1986) proposed that the geology of the area has an important bearing on the composition of the water that enters the lake, implying that salinity in surface water and shallow groundwater from the tributaries comes from the rocks of the Malmesbury Group, which contains high concentrations of salts mainly as sodium and chloride. In contrast, the CSIR (2009) proposed that salinity levels are due to land use change from natural cover of land to intensive and extensive agricultural activities.

It is important to understand and identify sources of salinity, the mechanisms of salinisation and the contribution of total salt loads of each tributary into the Verloren confluence in order to be able to put salinity mitigation plans in place. If the source and spatial variation of the salts can be determined in each tributary, it can be used to determine how salt loads are transported into the lake and what impact this will have on the salt levels in the lake. This study utilises an array of physiochemical parameters (pH, EC), major ion geochemistry (Na, Ca, Mg, K, Cl, Br, $SO_4$, $HCO_3$) and environmental isotope tracers ($\delta^2H$, $\delta^{18}O$, $^{87}Sr/^{86}Sr$) to characterise the nature and origins of salts in each tributary. This information is then compared to modelled discharge data to quantify the relative contribution of salt loads from each tributary being transferred into the Verloren confluence. The results obtained will help to develop appropriate management strategies for the Verlorenvlei estuarine lake and will further help to better understanding the

impacts of climate change on the long-term salinity management strategies for the estuarine system.

## 1.2 Problem statement

The Verlorenvlei estuarine lake is a semi-fresh system where the lake salinity varies as a result of several factors. These include ingress and mixing with sea water, evaporation, and salt transported into the lake from terrestrial sources. Management of the lake requires an understanding of how much each of these processes contributes to lake salinity. It is necessary to understand the salt loads in each of the tributaries that feed into the lake and how much each tributary contributes to overall inflows. To fully evaluate the contribution from each tributary, the salt levels in both the surface and shallow groundwater needs to be quantified, the daily flow rate in each tributary needs to be established and the relative contributions of runoff (likely to be saline) and baseflow (likely to be fresher) into each tributary needs to be determined. These parameters must also be evaluated on a temporal basis to understand the role of seasonality in salt transfer into the lake.

## 1.3 Aims and Objectives

Based on the above, the aim of this study is to characterise the nature of salinity within surface water and shallow groundwater in the catchment to the Verlorenvlei estuarine lake. To do this a number of different geochemical tools have been employed to address the following objectives.

1. To characterise the nature and distribution of salinity in each of the tributaries to the Verloren River.
    - 1.1. How saline is the surface water and shallow groundwater in each tributary and how does the salinity vary along the tributary length?
    - 1.2. What is the composition of the salts in surface water and shallow groundwater in each tributary and does this vary along the tributary length?
    - 1.3. How do the above patterns vary between seasons?
    - 1.4. What are the likely source of the salts in each tributary?

2. To determine the relative contribution of each tributary to the total salt load entering the Verloren River.
    - 2.1. What are the contributions of surface runoff vs baseflow to the total inflow from each tributary?
    - 2.2. How does seasonality in discharge impact on surface runoff vs baseflow and hence total salt loads?

2.3. Based on discharge data for each tributary, how much salt is each tributary contributing to the Verloren River?

3. To evaluate how the different salt loads and tributary contributions impact on the Verlorenvlei lake salinity levels and the long term health of the estuarine system.

3.1. What implications will the salt loads contributions from each tributary have on the salinity variation of the lake?

3.2. How will predicted climate change impact on salt transfer into the lake and future lake salinity levels?

## 1.4 Salinity

Salinisation is the process that increases the salinity of fresh waters and is reflected in an increase in total dissolved solids (TDS) and in the overall chemical content of water and sediments (Richter & Kreitler, 1993). Salinity is usually expressed as chloride content (mg/l) or Electrical Conductivity (EC, in µS/cm) (Van Weert, et al., 2009). The classifications differ in class names, used value limits and the parameters used. Surface water and groundwater can be classified according to TDS as follows: freshwater 1000mg/L; brackish water between 1000 and 10000mg/L; Saltwater >10000mg/L and brine > 100000mg/L. Since EC is measured directly in the field rather than TDS, TDS in the study is based on the formula:

$$TDS(mg/L) = \Sigma(Cations\ (mg/L) + Anions\ (mg/L))$$

Where the cations include $Na^{+}$, $Mg^{2+}$, $Ca^{2+}$, $K^{+}$, $Sr^{2+}$, As, Al, W, B, Se, and anions include $Cl^{-}$, $Br^{-}$, $HCO_3^{-}$, $SO_4^{2-}$, $NO_3^{-}$, $PO_4^{3-}$.

There are two distinguishable types of salinity (Williams, 1999): (1) primary salinity caused by natural occurring processes such as weathering of rocks at local and regional geological scales, rainfall, wind deposition, ingress of seawater and evaporite deposits (McDowell, 2008 Bridgman et al., 2008). These processes of primary salinity occur mostly in arid and semi-arid regions, which are dominated by high evaporation rates and low rainfall events; and (2) secondary salinity which includes dryland salinity, urban salinity, irrigation salinity and industrial salinity and occurs because of human-induced activities that alter or catalyse the natural processes of the hydrological system (Salama et al., 1999).

### *1.4.1 Sources of Salts*

*1.4.2.1. Natural Salts*

Natural salts affecting primary salinity include: a) deposition of marine sediments, b) sea level variations, c) meteorological processes and d) climate change (Van Weert, et al., 2009). There are different types of natural salt sources and these are:

(a) Seawater intrusions are common in coastal aquifers systems due to coastal aquifers being hydraulically connected to the sea. Therefore, changes in the hydraulic head of a coastal aquifer could allow for seawater intrusion (Kim et al., 2003). This happens when over abstraction of aquifers decreases the hydraulic head of the aquifer and as a result there is a decrease in groundwater quantity, which allows seawater intrusion to occur. Therefore, seawater intrusion increases salinity of coastal groundwater systems (Van Weert et al., 2009; Hudak, 2002; Vengosh et al., 2002).

(b) Connate saline waters are a result of sedimentation in seawater and seawater gets trapped as pockets in the interstitial spaces of the sediments. The trapped seawater then interacts with recent precipitation and gets flushed into groundwater. Salinity increases with depth below land surface as recharge water has longer residence time to interact with trapped seawater (Van Weert, et al., 2009; Vengosh et al., 2002; Monjerezi, 2012).

(c) Rainfall contains seawater sodium chloride salts although at low concentrations. Dissolved solutes and insoluble particles are carried to the ground by rainfall (Williams, 1982). Over time, the salts continually deposited by rain inland become concentrated and later on the salts are dissolved during recharge, causing salinisation in groundwater or rivers (Yechieli & Wood, 2002).

(d) Aeolian deposited salts are windblown salts from ocean surfaces and from inland lithologies as aerosol and dust. The deposition of particulates and aerosols from the atmosphere happens without rain as a transport medium (Williams, 1982). These salts are carried from inland surfaces into rivers and groundwater by precipitation during recharge (Richter & Kreitler, 1993).

(e) Natural terrestrial salts include evaporation at or near land surface and dissolution of evaporites. Evaporation at or near land surfaces, mostly occurs in arid and semi- arid countries where evaporation rates exceed precipitation resulting to concentration of salts in groundwater (Herczeg, et al., 2001). Dissolution of evaporites (halite, gypsum, anhydrite) on the surface and unsaturated zones mostly in sedimentary basins results in salinisation of groundwater (Richter & Kreitler, 1993).

#### *1.4.1.2 Anthropogenic Salts*

Anthropogenic salts are human induced salts driven by activities such as groundwater abstraction, disposal of waste-water, land reclamation, and disposal of road salt, all of which contribute too salt levels in in rivers and groundwater. Anthropogenic salts are more spatially localised in shallow groundwater (Phillips, et al., 2003; Salama, et al., 1999; Moore, et al., 2008). The different secondary salinity types are summarised below:

(a). Dryland salinity is common in agricultural areas, where the natural vegetation which has deep root systems is replaced by crops that have shallow root systems (Scanlon et al., 2002). Dryland salinity is when the water table rises due to increase in groundwater recharge, causing the water table to rise and salts are mobilised and redistributed closer to the soil surface and concentrated as groundwater evaporates. According to Phillips et al. (2003) these processes may expose natural and sodic soils and cause poor soil structures and reduce water infiltration.

(b). Irrigation salinity is when there is increased levels of salts in groundwater which reflect the change in balance between the inputs of water and salt, as well as the changes in water and salt drainage. This type of salinity is usually characterised by waterlogging, which can lead to saline seepages into low lying areas (Williams, 1999).

(c). Urban salinity is groundwater salinisation as a result of urban development activities. These activities include, leakage of sewage water into groundwater systems, de-icing of snow which may increase salts in groundwater. Disturbance of soil surface during building may expose saline subsoil, intercept lateral flows of groundwater which may have an influence on the water table. The rise of the water table allows for the mobilisation of salts across the landscape with redistribution near the soil surface causing salinisation (Slinger and Tenison, 2005 and Van Weert, et al., 2009).

(d). Industrial salinity is a result of industrial processes such as waste water from mining activities being discharge into groundwater systems (Williams, 1999) and the discharge of effluents into rivers groundwater systems. The contamination from industries can lead to accumulation and salinisation of the sediments, rivers and groundwater. Abandoned mines have been source of salts as rainwater come into contact with mine workings leading to contamination of water resources (Van Weert et al., 2009).

### *1.4.2 Geochemical Tracers of Salinity*

Studies conducted in semi-arid to arid regions have shown the use of multi-geochemical tracers as important and powerful tools for the identification of salinity sources and processes

affecting groundwater and surface water systems (Currell. et al., 2015; Anders et al., 2013; Monjerezi, 2012). These tracers are further discussed below.

*1.4.2.1 Major Ions*

Major ion concentrations are important tracers as they give an indication of the geochemical processes and water-rock interactions occurring in the aquifer system (Chen et al., 2002). For example, ion exchange within clay rocks leads to replacement of calcium (Ca) and magnesium (Mg) with sodium (Na). Therefore, deep groundwater that has a longer residence times should have a higher Na concentration and higher (Na+K)/(Ca+Mg) ratio than shallow groundwater (Chetelat et al., 2008; Anders et al., 2013; Farbe et al., 2004). Chloride and bromide ions have been used to trace sources of salinity and assess different salinity processes because of their conservative nature (Davis et al., 2004).

Molar and mass ratios of major ions such as Na/Cl, Cl/Br, Mg/Cl and Cl/$NO_3$ are used to distinguish between different sources of salinity. Ionic mass ratios, because of their characteristic and well-defined range for rainwater, sea water, sewage water, septic effluent, and animal waste, have been used in many studies to trace origin of groundwater contamination (Panno et al., 2006). These ratios have been illustrated in several groundwater salinity studies those conducted by Panno et al. (2006), Alcalά & Custadio (2008), Marie and Vengosh, (2001) and Davis et al. (1998). For example, Mg/Ca molar ratio is often used to explain the sources of $Ca^{2+}$ and $Mg^{2+}$ in groundwater. If the ratio Mg/Ca = 1, dissolution of dolomite should occur. Higher Mg/Ca molar ratio (> 2), indicates the dissolution of silicate minerals which contribute more $Mg^{2+}$ to the groundwater (Xiao et al., 2012). Sodium/Chloride molar ratios have been used to distinguish whether the origins of salts are either from weathering of silicate rocks or halite dissolution or of seawater origin. Chloride and bromide are normally conservative in a groundwater system; therefore, the molar ratio is a good tracer for source of chloride and bromide in water. The most common ratios of chloride/bromide in potable ground water are between 40 and 400 based on mass (Davies et al., 2004). Chloride/nitrate molar or mass ratios have been used to understand sources of nitrate in surface and groundwater. Saffigna & Keeney (1977) used chloride/nitrate molar ratios and found that the source of nitrate and chloride ions in groundwater of the central Wisconsin sand plains was mainly from irrigated agriculture water from the use of fertilisers.

*1.4.2.2 Isotopes*

There are several environmental isotopes that have been employed to determine salinity sources and transfer mechanisms such as $^{11}B$, $^{34}S$, $^{18}O$, $^{2}H$, $^{36}Cl/Cl$ $^{87}Sr/^{86}Sr$, but only isotopes relevant to this study are discussed further:

Stable isotopes of oxygen -18 and deuterium are commonly used in regional groundwater studies to identify flow regimes and sources of recharge (Hamouda et al 2011; Aggarwal, et al., 2005). Hydrogen and oxygen stable isotopes considered to be transported conservatively in shallow aquifer system, meaning if there is no significant evaporation of rainwater or any mixing processes, the oxygen and hydrogen isotopes can provide important information on the salinisation processes (Yechieli, et al., 2001; Bozdag & Göçmez, 2016). Stable isotope ratios expressed as $\delta^{2}H$ and $\delta^{18}O$ are commonly used to determine saline and fresh groundwater mixing and further differentiate remnants meteoric fallout from seawater intrusion (Herczeg et al., 2001).

Strontium isotopes can be used as an indicator for sources of salinity from the rock matrix, and to determine mixing relationships to fingerprint and quantify the sources of salinity in a water system (Vengosh et al., 1999; Richter & Kreitler, 1993). The $^{87}Sr/^{86}Sr$ ratios can be used for tracing the evolution and origin of groundwater chemistry (Moore et al., 2008). Strontium isotope compositions are useful for geochemical studies because of the strong association of $Sr^{2+}$ with $Ca^{2+}$ ions in carbonate and clay minerals thereby providing important insight into dissolution and precipitation of these minerals (Skrztpek and Dagramaci, 2013). Furthermore, they are not fractioned in nature as a result of surficial process, which therefore, makes Sr isotopes good tracers (Shand et al., 2009).

The use of Sr isotopes has been well established as indicted by numerous journal publications and review articles. For example, Wang et al. (2006) used Sr isotopes and chemical composition to identify the flow paths of karst water and hydrochemical processes in the Shentou karst system of northern China. Négrel et al. (2004) used a combination of Sr isotopes and major ion geochemistry to trace chemical transfer between surface and groundwater and to trace aquifer recharge. In a study conducted by Lemière & Négrel (2015) the chemistry of the Subarmarekha river system was caused by mixing of waters of various origins with different $^{87}Sr/^{86}Sr$ ratios and Sr contents, which were rainwater input, water-rock interaction and anthropogenic inputs. Strontium isotopes are used alongside Sr concentrations. In this study strontium isotopes and reciprocal of Sr have been used to construct a simple mixing model to quantify geochemical contributions of various end members to surface water and shallow groundwater chemistry of the Verloren confluence.

Tritium ($^{3}H$) concentrations can be used to qualitatively determine whether groundwater is modern, defined as less than 50 years in age, or pre-modern defined as older than about 50 years in age (Gleeson et al., 2016). Similarly, tritium is transported to shallow groundwater through recharge (Ravikumar & Somashekar, 2011; Aggarwal et al., 2005). Large amounts of atmospheric tritium were added by hydrogen bomb testing in the 1950s. However, $^{3}H$ values in southern African rainfall recorded as high as 100 TU in the 1960s have steadily decreased

to the present 2-3 TU which is regarded as background levels (Talma & Van Wyk, 2013). Because of the variable concentration of tritium in the atmosphere, tritium concentrations are not as a tracer for shallow groundwater age dating (Ravikumar et al, 2011). To overcome this, tritium has been combined with its radiogenic daughter product helium-3 ($^{3}He$) and the two combined can give reliable estimates of the groundwater residence time.

# 2. STUDY AREA

## 2.1 Study Location

The study area is in the northern area of the Sandveld region, 23km north-west of Piketberg, in the Western Cape Province. It is characterised by four major tributaries that drain into the Verloren River, the latter draining into the Verlorenvlei estuarine lake (Figure 2). Surface and shallow groundwater samples were collected from the four tributaries: Hol, Kruismans, Krom Antonies (north of the Kruismans), Bergvallei and the Verolren confluence in the period of June 2015 to June 2016.

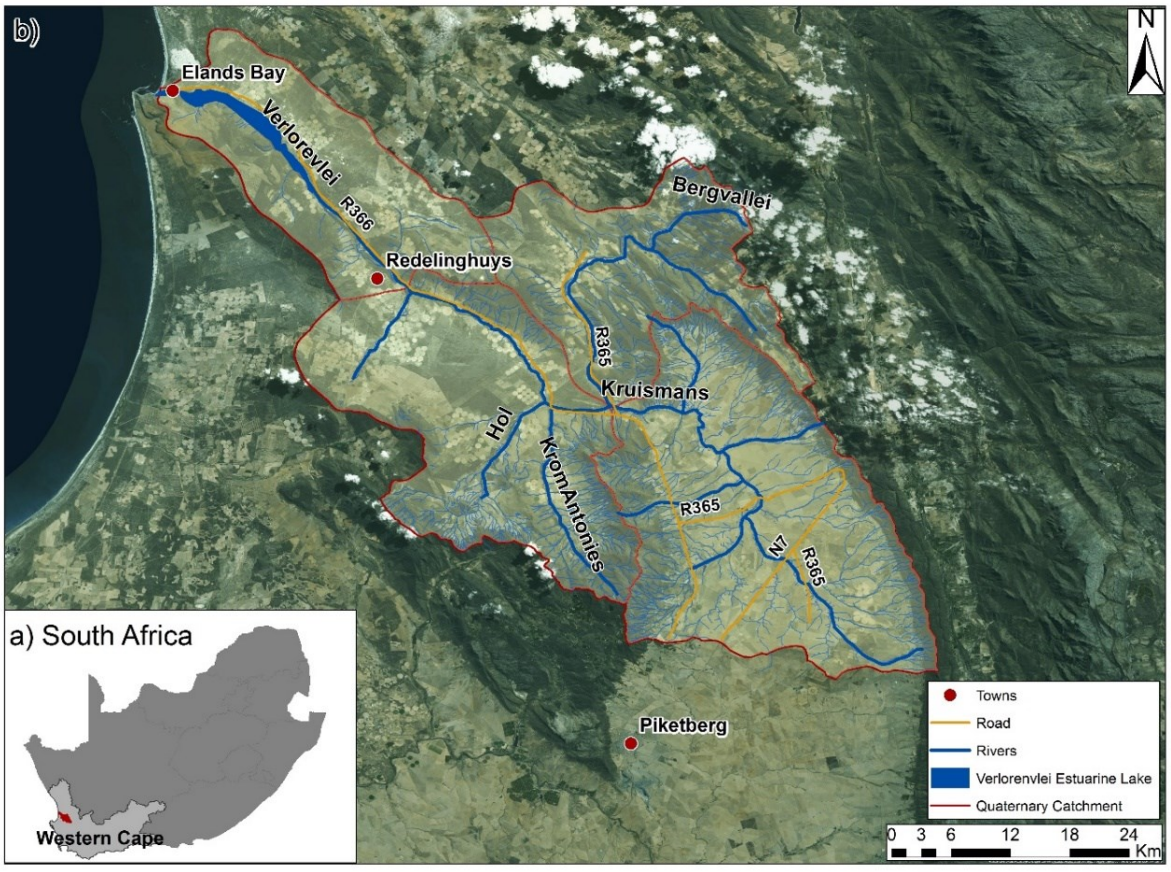


**Figure 2:** *Study area map, indicating the catchment boundaries and tributaries that drain into the Verloren River and its situation in South Africa.*

## 2.2 Geological Context

The catchment surface geology is characterised by low grade to un-metamorphosed sedimentary rocks of the Malmesbury Group, Klipheuwel Formation, and Table Mountain Group, as well as Tertiary to recent deposits (Figure.3). The Proterozoic Malmesbury Group

in the area consists of the Piketberg Formation that forms the valley floor of the four tributaries in the catchment. Calcareous, phyllitic greywacke, schists and minor quartzite constitute the Malmesbury Group. The calcareous series of the Porterville Formation are limestones and dolomites and these are observed along the Hol River (Meadows et al 1996; Rozendaal et al, 1999). The Riviera Granite pluton of the Cape Granite Suite, which intruded the Malmesbury Group, is located at the foothills of the Piketberg Mountains in the Moutonshoek area and is associated with vein-related Molybdenum(Mo) mineralization. The Klipheuwel Formation, which is Proterozoic in age, comprises of red micaceous shale grading into mudstone, interbedded with alternating beds of sandstones (Rozendaal & Scheepers, 1995).

The Table Mountain Group (TMG), which is Upper Silurian to Lower Devonian in age, extends throughout the whole study area but at higher elevations as it is preserved in the mountains that border the field area. The upper parts of the TMG predominately consist of thick bedded white to reddish brown sandstones, siltstones and shale beds. The Peninsula Formation is mostly characterised by mature sandstones and quartzites that form the mountains that surround the catchment. The Tertiary to recent deposits are characterised by white unconsolidated alluvial sands inclusive of clay deposits (Figure 3) and these cover the valley floor of each tributary in the catchment.

Structural displacements in the catchment have been documented by Rozendaal et al. (2004). This includes older north-west trending isoclinal fold structures that developed during an earlier deformation of the Malmesbury Group and intruded by the Riviera Granite pluton. Mesozoic tensional tectonics have resulted in north-west trending normal faults forming graben-horst structures in the catchment (Rozendaal et al., 1999). The Riviera Granite pluton is terminated on its western periphery by a major fault, the Krom Antonies fault, which has a possible downthrow of 450m to the west (Rozendaal et al., 1994).

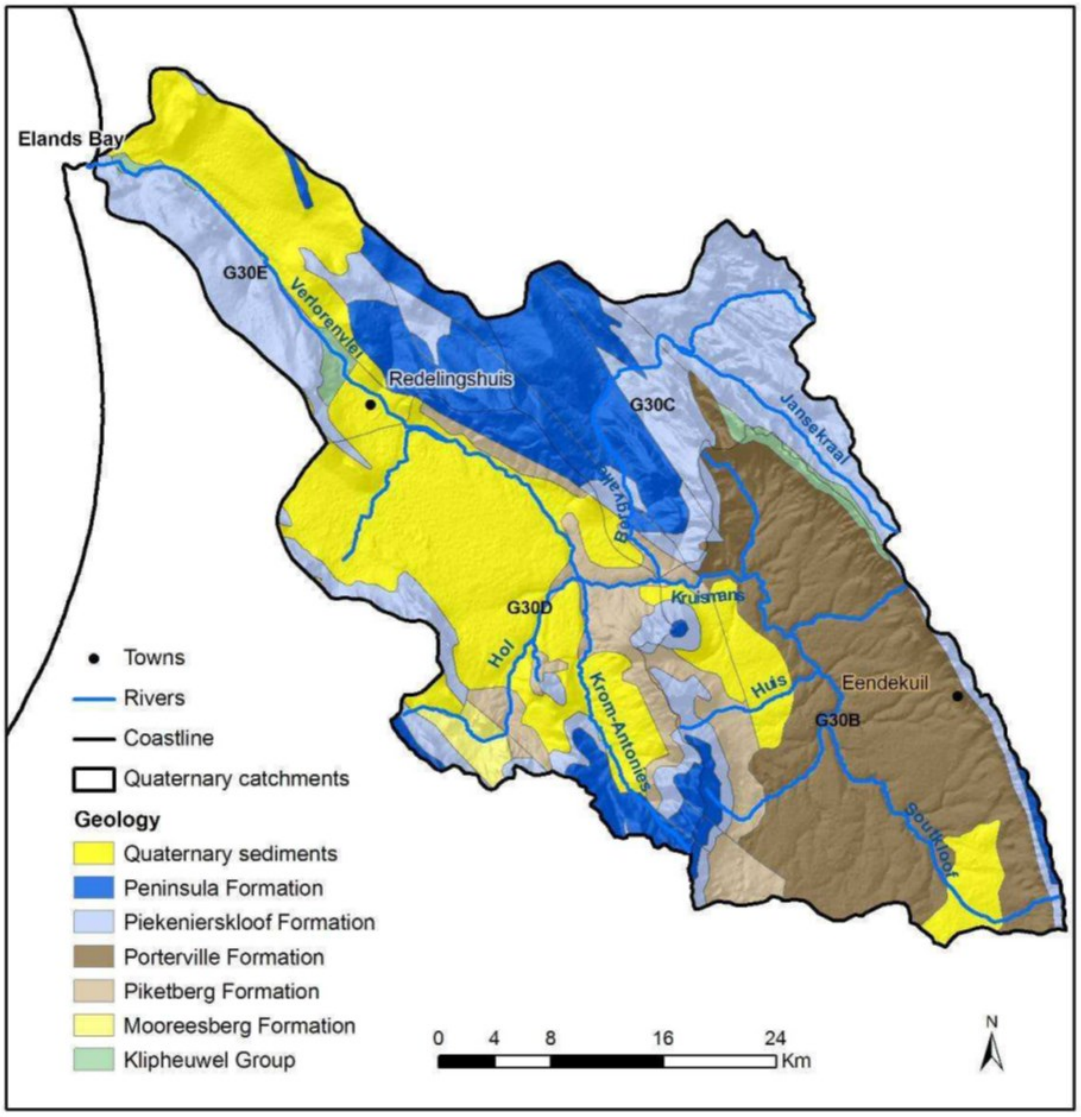


**Figure 3***: Geological map of the Verlorenvlei catchment (CSIR, 2009).*

## 2.3 Climate

The study area is classified as a semi-arid climate regime with mean annual temperatures ranging between 6ºC in winter and 32ºC in summer. In contrast to the winter season, the summer season is dry with high temperatures of up to 42°C that contribute to large evaporative losses from the hydrological system. The mean annual evaporation (MAE) is relatively high with a total potential rate ranging from 1800 to 2400 mm/year (Meadows et al., 1996). The mean annual precipitation (MAP) is ± 300mm, and follows a Mediterranean precipitation pattern receiving 80% of its rainfall during the winter season between the months of April to September. The precipitation is topographically controlled. The high lying areas which are more than 1000m above sea level (masl) receive mean annual rainfall between 300 and

500mm/annum. The low-lying areas which are less than 1000m above sea level (mamsl) receive mean annual precipitation of about 300mm/annum.

## 2.4 Catchment Characterisation

### *2.4.1 Catchment Delineation*

The catchment is 87km long and 43km wide, and situated south-east of the Sandveld plains, in the Piketberg and the Olifantsriver Mountains respectively (Meadows, et al, 1996; Baxter & Meadows, 1999). The catchment consists of four tributaries that drain into the 30km in length Verloren River the latter contributing water into the Verlorenvlei estuarine lake. The four tributaries are: (1) the 22.5 km long north westerly flowing perennial Krom Antonies; (2) the Kruismans which is the longest river in the catchment at 50km in length that confluences with the; (c) 36 km in length non-perennial Bergvallei and; (4) the 25 km long non-perennial Hol River that confluences with the Verloren River (Figure 1). It is from this confluence (between the Hol and Verloren) that salt input from each tributary is quantified into the Verloren River. (Sinclair et al, 1986).

### *2.4.2 Hydrogeology*

There are three major aquifer systems present within the study area. The first is the unconfined primary aquifer consisting mostly of unconsolidated alluvial sediments and sands in the valley floor of the catchment. The aquifer varies in thickness from <5m near the flanks and the upper reaches of the valley, to ~30m in the valley floor of the four tributaries. The groundwater abstracted from the primary aquifer is used for irrigation and domestic purposes. The aquifer is typically shallow about 15m in thickness throughout the area. Groundwater quality of the primary aquifer varies significantly following the general groundwater flow direction, which is westwards towards the coast, with salinity increasing towards the coast (Conrad et al, 2004; CSIR, 2009). The second aquifer, which is a semi-confined secondary aquifer, is characterized by faulted and fractured rocks of the Piketberg Formation of the Malmesbury Group and located in the valley of the catchment. The secondary aquifer is thought to have low concentrations of salts with groundwater having recorded average EC values of up to 126.8mS/m (CSIR, 2009). The flow direction of groundwater follows the surface topography of the catchment towards the coast, in association with springs occurring in the upper reaches of the Krom Antonies tributary, suggesting discharge from the secondary aquifer into the primary aquifer. The third aquifer is the TMG fractured rock aquifer that is in the high lying areas of the catchment. The TMG aquifer is significant throughout the area consisting of secondary openings (fractures, joints and solution cavities) in the crystalline and sedimentary

hard-rock formations, largely controlling groundwater flow in the aquifer. In general, TMG groundwater quality is between 16.3mS/m to 613mS/m and is used for irrigation purposes.

#### *2.4.3 Land use*

Most of the land within the catchment area is privately owned with extensive agricultural activities, particularly in the northern and southern part of the catchment. The main crops are potatoes, sweet potatoes upstream near Het Kruis, with oats, barley and wheat grown on smaller scales. Near natural land cover still occurs but the upper parts of the catchment are much more heavily cultivated in comparison with the less cultivated lower parts of the catchment nearer to the Verlorenvlei lake (CSIR, 2009; Sinclair et al., 1986).

## 3. MATERIALS AND METHODS

### 3.1 Instrumentation

To understand the chemical composition of shallow groundwater, piezometers of different depths were installed in each tributary. Four level loggers were installed to measure shallow groundwater water level fluctuations, and to assess whether the fluctuations were due to rainfall or baseflow, to understand salt input sources and salt transfer mechanisms.

#### *3.1.1 Piezometers*

Twenty-one piezometers were installed at different depths along each of the tributaries (Table 1). Five piezometers were installed in the Kruismans, six in the Hol, seven in the Krom Antonies, one in the Bergvallei, one at the confluence of the Krom Antonies and Kruismans and one after the confluence of the Hol and the Verloren River (Figure 6C). The depth of the piezometers and the total number of piezometers installed in each tributary dependent on the presence of an impervious clay layer which hindered the ability to get the piezometer installed in many locations. Factors such as cattle, residential areas, accessibility and irrigation patterns were taken into consideration in determining the position and distance between each piezometer. The depth of each piezometer was determined by the level of the water table at the time of initial augering (Figure 5A). The piezometers were constructed from an outer 110mm diameter PVC pipe with holes drilled in the ends for water to enter the pipe (Figure 5B) and an inner 90mm diameter PVC pipe also with holes drilled in the ends and wrapped with a geotextile material (bidem) (Figure 5C) to prevent the piezometer clogging up with silt. All materials used to construct the piezometers were inert to avoid any contamination.

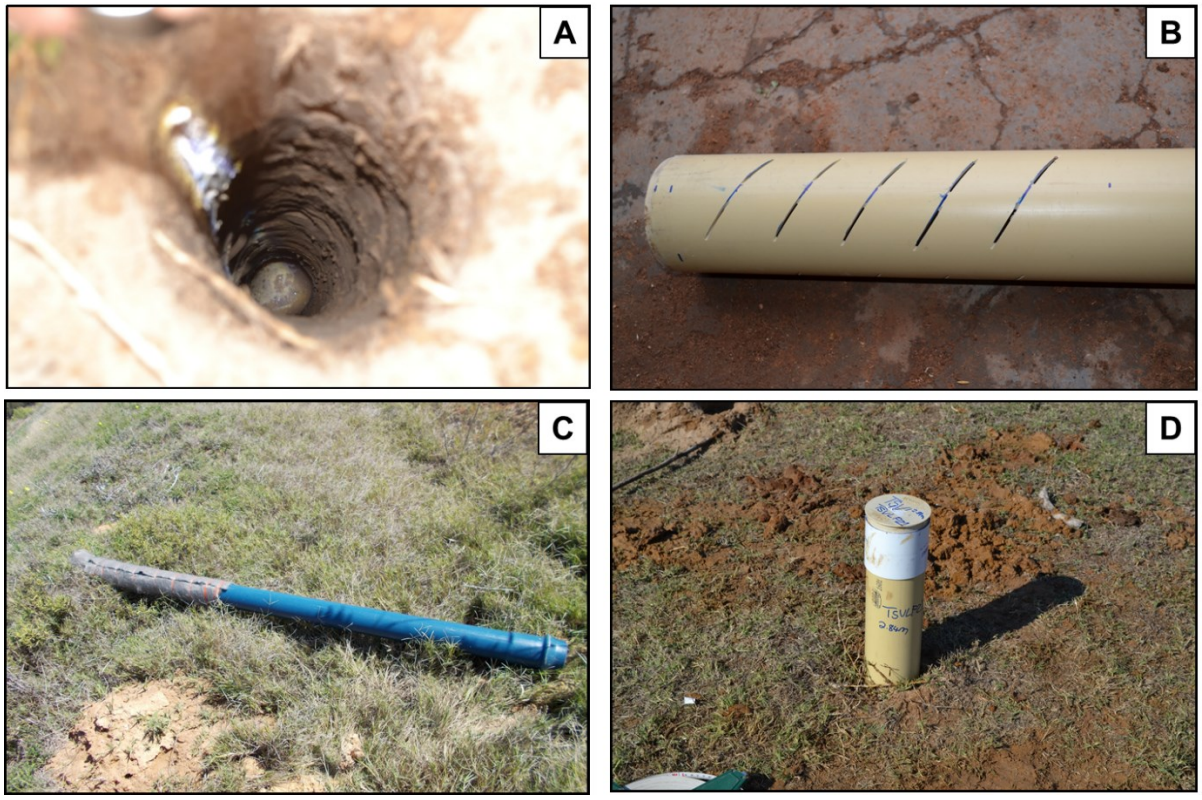


**Figure 4:** *Piezometer construction, A) augered hole; B) outer 10mm PVC piping; C) inner 90 mm diameter PVC piping wrapped with bedim; D) Finished piezometer.*

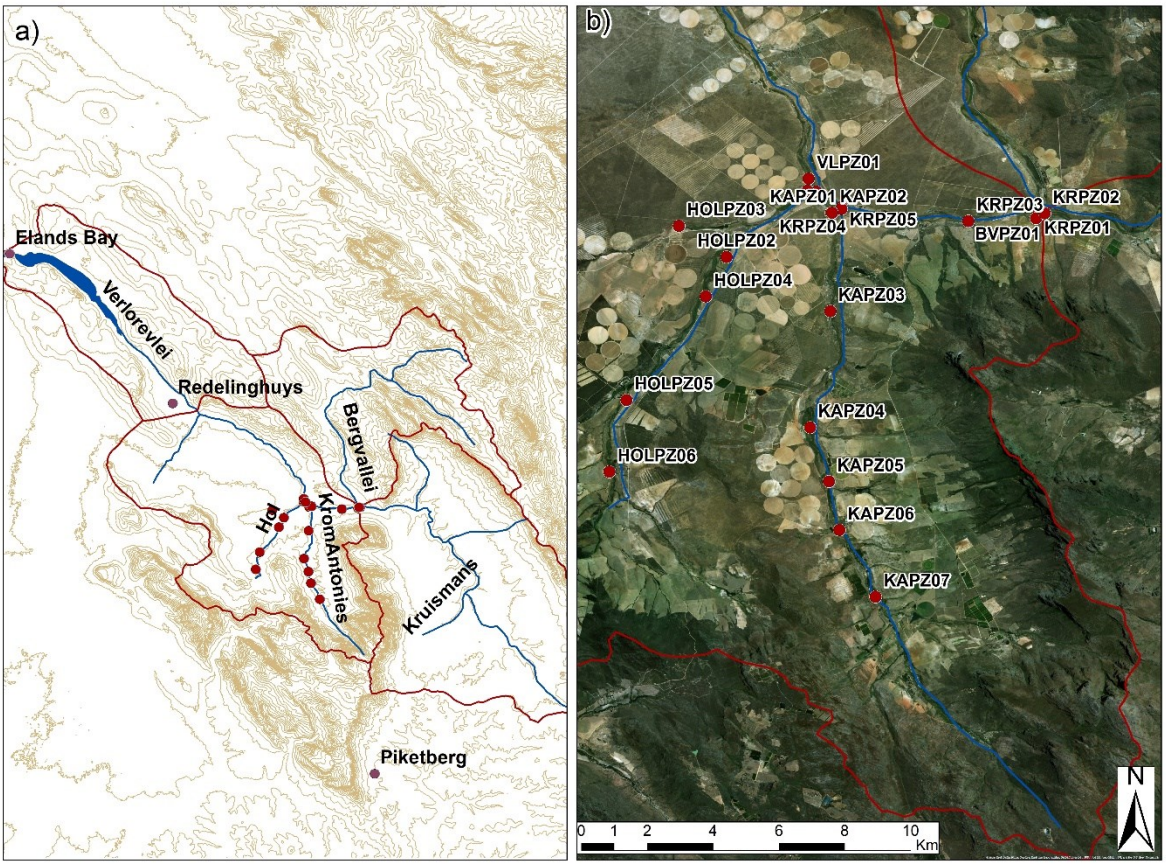


**Figure 5:** *A) Verlorenvlei Catchment; red dots: piezometers and purple dots: nearest towns; C) location of the 21 installed piezometers, KA: Krom Antonies tributary, KR: Kruismans tributary, HOL: Hol tributary, BV: Bergvallei tributary and VL: Verloren River and confluence.*

### *3.1.2 Water Level Loggers*

Four Heron level loggers were calibrated and set to measure at 15-minute intervals and installed in four piezometers (Table 2). Security, accessibility and depth (Table 1) of the piezometer were taken into consideration during installation. The purpose of the level loggers was to record fluctuations in water level particularly in response to seasonal variations in rainfall and base flow from groundwater. The barometric pressure from the nearby weather station (latitude: -32.72289 longitude: 18.73757) was used to cancel out the atmospheric pressure in the piezometer, required to calculate the water level for each level logger. Depth to water for piezometers without level loggers was measured using a dip meter during each sampling trip (Table 2).

**Table 1:** *Depths of all piezometers installed in each tributary.*

| Krom Antonies | Depth (m) | Kruismans | Depth (m) | Hol | Depth (m) | Bergvallei | Depth (m) | Verloren | Depth (m) |
|---|---|---|---|---|---|---|---|---|---|
| KAPZ01 | 1.2 | KRPZ01 | 2.4 | HOLPZ01 | 3.4 | BVPZ01 | 2.34 | VLPZ01 | 2.6 |
| KAPZ02 | 1.65 | KRPZ02 | 2.4 | HOLPZ02 | 2.6 | | | VLPZ02 | 1.43 |
| KAPZ03 | 1.8 | KRPZ03 | 1.3 | HOLPZ03 | 2.3 | | | | |
| KAPZ04 | 1.35 | KRPZ04 | 1.6 | HOLPZ04 | 1.36 | | | | |
| KAPZ05 | 2.2 | KRPZ05 | 1.66 | HOLPZ05 | 1.59 | | | | |
| KAPZ06 | 2.45 | | | HOLPZ06 | 1 | | | | |
| KAPZ07 | 2.1 | | | | | | | | |

**Table 2:** *Depths(m) at which each level logger was installed. KA: Krom Antonies tributary, KR: Kruismans tributary, HOL: Hol tributary and VL: Verloren confluence.*

| Piezometer | Level logger name | Depth (m) of level logger |
|---|---|---|
| HOLPZ04 | HOLP03 | 1.29 |
| KAPZ07 | KAP04 | 1.44 |
| KRPZ04 | KRP02 | 1.8 |
| VLPZ01 | VLP01 | 2.5 |

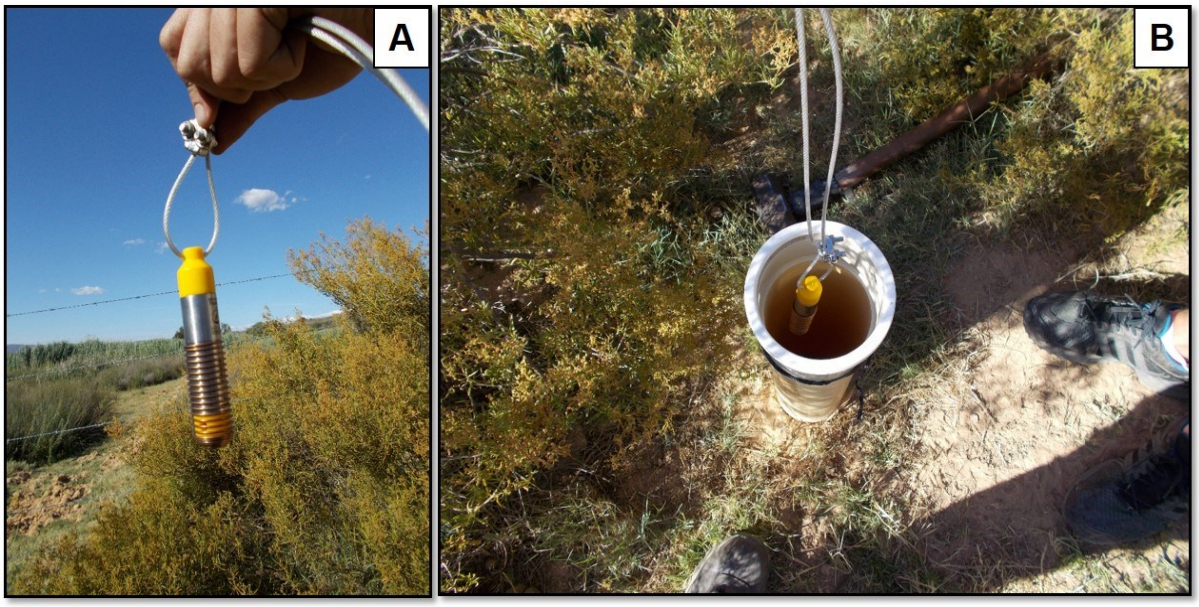


**Figure 6:** *A) Heron level logger; B) Heron level logger being submerged in the piezometer.*

## 3.2 Water Sampling

A total of 42 surface water samples were collected from four tributaries during the June 2015, July 2015, September 2015, November 2015, March 2016 and June 2016 sampling field trips. One hundred and ten shallow ground water samples were collected from piezometers in the same months as mentioned above. The monthly sampling was conducted to account for any seasonal variations of salinity within the catchment. Surface water samples were collected when the rivers were flowing and limited samples were collected for surface water samples. The current drought conditions across much of South Africa resulted in decreased surface

runoff in the catchment and restricted the total number of surface water samples that could be collected in 2015 and 2016. During the sampling field trip of November 2015 and March 2016, the majority of the piezometers were dry as a result of these drought conditions. Shallow groundwater samples were collected using a 1L stainless steel bailer and each piezometer was purged to remove stagnant water before each sample collection. Surface water and shallow groundwater samples were collected in pre-cleaned polyethylene 250 and 500ml bottles. The bottles were rinsed 3 times thoroughly with sample waters and then the sample was filtered into 15 and 50ml Polypropylene tubes.

Physiochemical parameters such as temperature (T), pH and electrical conductivity (EC) were measured at each sampling point using a portable EXTECH EC500 pH/Electrical Conductivity probe. The probe was calibrated every sampling day using pH and EC standard solutions, 4,7,10 and 84µS/cm, 1413µS/cm, 12880µS/cm respectively. Samples for cations and H, O stable isotopes were filtered into 15ml polypropylene (PP) tubes using a 0.45 micro-meter cellulose acetate filter and the cation samples were acidified with 1ml nitric acid ($HNO_3$) to avoid precipitation of metals. Anions and Sr isotopes were filtered into 50ml PP tubes and approximately 10ml of each anion sample was used to determine alkalinity. Ten tritium samples were collected into 1-L polyethylene (PE) bottles. All samples were kept cool prior analyses.

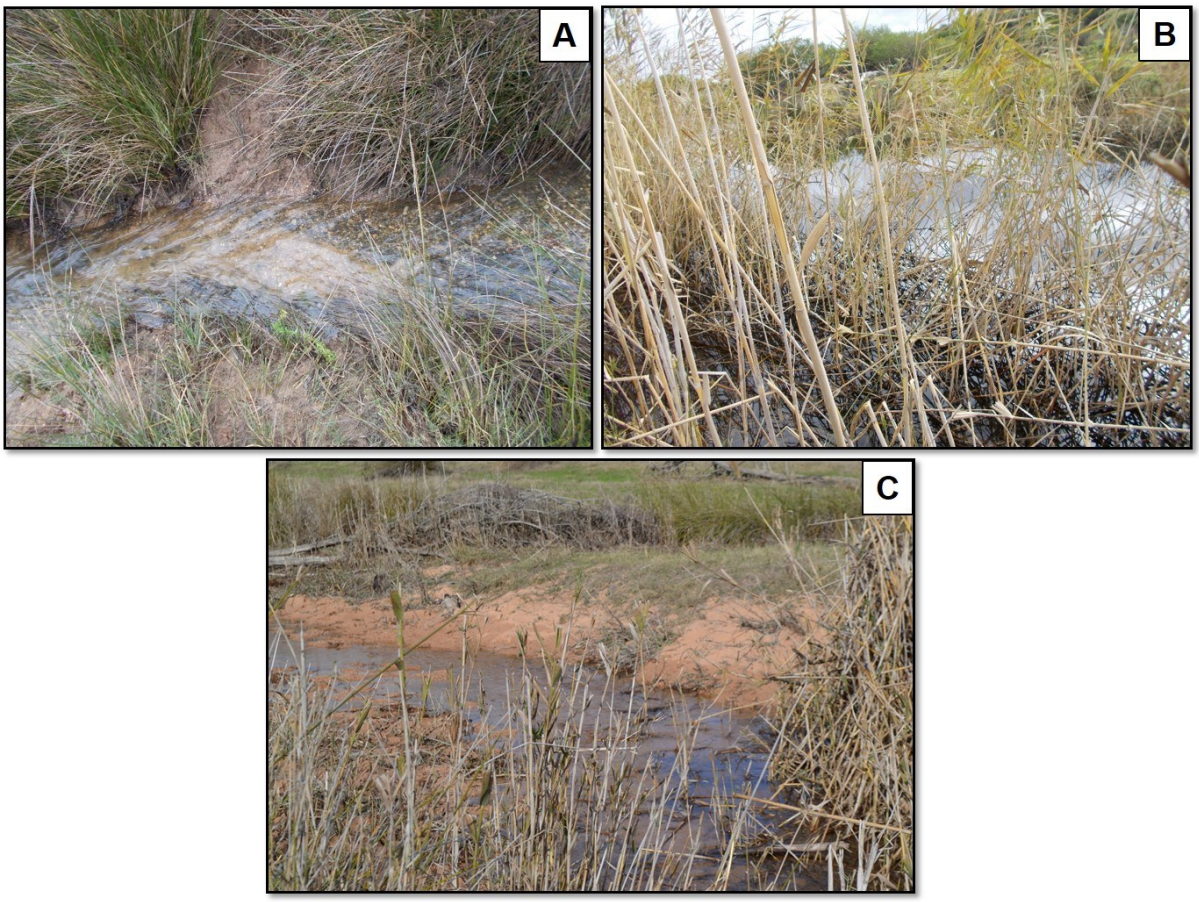


**Figure 7:** *Pictures showing surface water runoff during the wet season, A) Hol tributary; B) Bergvallei tributary and D) Kruismans tributary.*

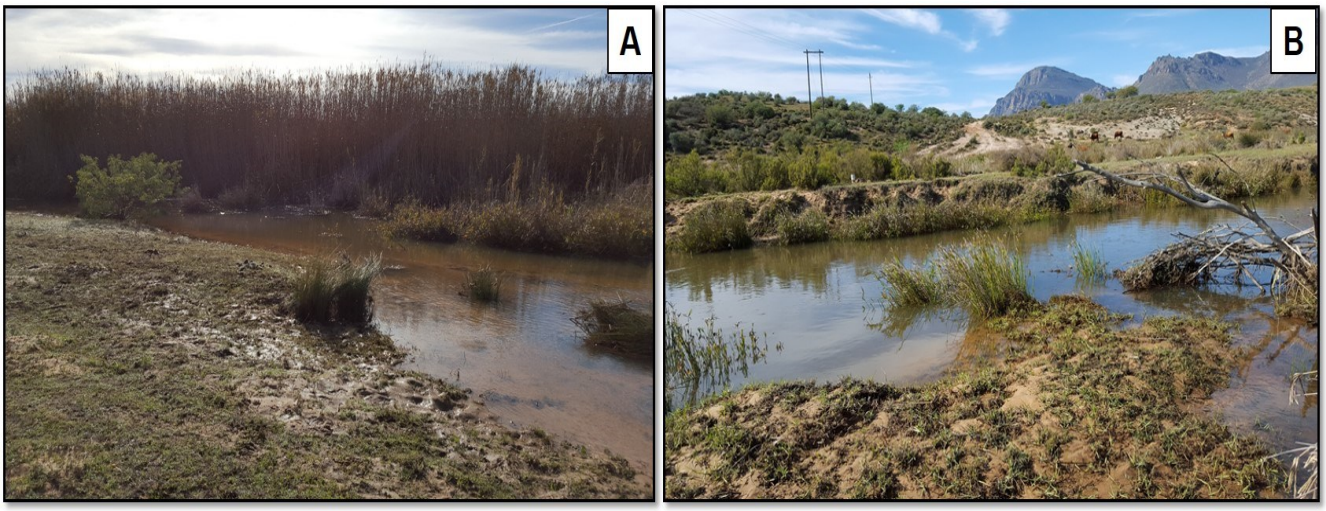


**Figure 8***: Pictures showing surface water runoff during the wet season, A) Verloren Confluence and B) Krom Antonies tributary.*

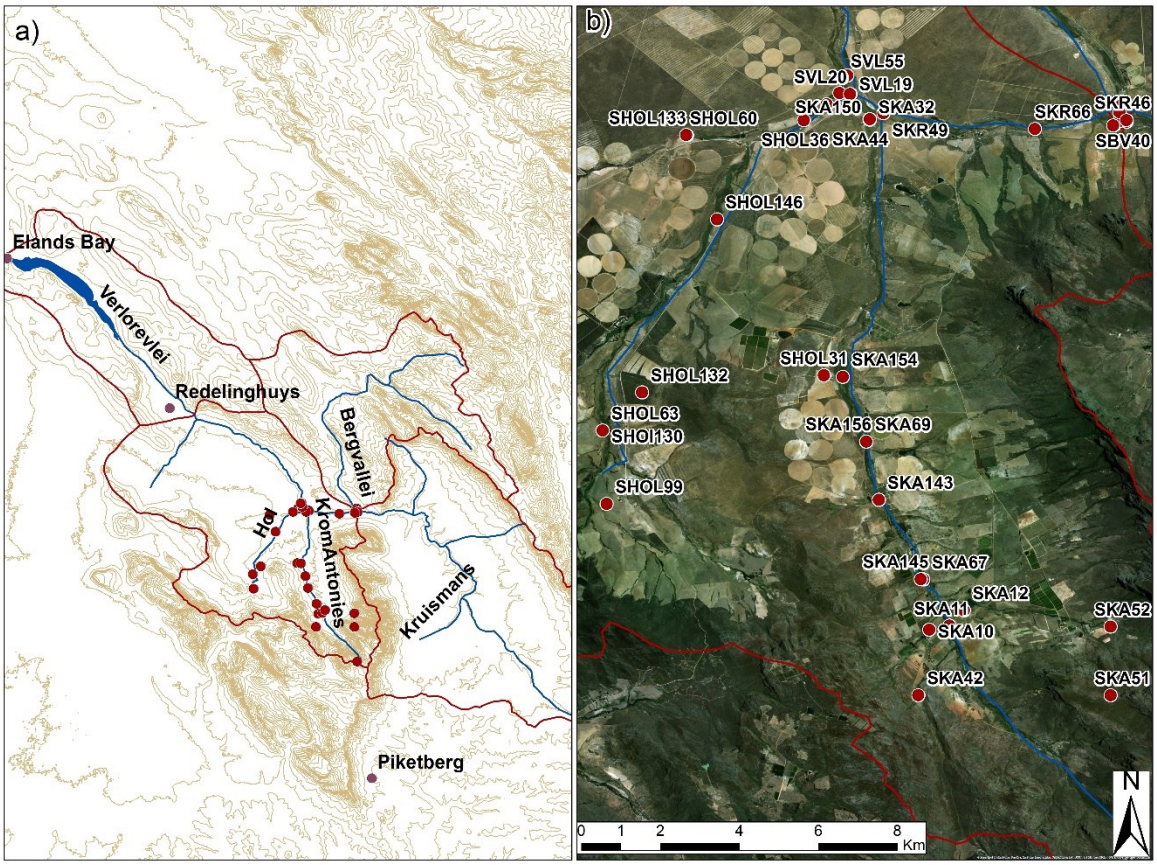


**Figure 9:** *A) Verlorenvlei Catchment, red dots: surface water sample locations and purple dots: nearest towns; C) Map showing location for surface water samples during the wet season of June 2015 to June 2016.*

## 3.3 Analytical Procedures

### *3.3.1 Major Ions*

Cations ($Na^+$, $Mg^{2+}$, $Ca^{2+}$, $K^+$) were determined at the Central Analytical Facility (CAF) Laboratory at Stellenbosch University using an Agilent 7700 Inductively coupled plasma mass spectrometry (ICP-MS). Anions ($Cl^-$, $SO_4^{2-}$, $NO_3^-$, $PO_4^{2-}$) were determined at the Department of Soil Sciences at the University of Stellenbosch using a Dionex DX-129 ion chromatograph (IC). Chloride, sulphate and nitrate of samples 128 to 156 were analysed at the Institute of Groundwater Studies (IGS) at the University of Free State using a Dionex Dx-120 ion chromatograph (IC) instrument. The minimum detection limit for $Cl^-$ was 0.2mg/L and for $SO_4^{2-}$, $NO_3^-$and $PO_4^2$ was 0.5mg/L. The maximum detection limits were undiluted but with a factor of adjusting up to 100mg/L for $Cl^-$, $SO_4^{2-}$, $NO_3^-$and $PO_4^{2-}$. The instruments were calibrated daily using the National Institute of Standards and Technology (NIST) traceable standards. For instrument stability, regular control standards are analysed throughout the run. Anions samples were run either as undiluted, volumetrically diluted x10 or volumetrically diluted x100

depending on EC values to bring anion concentrations to within range of the standards. Trace elements (W, B, As, Sr, Al, Se, and Br) were determined using ICP-MS at the CAF labs, where calibrations were done using Spectrascan SS-028555 standards and analytical errors did not exceed 10%.

Laboratory alkalinity and pH were determined from 50ml anion samples using 10ml of each sample and titrated using the Metrohm 702 SM Tritrino auto titrator. The instrument was calibrated for pH 4 and 7 standard solutions and a concentration of 0.02M of hydrochloric acid (HCl) was used as a titrant. The calculation for determining $HCO_3^-$ concentration is defined as follows:

$$HCO_3 = \frac{\big(EP2(ml) - EP1(ml)\big)\ x\ 0.02\ M\ x\ 50000}{10\ (ml)}$$

Where: EP2 represent $CO_3^{2-}$ and EP1 is $HCO_3^-$ in ml is the amount of acid titrated into sample, 0.02M is the acid (HCl) concentration and 10ml is the sample volume.

Total dissolved solids (TDS in mg/L) was obtained by adding concentrations of all cations, anions and trace elements: TDS = $Na^+$ + $Mg^{2+}$ +$Ca^{2+}$ + $K^+$ + $Sr^{2+}$ +As +Al+ W + B + Se+ $Cl^-$ + $Br^-$ + $HCO_3^-$ + $SO_4^{2-}$ + $NO_3^-$ + $PO_4^{3-}$. Trace element concentrations may be regarded as negligible, hence their low concentrations in surface water and shallow groundwater.

### *3.3.2 Evaluation of data using Charge Balance*

Cation–anion charge balance is a standard method for checking the correctness of analyses of portable water samples. The method is based on a percentage difference between the total positive charged cations and the total negative charged anions, on the assumption that the water sample should be electrically neutral, and is determined as follows:

$$\%\ Difference = 100 * (\frac{\sum cations\ -\ \sum anions}{\sum cations\ +\ \sum anions})$$

A percentage difference of ± 10% is considered as acceptable and that of ±5% is considered as accurate (Murray and Wade, 1996.) Most of the samples show ion balance errors within ±10 % (Table 3 and 4) which indicated the overall precision of the analytical procedure.

### *3.3.3 Oxygen and Hydrogen Isotopes*

Stable isotopes of $\delta^2H$ and $\delta^{18}O$ for surface water and shallow groundwater samples were determined in the laboratory of the Environmental Isotope Group (EIG) of the i-Themba Laboratories Gauteng using the PDZ Europa Geo 20-20 gas mass-spectrometer connected to peripheral sample preparation devices The standards used have been prepared by

calibration against the following known standards: LGR2 ($\delta^2H$ -117.00, $\delta^{18}O$ -15.55), VSMOW2 (IAEA) ($\delta^2H$ 0.0, $\delta 1^8O$ 0.0) and IA-RO53 (IAD) ($\delta^2H$ -61.97, $\delta^{18}O$ -10.18). Each sample and standard was sub-sampled and analysed 6 times. The standard deviation of the $\delta^2H$ results was less than 1.5 ‰ and for the $\delta^{18}O$ samples, less than 0.3 ‰. Deviation from the $^2H/^1H$ and $^{18}O/^{16}O$ ratios relative to the international reference material the Standard Mean Ocean Water (SMOW) which is assigned $\delta^2H$ and $\delta^{18}O$ values of zero ‰, with analytical precision estimated at 0.1‰ for $\delta^{18}O$ and 0.5 ‰ for $\delta^2H$. The analytical results are presented in the common delta notation:

$$\delta\ (‰) = ((R_{sample} - R_{standard}) / (R_{standard})) \times 1000$$

where R represents the $^{18}O/^{16}O$, D/H, per the standard SMOW.

### *3.3.4 Strontium Isotopes*

A standard procedure was adopted for the chemical separation and mass spectrometry of strontium. The $^{87}Sr/^{86}Sr$ isotope ratios were measured on a NuPlasma HR MC-ICP-MS in the Department of Geological Sciences at the University of Cape Town, South Africa. Filtered groundwater samples, were used for the analysis with 6ml of each sample dried down in a Teflon beaker. After drying 2M nitric acid (HNO3) was added and the sample was dried down once more, and process repeated. After the second drying, 1.5ml of 2M $HNO_3^-$ was added and the sample was ready for Sr chemistry. The Sr chemistry involved placing the sample through a standard cation exchange column which extracted the Sr for analysis. Strontium isotopes were analysed as 200ppb in 0.2% $HNO_3^-$ solution and calibrated to the standard reference NIST987 that has a standard value of 0.710255. The Sr isotope data was corrected for Rubidium (Rb) interference and instrumental mass fractionation using the exponential law and a $^{86}Sr/^{88}Sr$ value of 0.1194.

### *3.3.5 Tritium*

Unfiltered 1-L samples of tritium were analysed in the laboratory of the Environmental Isotope Group (EIG) of the i-Themba laboratories Gauteng. The samples were distilled with an electrolyte of sodium hydroxide and subsequently enriched by electrolysis. Five hundred millilitres of the sample was used and after several days of electrolysis this volume is then reduced to 20ml for tritium enrichment by a factor of about 20. Known standards (spikes) of tritium concentrations were run to check whether enrichment was attained. Ten millilitres of the enriched distilled water samples went through liquid scintillation counting 2 to 3 cycles for 4 hours. The detection limits were 0.2 TU for enriched samples.

# 4.RESULTS

Physiochemical parameters such as pH, temperature and EC, major ions, trace elements and environmental isotopes ($\delta^{18}O$, $\delta^{2}H$, $^{87}Sr/^{86}Sr$ and $^{3}H$ ) are represented in Tables 3 and 4. The data is described for each individual tributary, because each tributary has its own unique chemical characteristics and chemical variation between surface water and shallow groundwater samples. Sodium is represented as a percentage of all cations in mili equivalents [100 * Na/ (Ca + K + Mg + Na)]. Alkalinity is represented as $HCO_3^-$. Six trace elements (W, Se, Sr, B, As, Al) were analysed for each surface water and shallow groundwater sample.

The standard $\delta^{2}H$ versus $\delta^{18}O$ plots show results for surface water and shallow groundwater samples collected from each tributary in relation with the Global Meteoric Water Line (GMWL: $\delta\ ^{2}H = 8\ \delta^{18}O + 10$) (Craig, 1961). The Local Meteoric Water Line (LMWL) $\delta^{2}H = 6.8\ \delta^{18}O + 9.8$) was simulated by $\delta^{2}H$ and $\delta^{18}O$ content of precipitation of samples collected in the study area (Eilers, 2018). The values of $^{87}Sr/^{86}Sr$ of 16 selected shallow groundwater samples, range from 0.71418 to 0.71597 (Table 4). Strontium concentration of the selected shallow groundwater samples range from 125.4 to 2468.8 µg/L (average =1043.7µg/L).

**Table 3***: Surface water results of field measurements, major ion chemistry, stable and radiogenic isotopes. Blank spaces: not detected (anions) and not determined (stable isotopes). The respective laboratories used for analyses are shown:*

| Sample ID | EC | pH | $Ca^{1}$ | $Mg^{1}$ | $Na^{1}$ | $K^{1}$ | $Cl^{1,2}$ | $Br^{1}$ | $SO_4^{1,2}$ | $HCO_3$ | $NO_3^{1,2}$ | $PO_4^{1,2}$ | TDS | %CAB | Na% | Na/Cl | Cl/Br | Mg/Ca | Na/Ca | Sr/Ca | $\delta D^{3}$ | $\delta^{18}O^{3}$ |
|---|---|---|---|---|---|---|---|---|---|---|---|---|---|---|---|---|---|---|---|---|---|---|
| | (mS/m) | | [mg/L] | [mg/L] | [mg/L] | [mg/L] | [mg/L] | [mg/L] | [mg/L] | [mg/L] | [mg/L] | [mg/L] | [mg/L] | | | Molar ratios | | | | | (‰) | (‰) |
| Krom Antonies | | | | | | | | | | | | | | | | | | | | | | |
| TS15VLR010 | 15 | 6.67 | 8.80 | 3.60 | 15.20 | 1.90 | 29.50 | 0.15 | 6.90 | 22.4 | 0.2 | 4.5 | 93.15 | -1.53 | 51.53 | 0.80 | 441.65 | 0.68 | 3.01 | 0.002 | -1.2 | -0.42 |
| TS15VLR011 | 12.68 | 6.53 | 5.10 | 2.80 | 12.70 | 0.70 | 26.80 | 0.06 | 4.60 | 15.4 | | 0.8 | 68.96 | -3.40 | 59.62 | 0.73 | 1094.95 | 0.91 | 4.34 | 0.002 | -13.5 | -3.71 |
| TS15VLR013 | 5.16 | 6.23 | 2.70 | 1.30 | 12.00 | 0.40 | 15.40 | 0.06 | 10.40 | 10.0 | | | 52.26 | -2.60 | 73.17 | 1.20 | 615.12 | 0.79 | 7.75 | 0.002 | -15.1 | -3.82 |
| TS15VLR032 | 112.1 | 7.47 | 35.89 | 26.67 | 151.72 | 2.11 | 289.00 | 0.91 | 41.00 | 104.2 | | 7 | 658.50 | -1.39 | 70.12 | 0.81 | 711.84 | 1.23 | 7.37 | 0.003 | -12.6 | -2.83 |
| TS15VLR042 | 62.8 | 5.92 | 1.80 | 1.60 | 20.80 | 0.30 | 37.00 | 0.16 | 2.00 | 7.4 | | | 71.06 | -3.15 | 84.90 | 0.87 | 519.97 | 1.47 | 20.15 | 0.001 | -13.3 | -3.67 |
| TS15VLR044 | 115.4 | 7.49 | 42.85 | 31.86 | 178.79 | 2.05 | 355.00 | 1.05 | 47.00 | 118.2 | 2 | | 778.80 | -1.47 | 69.96 | 0.78 | 758.53 | 1.23 | 7.28 | 0.003 | -16.3 | -3.72 |
| TS15VLR051 | 5.79 | | 2.00 | 1.50 | 16.10 | 0.30 | 26.27 | 0.12 | 7.00 | 0.0 | | | 53.29 | 2.41 | 80.90 | 0.95 | 506.40 | 1.24 | 14.04 | 0.002 | | |
| TS15VLR052 | 4.71 | 6.28 | 2.10 | 1.60 | 16.00 | 0.30 | 30.00 | 0.09 | 2.00 | 9.8 | 1 | | 62.89 | -6.23 | 80.00 | 0.82 | 730.51 | 1.26 | 13.28 | 0.002 | | |
| TS15VLR067 | 25.4 | 7.05 | 7.90 | 4.20 | 16.73 | 0.70 | 36.00 | 0.13 | 8.00 | 26.0 | | | 99.67 | -3.98 | 56.66 | 0.72 | 614.70 | 0.88 | 3.69 | 0.003 | -10.0 | -2.99 |
| TS15VLR069 | 49.2 | 7.04 | 15.66 | 9.68 | 48.20 | 0.63 | 96.00 | 0.42 | 17.00 | 44.8 | 2 | | 234.40 | -1.87 | 64.98 | 0.77 | 509.32 | 1.02 | 5.37 | 0.003 | -3.1 | -2.65 |
| TS15VLR0110 | 233 | 7.98 | 72.91 | 60.56 | 337.08 | 3.15 | 641.00 | 2.06 | 81.00 | 200.9 | | | 1398.67 | 0.64 | 71.16 | 0.81 | 701.53 | 1.37 | 8.06 | 0.004 | -2.6 | 0.21 |
| TS15VLR0123 | 34.5 | 7.32 | 16.67 | 10.48 | 42.59 | 1.07 | 74.00 | 0.31 | 20.00 | 48.2 | | | 213.31 | 4.05 | 60.15 | 0.89 | 542.10 | 1.04 | 4.46 | 0.003 | -6.5 | -1.83 |
| TS16VLR0143 | 9.81 | 6.11 | 3.20 | 1.60 | 10.14 | 0.65 | 22.00 | 0.07 | 6.00 | 1.8 | | | 45.45 | -1.73 | 65.04 | 0.71 | 754.91 | 0.82 | 5.53 | 0.003 | -12.1 | -2.85 |
| TS15VLR0150 | 21.7 | 6.44 | 6.60 | 3.92 | 22.90 | 1.43 | 52.00 | 0.11 | 12.00 | 2.6 | | | 101.56 | -2.17 | 65.72 | 0.68 | 1072.57 | 0.98 | 6.05 | 0.003 | -11.3 | -2.72 |
| TS15VLR0154 | 18.34 | 6.09 | 5.14 | 2.94 | 19.25 | 0.95 | 43.00 | 0.09 | 11.00 | 1.8 | 1.43 | | 84.17 | -3.93 | 68.07 | 0.69 | 1077.30 | 0.94 | 6.53 | 0.003 | -11.9 | -2.66 |
| TS15VLR0156 | 16.92 | 6.17 | 5.54 | 3.17 | 19.90 | 0.69 | 43.00 | 0.09 | 11.00 | 1.8 | 1.33 | 4.10 | 86.61 | -2.55 | 67.93 | 0.71 | 1064.54 | 0.94 | 6.26 | 0.003 | -11.1 | -2.53 |
| Average | 46.41 | 6.72 | 14.68 | 10.47 | 58.76 | 1.08 | 113.50 | 0.37 | 17.93 | 38.46 | 1.33 | 4.10 | 256.42 | -1.81 | 68.12 | 0.81 | 732.25 | 1.05 | 7.70 | 0.003 | -10.04 | -2.58 |
| Standard Deviation | 57.18 | 0.63 | 19.68 | 16.18 | 89.69 | 0.82 | 171.65 | 0.54 | 21.16 | 56.30 | 0.76 | 3.12 | 375.03 | 2.49 | 8.93 | 0.13 | 227.06 | 0.22 | 4.49 | 0.001 | 4.79 | 1.20 |
| Kruismans | | | | | | | | | | | | | | | | | | | | | | |
| TS15VLR014 | 698 | 7.34 | 119.80 | 225.30 | 1202.00 | 25.63 | 2717.60 | 7.92 | 301.00 | 299.8 | 8 | | 4907.049 | -6.37 | 76.43 | 0.68 | 772.36 | 3.10 | 17.49 | 0.008 | -13.5 | -2.97 |
| TS15VLR038 | | 7.51 | 137.02 | 235.34 | 1225.98 | 23.01 | 2514.00 | 8.37 | 246.00 | 316.0 | 0 | | 4705.707 | -0.70 | 75.62 | 0.75 | 676.29 | 2.83 | 15.60 | 0.006 | -12.8 | -2.80 |
| TS15VLR046 | 749 | 7.17 | 144.52 | 248.30 | 1295.85 | 24.11 | 2617.00 | 8.74 | 277.00 | 671.2 | 10 | | 5296.725 | -3.51 | 75.66 | 0.76 | 674.09 | 2.83 | 15.63 | 0.006 | -14.7 | -2.86 |
| TS15VLR049 | 731 | 7.9 | 145.61 | 244.70 | 1280.77 | 25.55 | 2515.00 | 8.66 | 280.00 | 298.8 | | | 4799.097 | 1.24 | 75.49 | 0.79 | 653.33 | 2.77 | 15.34 | 0.006 | -13.4 | -2.49 |
| TS15VLR066 | 585 | 7.55 | 84.50 | 185.50 | 766.83 | 15.20 | 1665.00 | 5.44 | 227.00 | 173.4 | | | 3122.866 | -1.23 | 72.89 | 0.71 | 689.06 | 3.62 | 15.82 | 0.005 | -12.0 | -2.51 |
| TS16VLR0135 | 715 | 7.02 | 125.20 | 223.30 | 980.70 | 24.51 | 2460.00 | 1.70 | 328.10 | 24.8 | 2.62 | | 4170.935 | -6.03 | 72.45 | 0.62 | 3247.95 | 2.94 | 13.66 | 0.006 | -10.7 | -2.32 |
| TS16VLR0140 | 685 | 7.11 | 131.30 | 226.20 | 988.30 | 24.27 | 2505.00 | 1.70 | 345.00 | 24.8 | 1.93 | | 4248.505 | -6.43 | 72.14 | 0.61 | 3307.36 | 2.84 | 13.12 | 0.006 | -10.7 | -2.39 |
| Average | 693.83 | 7.37 | 126.85 | 226.95 | 1105.78 | 23.18 | 2427.66 | 6.08 | 286.30 | 258.40 | 4.51 | | 4464.41 | -3.29 | 74.38 | 0.70 | 1431.49 | 2.99 | 15.24 | 0.01 | -12.5 | -2.62 |
| Standard Deviation | 52.94 | 0.28 | 19.40 | 19.18 | 183.14 | 3.36 | 321.53 | 2.95 | 39.05 | 204.74 | 3.82 | | 653.71 | 2.89 | 1.67 | 0.07 | 1168.25 | 0.28 | 1.35 | 0.00 | 1.4 | 0.23 |

Notes: Superscripts :(1) Stellenbosch University Central Alalytical Faculty, South Africa; (2) University of Free State Institute of Groundwater Studies, South Africa; (3) iThemba LABS, South Africa.

*Table 3 continued....*

| Sample ID | EC | pH | Ca 1 | Mg [1] | Na [1] | K [1] | Cl [1,2] | Br [1] | $SO_4$ [1,2] | $HCO_3$ | $NO_3$ [1,2] | $PO_4$ [1,2] | %CAB | Na% | Na/Cl | Cl/Br | Mg/Ca | Na/Ca | Sr/Ca | δ D [3] | $\delta^{18}O$ [3] |
|---|---|---|---|---|---|---|---|---|---|---|---|---|---|---|---|---|---|---|---|---|---|
| | (mS/m) | | [mg/L] | [mg/L] | [mg/L] | [mg/L] | [mg/L] | [mg/L] | [mg/L] | [mg/L] | [mg/L] | [mg/L] | Molar ratios | | | | | | | (‰) | (‰) |
| **Hol** | | | | | | | | | | | | | | | | | | | | | |
| TS15VLR030 | 514 | 7.77 | 125.60 | 162.00 | 722.60 | 12.50 | 1582.12 | 1.22 | 318.00 | 109.8 | 0 | 0 | -1.60 | 70.66 | 0.70 | 2911.74 | 2.13 | 10.03 | 0.001 | -12.1 | -2.28 |
| TS15VLR031 | 124.7 | 6.88 | 35.89 | 26.67 | 151.72 | 2.11 | 265.14 | 0.91 | 41.00 | 57.6 | | | 6.82 | 70.12 | 0.88 | 653.07 | 1.23 | 7.37 | 0.003 | -15.0 | -3.11 |
| TS15VLR036 | 592 | 7.15 | 122.10 | 186.75 | 947.70 | 16.63 | 1843.43 | 6.91 | | 162.6 | 0 | 0 | 7.14 | 74.44 | 0.79 | 600.68 | 2.52 | 13.53 | 0.005 | -11.2 | -2.58 |
| TS15VLR060 | 57 | 6.32 | 9.70 | 12.10 | 70.18 | 0.70 | 124.00 | 0.39 | 19.00 | 19.8 | 5 | 2 | 2.10 | 75.72 | 0.87 | 715.50 | 2.06 | 12.61 | 0.005 | -16.7 | -3.37 |
| TS15VLR063 | 371 | 7.73 | 98.50 | 113.70 | 413.34 | 2.70 | 837.00 | 2.58 | 227.00 | 205.8 | 0 | 0 | 0.94 | 65.79 | 0.76 | 729.12 | 1.90 | 7.32 | 0.004 | -11.6 | -2.31 |
| TS15VLR099 | 266 | 7.07 | 109.61 | 48.32 | 444.14 | 3.24 | 628.00 | 2.29 | 231.00 | 376.4 | 18 | 17 | -1.18 | 73.37 | 1.09 | 615.89 | 0.73 | 7.06 | 0.002 | -14.1 | -3.68 |
| TS15VLR0108 | 605 | 8.17 | 112.48 | 171.88 | 1000.47 | 2.53 | 2062.00 | 6.48 | 35.00 | 394.4 | 0 | 0 | -1.59 | 77.71 | 0.75 | 715.69 | 2.52 | 15.51 | 0.005 | 7.8 | 2.85 |
| TS15VLR0113 | | 6.01 | 14.23 | 16.22 | 89.72 | 0.38 | 181.00 | 0.53 | 32.00 | 27.6 | 0 | 0 | -2.21 | 74.43 | 0.77 | 774.29 | 1.88 | 10.99 | 0.005 | -11.4 | -3.21 |
| TS16VLR0130 | 217 | 6.89 | 89.44 | 59.56 | 256.90 | 8.74 | 596.00 | 1.36 | 259.30 | 8.0 | 7.92 | | -3.95 | 61.96 | 0.67 | 986.14 | 1.10 | 5.01 | 0.003 | -9.0 | -2.03 |
| TS16VLR0132 | 770 | 7.29 | 132.10 | 228.20 | 1054.00 | 24.66 | 2703.00 | 7.49 | 391.70 | 23.6 | 1 | | -8.28 | 73.25 | 0.60 | 812.23 | 2.85 | 13.91 | 0.006 | -8.8 | -2.22 |
| TS16VLR0133 | 247 | 5.67 | 68.23 | 75.02 | 312.00 | 4.08 | 693.00 | 1.48 | 236.10 | 4.0 | 3.04 | | -2.76 | 67.92 | 0.69 | 1057.03 | 1.81 | 7.97 | 0.005 | -11.9 | -2.70 |
| TS16VLR0146 | 522 | 6.94 | 118.80 | 139.80 | 720.50 | 14.38 | 1753.00 | 4.74 | 272.00 | 16.6 | | | -5.98 | 72.52 | 0.63 | 832.72 | 1.94 | 10.57 | 0.004 | -7.7 | -2.16 |
| Average | 389.61 | 6.99 | 86.39 | 103.35 | 515.27 | 7.72 | 1105.64 | 3.03 | 187.46 | 117.18 | 3.50 | 2.71 | -0.88 | 71.49 | 0.77 | 950.34 | 1.89 | 10.16 | 0.004 | -10.1 | -2.23 |
| Standard Deviation | 215.66 | 0.70 | 42.13 | 70.51 | 345.52 | 7.39 | 811.99 | 2.53 | 125.82 | 134.99 | 5.47 | 5.87 | 4.40 | 4.28 | 0.13 | 605.90 | 0.59 | 3.13 | 0.001 | 6.0 | 1.62 |
| **Bergvallei** | | | | | | | | | | | | | | | | | | | | | |
| TS15VLR015 | 166.5 | 6.31 | 30.19 | 48.29 | 262.13 | 6.45 | 563.80 | 1.83 | | 43.0 | 0 | 0 | 1.29 | 75.53 | | 692.68 | 2.64 | 15.14 | 0.004 | | |
| TS15VLR047 | 165.8 | 6.81 | 29.44 | 48.07 | 261.74 | 5.98 | 518.00 | 1.79 | 55.00 | 40.4 | 2 | 0 | 1.51 | 75.81 | 0.78 | 652.04 | 2.69 | 15.50 | 0.004 | -16.5 | -3.28 |
| TS16VLR0138 | 183.4 | 6.56 | 30.72 | 50.05 | 243.20 | 15.35 | 580.00 | 1.70 | 73.20 | 5.8 | | | 0.49 | 71.67 | 0.65 | 765.78 | 2.69 | 13.80 | 0.004 | -12.3 | -2.83 |
| Average | 171.90 | 6.56 | 30.12 | 48.80 | 255.69 | 9.26 | 553.93 | 1.77 | 64.10 | 29.73 | 1.00 | 0.00 | 1.10 | 74.34 | 0.71 | 703.50 | 2.67 | 14.81 | 0.004 | -14.4 | -3.06 |
| Standard Deviation | 8.14 | 0.20 | 0.53 | 0.89 | 8.83 | 4.31 | 26.26 | 0.05 | 9.10 | 16.96 | 1.00 | 0.00 | 0.44 | 1.89 | 0.07 | 47.06 | 0.02 | 0.73 | 0.000 | 2.1 | 0.22 |
| **Veerloren** | | | | | | | | | | | | | | | | | | | | | |
| TS15VLR020 | 37.5 | 5.64 | 3.40 | 8.70 | 61.52 | 0.90 | 107.00 | 0.36 | 6.00 | 9.4 | 8 | 22 | -4.01 | 68.59 | 0.73 | 934.12 | 1.12 | 6.89 | 0.003 | -13.8 | -3.67 |
| TS15VLR019 | 70.2 | 6.36 | 25.24 | 17.06 | 99.75 | 3.39 | 212.00 | 0.51 | 36.00 | 55.8 | 2.2 | 0 | -7.01 | 82.56 | 0.89 | 678.15 | 4.22 | 31.55 | 0.005 | -16.2 | -3.79 |
| TS15VLR028 | 200 | 7.04 | 59.89 | 67.97 | 337.63 | 8.20 | 689.00 | 2.27 | 162.00 | 137.2 | 0 | 0 | -3.27 | 71.28 | 0.76 | 683.08 | 1.87 | 9.83 | 0.005 | -7.9 | -1.97 |
| TS15VLR055 | 414 | 6.90 | 107.00 | 134.90 | 1048.00 | 9.90 | 1650.00 | 4.42 | 321.00 | 98.8 | 0 | 0 | -12.86 | 35.50 | 0.98 | 79.90 | 2.08 | 0.06 | 0.004 | -10.6 | -2.17 |
| Average | 180.43 | 6.49 | 48.88 | 57.16 | 386.73 | 5.60 | 664.50 | 1.89 | 131.25 | 75.30 | 2.55 | 5.50 | -6.78 | 64.48 | 0.84 | 593.81 | 2.32 | 12.08 | 0.004 | -12.1 | -2.90 |
| Standard Deviation | 147.92 | 0.55 | 39.14 | 50.29 | 396.17 | 3.61 | 609.79 | 1.64 | 124.21 | 47.72 | 3.27 | 9.53 | 3.77 | 17.53 | 0.10 | 314.24 | 1.15 | 11.78 | 0.001 | 3.1 | 0.83 |

Notes: Superscripts :(1 ) Stellenbosch University Central Alalytical Faculty, South Africa (2) University of Free State Institute of Groundwater Studies, South Africa; (3) iThemba LABS, South Africa.

**Table 4:** *Shallow groundwater results of field measurements, major ion chemistry, stable and radiogenic isotopes. Blank spaces: not detected (anions) and not determined (isotopes). Piezometer coordinates are shown in Appendix 1. The respective laboratories used for analyses are shown:*

| Krom Antonies | Sample ID | EC | pH | $Ca^{1}$ | $Mg^{1}$ | $Na^{1}$ | $K^{1}$ | $Cl^{1,2}$ | $Br^{1}$ | $SO_4^{1,2}$ | $HCO_3$ | $NO_3^{1,2}$ | $PO_4^{1,2}$ | TDS | Na% | Na/Cl | Cl/Br | Mg/Ca | Sr/Ca | δ D [3] | $\delta^{18}O$ [3] | $^{87}Sr/^{86}Sr$ [4] |
|---|---|---|---|---|---|---|---|---|---|---|---|---|---|---|---|---|---|---|---|---|---|---|
| Piezometer | | (mS/m) | | [mg/L] | [mg/L] | [mg/L] | [mg/L] | [mg/L] | [mg/L] | [mg/L] | [mg/L] | [mg/L] | [mg/L] | [mg/L] | | Molar ratios | | | | (‰) | (‰) | |
| KAPZ07 (LL) | TS15VLR0102 | 32.8 | 6.92 | 18.87 | 6.72 | 31.63 | 1.14 | 50.00 | 0.22 | 34 | 42.8 | 20 | | 205.38 | 54.20 | 0.98 | 511.31 | 0.59 | 0.002 | -12.6 | -3.50 | |
| | TS15VLR0122 | 18.18 | 6.89 | 13.90 | 5.76 | 24.51 | 1.09 | 35.00 | 0.21 | 6 | 55 | | | 141.47 | 54.14 | 1.08 | 382.68 | 0.68 | 0.030 | -10.5 | -3.24 | |
| KAPZ06 | TS15VLR068 | 218 | 5.65 | 132.80 | 52.10 | 179.70 | 1.00 | 342.00 | 1.32 | 489 | 49.4 | 3 | | 1250.32 | 49.15 | 0.81 | 583.44 | 0.65 | 0.002 | -12.0 | -3.06 | |
| | TS15VLR0124 | 190.3 | 6.95 | 334.20 | 32.86 | 204.97 | 1.26 | 343.00 | 1.32 | 786 | 14.4 | | | 1718.01 | 35.75 | 0.92 | 585.66 | 0.16 | 0.001 | -11.0 | -2.88 | |
| | TS16VLR0142 | 145.7 | 6.29 | 84.64 | 27.18 | 166.90 | 0.57 | 304.00 | 1.19 | | 22.8 | | | 789.28 | 59.76 | 0.85 | 574.50 | 0.53 | 0.002 | -8.2 | -2.19 | |
| KAPZ05 | TS15VLR070 | 205 | 7.06 | 77.40 | 41.70 | 197.40 | 1.70 | 400.00 | 1.16 | 93 | 221.6 | 42 | | 1075.96 | 62.04 | 0.76 | 777.50 | 0.89 | 0.003 | -11.9 | -2.84 | |
| | TS15VLR0101 | 143.3 | 7.57 | 61.75 | 29.65 | 208.56 | 0.61 | 302.00 | 1.00 | 82 | 175.6 | 43 | 6 | 910.17 | 69.39 | 1.07 | 680.15 | 0.79 | 0.003 | -13.3 | -3.04 | |
| | TS16VLR0155 | 197.4 | 7.06 | 90.73 | 40.81 | 232.40 | 0.73 | 526.00 | 1.22 | | 34.2 | | | 1034.36 | 63.73 | 0.68 | 964.41 | 0.74 | 0.003 | -9.3 | -2.33 | |
| KAPZ04 | TS15VLR072 | 127.6 | 6.67 | 50.20 | 27.90 | 102.90 | 2.10 | 256.00 | 0.74 | 22 | 73 | | | 534.84 | 56.20 | 0.62 | 782.94 | 0.92 | 0.004 | -9.1 | -2.36 | |
| | TS15VLR0100 | 178.3 | 6.89 | 97.44 | 43.11 | 228.39 | 2.35 | 439.34 | 1.16 | 211 | 168.6 | 37 | | 1228.39 | 61.51 | 0.80 | 854.86 | 0.73 | 0.004 | -7.9 | -2.34 | |
| | TS15VLR0125 | 63 | 7.11 | 29.76 | 14.46 | 82.63 | 1.31 | 132.00 | 0.46 | 10 | 134.8 | | | 405.43 | 64.47 | 0.97 | 650.17 | 0.80 | 0.004 | -11.2 | -2.82 | |
| | TS16VLR0153 | 87.8 | 6.42 | 38.12 | 18.87 | 100.60 | 1.56 | 212.00 | 0.46 | | 11.4 | | | 480.01 | 63.21 | 0.73 | 1039.86 | 0.82 | 0.003 | -7.7 | -2.24 | |
| KAPZ03 | TS15VLR071 | 177.9 | 6.67 | 45.10 | 40.10 | 159.30 | 0.70 | 401.00 | 0.88 | 71 | 73 | 4 | | 795.08 | 64.97 | 0.61 | 1031.37 | 1.47 | 0.004 | -12.9 | -2.89 | |
| | TS15VLR098 | 46.4 | 7.17 | 12.30 | 9.50 | 52.10 | 2.70 | 112.20 | 0.50 | 0 | 40 | | | 229.30 | 68.02 | 0.72 | 508.76 | 1.27 | 0.004 | -11.8 | -3.58 | |
| | TS16VLR0152 | 31.1 | 6.29 | 9.59 | 6.09 | 34.30 | 1.34 | 75.00 | 0.16 | 2.4 | | | | 151.88 | 66.84 | 0.71 | 1071.53 | 1.05 | 0.003 | -11.5 | -2.83 | |
| KAPZ02 | TS15VLR053 | 257 | 7.15 | 70.20 | 72.70 | 285.40 | 3.40 | 730.00 | 2.29 | 64 | 258.8 | 3 | | 1489.79 | 66.11 | 0.60 | 716.35 | 1.71 | 0.003 | -8.8 | -1.83 | |
| | TS15VLR077 | 213 | 7.01 | 60.30 | 58.80 | 256.00 | 3.00 | 610.00 | 1.60 | 79 | 178 | | 5 | 1251.70 | 67.71 | 0.65 | 856.52 | 1.61 | 0.003 | -11.5 | -2.67 | 0.715 |
| | TS15VLR088 | 132.9 | 6.98 | 41.56 | 34.61 | 188.11 | 2.29 | 326.00 | 1.05 | 40 | 136.8 | | | 770.41 | 70.57 | 0.89 | 700.02 | 1.37 | 0.003 | -11.4 | -3.69 | |
| | TS15VLR0109 | 65 | 7.07 | 42.25 | 34.59 | 97.57 | 3.75 | 197.00 | 0.81 | 6 | 190.8 | | | 572.77 | 54.77 | 0.76 | 549.91 | 1.35 | 0.003 | -8.3 | -2.69 | 0.715 |
| | TS16VLSR0149 | 210 | 6.38 | 69.11 | 57.26 | 250.50 | 3.95 | 594.00 | 1.62 | | 22.2 | | | 1103.65 | 65.78 | 0.65 | 823.47 | 1.37 | 0.003 | -5.2 | -1.81 | |
| KAPZ01 | TS15VLR078 | 321 | 5.32 | 87.30 | 67.50 | 351.10 | 2.60 | 910.00 | 2.19 | 152 | 18 | | | 1590.69 | 69.05 | 0.60 | 936.19 | 1.28 | 0.003 | -7.3 | -1.38 | |
| | TS15VLR087 | 54.3 | 6.64 | 17.06 | 10.91 | 68.97 | 2.93 | 139.00 | 0.39 | 26 | 49 | 2 | 5 | 321.25 | 69.06 | 0.77 | 811.99 | 1.05 | 0.003 | -6.9 | -1.90 | |
| | TS15VLR0111 | 77 | 6.63 | 24.35 | 18.51 | 103.25 | 2.63 | 162.00 | 2.06 | 25 | 125.2 | | | 462.99 | 69.42 | 0.98 | 177.30 | 1.25 | 0.004 | -10.6 | -2.73 | |
| | TS16VLSR0151 | 26 | 6.34 | 7.85 | 4.77 | 28.40 | 3.35 | 61.00 | 0.13 | | 2.8 | | | 124.29 | 64.02 | 0.72 | 1090.90 | 1.00 | 0.003 | -13.1 | -2.99 | |
| Average | | 134.12 | 6.71 | 63.20 | 31.52 | 151.48 | 2.00 | 319.11 | 1.00 | 115.71 | 91.23 | 19.25 | 5.33 | 776.56 | 62.08 | 0.79 | 735.91 | 1.00 | 0.004 | -10.2 | -2.66 | |
| Standard Deviation | | 81.82 | 0.49 | 64.96 | 19.84 | 89.59 | 1.03 | 223.14 | 0.62 | 192.72 | 75.00 | 17.52 | 0.47 | 477.39 | 7.90 | 0.14 | 224.93 | 0.37 | 0.005 | 2.2 | 0.57 | |
| Kruismans | | | | | | | | | | | | | | | | | | | | | | |
| KRPZ01 | TS15VLR045 | 627 | 7.11 | 137.40 | 189.52 | 1078.23 | 17.54 | 2015.00 | 6.89 | 233 | 376.8 | | | 4054.39 | 75.79 | 0.83 | 658.33 | 2.28 | 0.001 | -13.7 | -3.33 | |
| | TS15VLR081 | 580 | 7.48 | 109.50 | 183.10 | 814.00 | 13.60 | 1750.00 | 5.83 | 202 | 299.4 | | | 3377.43 | 72.67 | 0.72 | 675.65 | 2.76 | 0.000 | -16.1 | -3.27 | 0.716 |
| | TS15VLR0105 | 530 | 7.5 | 115.09 | 150.25 | 826.89 | 13.99 | 1406.51 | 5.10 | 212 | 276.2 | | 14 | 3020.04 | 74.75 | 0.91 | 620.34 | 2.15 | 0.005 | -16.6 | -3.79 | |
| | TS15VLR0121 | 354 | 7.14 | 69.75 | 88.45 | 526.75 | 11.77 | 949.00 | 3.27 | 139 | 223.2 | | | 2011.19 | 75.60 | 0.86 | 653.44 | 2.09 | 0.005 | -16.8 | -5.08 | 0.716 |
| | T16VLSR0139 | 432 | 6.92 | 101.10 | 122.50 | 607.60 | 11.41 | 3768.00 | 4.21 | | 36 | | | 2567.52 | 72.11 | 0.61 | 827.90 | 2.00 | 0.004 | -13.2 | -3.16 | |
| KRPZ02 | TS15VLR082 | 563 | 6.84 | 153.30 | 272.10 | 1100.00 | 13.20 | 2858.00 | 8.56 | 263 | 301 | 6 | | 4975.16 | 71.49 | 0.59 | 751.55 | 2.93 | 0.006 | -7.1 | -2.17 | 0.716 |
| | TS15VLR0104 | 713 | 7.05 | 145.30 | 219.01 | 1148.13 | 15.93 | 2135.78 | 7.64 | 207 | 297.6 | | 9 | 4185.38 | 75.12 | 0.83 | 629.51 | 2.49 | 0.006 | -9.5 | -2.18 | |
| | TS15VLR0119 | 664 | 6.92 | 134.77 | 203.68 | 1116.50 | 17.62 | 2377.00 | 7.49 | 158 | 261.8 | | | 4276.86 | 75.82 | 0.72 | 714.39 | 2.49 | 0.006 | -6.4 | -1.76 | 0.716 |
| | T16VLSR0136 | 671 | 6.7 | 140.00 | 223.10 | 982.10 | 11.47 | 2474.00 | 7.39 | | 34 | | | 4075.36 | 72.39 | 0.61 | 753.75 | 2.63 | 0.006 | -8.1 | -2.00 | |
| KRPZ03 | TS15VLR065 | 905 | 6.85 | 151.90 | 278.20 | 1257.38 | 17.30 | 2883.00 | 9.21 | 295 | 312.6 | | | 5204.59 | 73.76 | 0.67 | 704.64 | 3.02 | 0.001 | -12.9 | -2.83 | |
| | TS15VLR095 | 738 | 6.96 | 119.56 | 192.08 | 1079.35 | 16.88 | 2168.00 | 7.51 | 183 | 266.6 | | | 4032.98 | 76.67 | 0.77 | 650.06 | 2.65 | 0.006 | -13.4 | -2.50 | |
| | T16VLSR0141 | 1031 | 7.04 | 214.60 | 339.90 | 1430.00 | 11.90 | 3837.00 | 15.64 | | 62 | | | 6239.04 | 71.63 | 0.58 | 550.78 | 2.61 | 0.006 | -6.3 | -1.48 | |
| KRPZ04 (LL) | TS15VLR035 | 382 | 7.01 | 196.83 | 301.92 | 1316.82 | 6.26 | 2941.13 | 10.27 | 160 | 468.2 | 5 | | 5406.43 | 72.28 | 0.69 | 644.66 | 2.53 | 0.001 | -1.4 | -0.14 | |
| | TS15VLR048 | 848 | 7.2 | 155.95 | 279.84 | 1559.41 | 4.20 | 3064.00 | 10.58 | 157 | 543.8 | | | 5774.78 | 77.99 | 0.79 | 651.77 | 2.96 | 0.001 | -3.1 | -0.65 | |
| | TS15VLR079 | 529 | 7.17 | 171.00 | 313.00 | 1231.99 | 6.60 | 2913.78 | 10.25 | 574 | 412.2 | | | 5632.82 | 71.52 | 0.65 | 639.72 | 3.02 | 0.001 | -4.1 | -0.62 | 0.716 |
| | TS15VLR093 | 953 | 7.64 | 195.65 | 302.91 | 1420.21 | 7.00 | 3382.99 | 10.33 | 179 | 370 | | | 5868.08 | 73.75 | 0.65 | 737.13 | 2.55 | 0.006 | -6.4 | -1.20 | |
| | TS15VLR0117 | 865 | 7.26 | 172.67 | 285.29 | 1345.24 | 7.14 | 3139.00 | 9.22 | 183 | 367.4 | | | 5508.97 | 74.31 | 0.66 | 766.54 | 2.73 | 0.007 | -4.7 | -0.95 | 0.716 |
| | T16VLSR0128 | 102.5 | 6.81 | 234.90 | 382.80 | 1364.00 | 7.77 | 4160.00 | 11.12 | | 55 | | | 6484.29 | 68.56 | 0.51 | 842.02 | 2.69 | 0.007 | -0.3 | -0.31 | |
| KRPZ05 | TS15VLR050 | 1197 | 6.94 | 288.51 | 363.08 | 2081.17 | 17.16 | 4704.00 | 14.35 | 530 | 186 | 6 | | 8190.27 | 75.68 | 0.68 | 737.64 | 2.08 | 0.000 | -12.6 | -2.49 | |
| | TS15VLR080 | 551 | 6.98 | 299.50 | 485.00 | 2156.22 | 13.70 | 5327.25 | 17.10 | 527 | 231.2 | | | 9056.96 | 72.98 | 0.62 | 701.27 | 2.67 | 0.000 | -11.1 | -2.56 | |
| | TS15VLR094 | 1795 | 7.18 | 421.99 | 563.91 | 3009.14 | 18.56 | 6273.77 | 20.94 | 641 | 232.2 | | | 11181.51 | 74.97 | 0.74 | 674.32 | 2.21 | 0.005 | -13.6 | -2.80 | |
| | TS15VLR0118 | 1988 | 6.89 | 472.12 | 662.47 | 3511.32 | 19.08 | 9248.00 | 24.24 | 692 | 294.4 | | | 14923.63 | 75.27 | 0.59 | 858.63 | 2.32 | 0.005 | -9.9 | -2.33 | |
| Average | | 773.57 | 7.07 | 190.97 | 291.01 | 1407.38 | 12.73 | 3353.42 | 10.32 | 307.50 | 268.53 | 5.67 | 11.50 | 5729.44 | 73.87 | 0.69 | 702.00 | 2.54 | 0.004 | -9.4 | -2.16 | |
| Standard Deviation | | 427.62 | 0.23 | 98.20 | 135.83 | 702.12 | 4.46 | 1778.15 | 5.14 | 183.86 | 131.87 | 0.47 | 2.50 | 2882.97 | 2.12 | 0.10 | 75.33 | 0.30 | 0.003 | 4.8 | 1.19 | |

Notes: Supercripts: (1) Stellenbosch University Central Alalytical Faculty, South Africa; (2) University of Free State Institute of Groundwater Studies, South Africa; (3) iThemba LABS, South Africa; (4) Department of Geological Sciences, University of Cape Town, South Africa.

| Hol | Sample ID | EC | pH | Ca [1] | Mg [1] | Na [1] | K [1] | Cl [1,2] | Br [1] | $SO_4$ [1,2] | $HCO_3$ | $NO_3$ [1,2] | $PO_4$ [1,2] | TDS | Na% | Na/Cl | Cl/Br | Mg/Ca | Sr/Ca | δ D [3] | $\delta^{18}O$ [3] | $^{87}Sr/^{86}Sr$ [4] |
|---|---|---|---|---|---|---|---|---|---|---|---|---|---|---|---|---|---|---|---|---|---|---|
| Piezometer | | (mS/m) | | [mg/L] | [mg/L] | [mg/L] | [mg/L] | [mg/L] | [mg/L] | [mg/L] | [mg/L] | [mg/L] | [mg/L] | [mg/L] | | | Molar ratios | | | (‰) | (‰) | |
| HolPZ06 | TS15VLR097 | 1200 | 7.17 | 337.92 | 367.51 | 1873.74 | 1.57 | 3849.16 | 12.83 | | 466.8 | | | 6909.53 | 82.92 | 0.75 | 675.40 | 1.79 | 0.004 | -12.7 | -3.27 | |
| | TS15VLR0115 | 1499 | 7.22 | 414.37 | 477.50 | 2385.09 | 2.39 | 6149.00 | 16.84 | 687 | 679 | | | 10811.2 | 82.65 | 0.60 | 821.76 | 1.90 | 0.005 | -12.3 | -3.08 | |
| | T16VLSR0129 | 1893 | 7.03 | 629.80 | 775.10 | 2585.00 | 0.79 | 7079.00 | 21.37 | | 82 | | | 12392.1 | 76.20 | 0.56 | 745.59 | 2.03 | 0.004 | -7.9 | -2.07 | |
| HolPZ05 | TS15VLR062 | 792 | 6.37 | 195.60 | 239.60 | 1052.12 | 0.05 | 2268.00 | 5.79 | 691 | 70.8 | 6 | | 4532.21 | 80.64 | 0.72 | 880.88 | 2.02 | 0.004 | -12.0 | -2.87 | |
| | TS15VLR089 | 804 | 5.93 | 239.17 | 273.31 | 1225.99 | 0.05 | 2774.00 | 7.29 | 725 | 37.8 | | | 5285.1 | 80.99 | 0.68 | 856.62 | 1.89 | 0.004 | -10.8 | -2.66 | |
| HolPZ04 | TS15VLR061 | 552 | 7.62 | 71.00 | 112.90 | 758.70 | 4.40 | 1411.00 | 4.46 | 143 | 467.4 | 2 | 20 | 2994.86 | 86.26 | 0.83 | 711.38 | 2.62 | 0.004 | -16.8 | -3.24 | |
| | TS15VLR090 | 1255 | 7.25 | 296.55 | 417.63 | 2125.86 | 9.71 | 4891.00 | 14.45 | 339 | 533.2 | 12 | | 8639.38 | 82.78 | 0.67 | 762.03 | 2.32 | 0.005 | -13.4 | -3.44 | |
| | TS15VLR0116 | 583 | 7.47 | 92.87 | 130.52 | 965.19 | 4.84 | 1742.00 | 5.52 | 107 | 356.8 | 11 | 106 | 3521.74 | 87.33 | 0.86 | 710.50 | 2.32 | 0.005 | -13.5 | -3.26 | |
| | T16VLSR0131 | 643 | 7.59 | 111.90 | 138.60 | 1008.00 | 4.15 | 2017.00 | 5.58 | | 106.4 | | | 3540.63 | 87.17 | 0.77 | 813.51 | 2.04 | 0.005 | -13.5 | -2.95 | |
| HolPZ03 | TS15VLR059 | 372 | 4.68 | 116.40 | 166.40 | 444.80 | 2.10 | 1053.00 | 2.84 | 607 | 5.8 | 3 | 19 | 2420.34 | 71.85 | 0.65 | 833.59 | 2.36 | 0.005 | -16.6 | -4.13 | |
| | TS15VLR091 | 387 | 5.4 | 93.13 | 112.20 | 523.23 | 2.51 | 1085.00 | 3.51 | 414 | 11.2 | 8 | | 2252.78 | 81.43 | 0.74 | 696.31 | 1.99 | 0.005 | -13.4 | -3.66 | |
| | TS15VLR0112 | 353 | 3.8 | 76.38 | 90.09 | 457.75 | 1.73 | 1071.00 | 2.72 | 292 | 0 | | | 1991.67 | 82.72 | 0.66 | 884.72 | 1.95 | 0.005 | 2.0 | 0.47 | |
| | T16VLSR0134 | 189.4 | 5.22 | 37.13 | 41.72 | 247.40 | 1.10 | 596.00 | 1.49 | | 2.8 | | | 1025.45 | 84.70 | 0.64 | 895.92 | 1.85 | 0.005 | -13.0 | -2.84 | |
| HolPZ02 | TS15VLR058 | 350 | 6.75 | 86.90 | 188.50 | 949.91 | 5.90 | 1550.15 | 5.56 | 460 | 110.2 | 70 | 143 | 3570.13 | 82.70 | 0.95 | 627.04 | 3.58 | 0.005 | -15.5 | -2.94 | |
| | TS15VLR092 | 562 | 6.91 | 79.35 | 145.30 | 844.30 | 3.53 | 1625.00 | 5.13 | 471 | 71.8 | 66 | | 3311.41 | 84.68 | 0.80 | 712.56 | 3.02 | 0.005 | -13.4 | -3.12 | |
| | TS15VLR0114 | 566 | 6.49 | 81.62 | 148.90 | 879.84 | 3.77 | 1698.00 | 4.73 | 419 | 64.8 | 75 | | 3375.66 | 84.88 | 0.80 | 807.64 | 3.01 | 0.005 | -14.7 | -2.70 | |
| HolPZ01 | TS15VLR075 | 452 | 7.53 | 83.30 | 173.00 | 1481.00 | 12.30 | 2644.00 | 9.96 | 439 | 716.8 | | 55 | 5614.36 | 88.66 | 0.86 | 597.39 | 3.43 | 0.005 | -11.9 | -2.33 | 0.715 |
| | TS15VLR085 | 997 | 7.6 | 108.80 | 192.38 | 2078.76 | 18.04 | 3231.00 | 11.66 | 456 | 1018.2 | 6 | | 7120.84 | 90.59 | 0.99 | 623.92 | 2.92 | 0.006 | -9.9 | -2.58 | |
| | TS16VLR0127 | 350 | 7.58 | 100.28 | 167.96 | 1925.42 | 15.11 | 3117.00 | 9.93 | 425 | 875 | | | 6635.71 | 91.10 | 0.95 | 706.30 | 2.76 | 0.006 | -11.6 | -2.53 | |
| Average | | 726.28 | 6.61 | 171.18 | 229.43 | 1253.27 | 4.95 | 2623.70 | 7.98 | 445.00 | 298.78 | 25.90 | 68.60 | 5049.74 | 83.70 | 0.76 | 755.95 | 2.41 | 0.005 | -12.2 | -2.80 | |
| Standard Deviation | | 440.28 | 1.09 | 147.64 | 169.11 | 689.96 | 5.02 | 1726.90 | 5.20 | 176.43 | 322.43 | 29.30 | 48.87 | 2973.81 | 4.50 | 0.12 | 90.62 | 0.54 | 0.001 | 3.9 | 0.90 | |
| Bergvallei | | | | | | | | | | | | | | | | | | | | | | |
| BVPZ01 | TS15VLR083 | 520 | 6.35 | 124.10 | 226.30 | 1195.84 | 15.30 | 2612.20 | 8.85 | 221 | 160 | 6 | | 4569.59 | 76.58 | 0.71 | 664.38 | 3.01 | 0.003 | -11.4 | -2.63 | 0.715 |
| | TS15VLR0103 | 784 | 6.38 | 102.70 | 188.30 | 1225.00 | 12.88 | 2789.91 | 9.21 | 218 | 228.4 | | 14 | 4788.4 | 80.12 | 0.68 | 681.78 | 3.03 | 0.004 | -12.4 | -2.75 | |
| | TS15VLR0120 | 741 | 6.09 | 108.08 | 215.16 | 1126.51 | 14.23 | 2675.00 | 7.63 | 255 | 130.8 | | | 4532.41 | 76.95 | 0.65 | 789.18 | 3.29 | 0.004 | -12.6 | -2.42 | |
| | TS16VLR0137 | 1020 | 6.34 | 196.5 | 383.2 | 1516 | 11.73 | 3768 | 10.08 | | 57.8 | | | 6825.32 | 71.86 | 0.62 | 841.38 | 3.22 | 0.004 | -12.284 | -2.8339 | |
| Average | | 766.25 | 6.29 | 132.84 | 253.24 | 1265.84 | 13.54 | 2961.28 | 8.94 | 231.33 | 144.25 | | | 5178.93 | 76.38 | 0.66 | 744.18 | 3.13 | 0.004 | -12.2 | -2.66 | |
| Standard Deviation | | 122.65 | 0.13 | 43.01 | 86.25 | 165.36 | 1.02 | 490.41 | 1.01 | 18.50 | 69.89 | | | 1025.89 | 3.41 | 0.02 | 66.44 | 0.11 | 0.000 | 0.1 | 0.18 | |
| Verloren | | | | | | | | | | | | | | | | | | | | | | |
| VLPZ02 | TS15VLR018 | 172.2 | 6.36 | 35.70 | 51.80 | 291.67 | 5.00 | 608.00 | 2.05 | 63 | 84.8 | | 0 | 1142.03 | 75.92 | 0.74 | 666.20 | 2.39 | 0.010 | -4.9 | -1.50 | |
| | TS15VLR074 | 275 | 7.27 | 58.30 | 66.90 | 339.76 | 5.60 | 675.00 | 2.17 | 74 | 160 | 3 | 74 | 1458.73 | 72.20 | 0.78 | 700.56 | 1.89 | 0.008 | -8.2 | -2.04 | |
| | TS15VLR086 | 243 | 7.5 | 63.24 | 67.12 | 345.49 | 4.46 | 705.00 | 2.15 | 84 | 196.8 | 2 | | 1470.27 | 71.93 | 0.76 | 738.10 | 1.75 | 0.008 | -6.9 | -1.90 | 0.715 |
| VLPZ01 (LL) | TS15VLR022 | 179.5 | 6.46 | 30.93 | 25.41 | 240.50 | 11.30 | 412.00 | 1.16 | 123 | 59.6 | | 12 | 915.893 | 78.05 | 0.90 | 801.75 | 1.36 | 0.010 | -14.2 | -3.33 | |
| | TS15VLR024 | 85.4 | 5.63 | 15.43 | 13.79 | 145.87 | 6.01 | 258.00 | 0.73 | 64 | 14.8 | 4.4 | 1.7 | 524.732 | 80.54 | 0.87 | 792.04 | 1.47 | 0.010 | -16.0 | -3.55 | |
| | T15VLSR055 | | 6.9 | 128.76 | 123.18 | 622.87 | 12.71 | 1057.37 | 3.97 | 321 | 98.8 | | | 2368.64 | 70.18 | 0.91 | 599.96 | 1.58 | 0.008 | -10.6 | -2.17 | |
| | TS15VLR076 | 113.8 | 6.32 | 17.20 | 16.30 | 136.71 | 6.00 | 239.00 | 0.74 | 49 | 25 | 5 | 7 | 501.95 | 77.58 | 0.88 | 726.04 | 1.56 | 0.007 | -17.5 | -3.83 | 0.714 |
| | TS15VLR084 | 116.5 | 5.79 | 17.34 | 19.88 | 165.50 | 6.61 | 321.00 | 0.95 | 66 | 14.8 | 5 | | 617.074 | 79.06 | 0.80 | 760.98 | 1.89 | 0.010 | -16.9 | -3.73 | |
| | TS15VLR0106 | 135.3 | 5.72 | 22.51 | 25.50 | 200.81 | 7.99 | 382.00 | 1.11 | 56.4 | 13 | 2.1 | 27.8 | 739.217 | 78.19 | 0.81 | 775.48 | 1.87 | 0.010 | -10.7 | -3.46 | 0.715 |
| | TS16VLR0126 | 103.2 | 5.78 | 11.92 | 14.24 | 146.93 | 6.45 | 249.00 | 0.72 | 49 | 15 | | | 493.266 | 81.83 | 0.91 | 774.72 | 1.97 | 0.011 | -20.6 | -3.83 | |
| | T16VLSR0147 | 92.4 | 5.35 | 12.27 | 13.34 | 124.60 | 5.88 | 1753.00 | 0.64 | | 2.2 | | | 457.925 | 79.83 | 0.76 | 891.04 | 1.79 | 0.010 | -16.6 | -3.60 | |
| Average | | 151.63 | 6.28 | 37.60 | 39.77 | 250.97 | 7.09 | 605.40 | 1.49 | 94.94 | 62.25 | 3.58 | 20.42 | 971.79 | 76.85 | 0.83 | 747.90 | 1.78 | 0.009 | -13.0 | -2.99 | |
| Standard Deviation | | 61.60 | 0.67 | 33.43 | 32.98 | 140.65 | 2.49 | 435.49 | 0.97 | 78.08 | 63.00 | 1.27 | 25.64 | 569.09 | 3.66 | 0.06 | 72.84 | 0.27 | 0.001 | 4.8 | 0.85 | |

Notes: Supercripts: (1 ) Stellenbosch University Central Alalytical Faculty, South Africa; (2) University of Free State Institute of Groundwater Studies, South Africa;
(3) iThemba LABS, South Africa; (4) Department of Geological Sciences, University of Cape Town, South Africa.

*Table 4 continued….*

**Table 5:** *Surface water and shallow groundwater results of trace elements. Blank spaces: Depth to water (m) not measured. The respective laboratories used for analyses are shown:*

| Krom Antonies Piezometer | Sample ID | Date | Time | DW (m) | Al [1] [µg/L] | B [1] [µg/L] | As [1] [µg/L] | Se [1] [µg/L] | Sr [1] [µg/L] | W [1] [µg/L] |
|---|---|---|---|---|---|---|---|---|---|---|
| KAPZ07 (LL) | TS15VLR0102 | 2015/09/11 | 12:20 | 0.86 | 47.41 | 34.39 | 1.28 | 0.50 | 82.40 | 0.012 |
| | TS15VLR0122 | 2015/11/26 | 12:08 | 1 | 302.91 | 47.99 | 0.26 | 0.35 | 905.98 | 0.003 |
| KAPZ06 | TS15VLR068 | 2015/07/16 | 17:56 | | 0.52 | 160.32 | 0.21 | < 0.6 | 668.41 | < 0.002 |
| | TS15VLR0124 | 2015/11/26 | 12:54 | 1.92 | 71.86 | 155.03 | 2.90 | 0.71 | 651.22 | 0.001 |
| | TS16VLR0142 | 2016/06/16 | 12:40 | 0.95 | 2.85 | 156.02 | 0.31 | 0.27 | 390.02 | 0.004 |
| KAPZ05 | TS15VLR070 | 2015/07/16 | 18:00 | | 2.85 | 143.05 | 0.39 | 2.88 | 484.29 | 0.006 |
| | TS15VLR0101 | 2015/09/11 | 11:45 | 1.54 | 10.93 | 160.22 | 0.43 | 3.00 | 414.14 | 0.016 |
| | TS16VLR0155 | 2016/06/17 | 15:04 | 1.16 | 32.01 | 145.26 | 0.41 | 3.43 | 599.18 | 0.015 |
| KAPZ04 | TS15VLR072 | 2015/07/17 | 11:00 | | 0.59 | 59.17 | 0.38 | < 0.6 | 397.03 | 0.004 |
| | TS15VLR0100 | 2015/09/11 | 11:15 | 0.54 | 1.86 | 66.72 | 0.40 | 0.29 | 784.05 | 0.003 |
| | TS15VLR0125 | 2015/11/26 | 14:07 | 0.98 | 19.78 | 56.64 | 0.39 | 0.29 | 241.57 | 0.003 |
| | TS16VLR0153 | 2016/06/17 | 14:32 | 0.36 | 9.61 | 53.38 | 0.08 | 0.23 | 239.63 | 0.004 |
| KAPZ03 | TS15VLR071 | 2015/07/17 | 10:05 | | 4.77 | 99.50 | 0.87 | < 0.6 | 345.80 | 0.009 |
| | TS15VLR098 | 2015/09/11 | 18:18 | 0.87 | 39.76 | 52.21 | 1.29 | 0.56 | 103.65 | 0.008 |
| | TS16VLR0152 | 2016/06/17 | 13:59 | 0.14 | 61.86 | 28.28 | 0.36 | 0.18 | 65.60 | 0.007 |
| KAPZ02 | TS15VLR053 | 2015/06/19 | 11:00 | 1.5 | 3.19 | 155.86 | 0.31 | 0.50 | 524.47 | 0.007 |
| | TS15VLR077 | 2015/07/17 | 14:15 | | 0.33 | 150.53 | 0.24 | < 0.6 | 412.03 | 0.006 |
| | TS15VLR088 | 2015/09/09 | 12:16 | 1.5 | 17.20 | 110.83 | 0.21 | 0.47 | 287.06 | 0.006 |
| | TS15VLR0109 | 2015/11/24 | 18:29 | 1.82 | 42.05 | 76.42 | 1.99 | 0.46 | 300.84 | 0.030 |
| | TS16VLSR0145 | 2016/06/17 | 11:40 | 1 | 5.70 | 115.60 | 0.22 | 0.23 | 481.15 | 0.002 |
| KAPZ01 | TS15VLR078 | 2015/07/17 | 14:20 | | 7.52 | 136.08 | 0.17 | < 0.6 | 644.68 | < 0.002 |
| | TS15VLR087 | 2015/09/09 | 12:00 | 0.47 | 8.83 | 51.74 | 0.26 | 0.51 | 118.60 | 0.003 |
| | TS15VLR0111 | 2015/11/24 | 18:58 | 0.941 | 11.72 | 84.66 | 0.83 | 0.78 | 189.86 | 0.006 |
| | TS16VLSR0151 | 2016/06/17 | 12:09 | 0.095 | 80.54 | 34.53 | 0.47 | 0.19 | 55.65 | 0.009 |
| Average | | | | 0.98 | 32.78 | 97.27 | 0.61 | 0.83 | 391.14 | 0.01 |
| Standard Deviation | | | | 0.52 | 61.01 | 47.06 | 0.65 | 1.00 | 231.37 | 0.01 |
| Hol | | | | | | | | | | |
| HolPZ06 | TS15VLR097 | 2015/09/10 | 15:10 | 1.33 | 9.59 | 597.52 | 1.11 | 0.66 | 3173.51 | 0.008 |
| | TS15VLR0115 | 2015/11/25 | 13:34 | 1.45 | 2.19 | 690.38 | 39.80 | 0.42 | 4094.12 | 0.009 |
| | T16VLSR0129 | 2016/06/15 | 15:42 | 0.84 | 5.07 | 554.63 | 1.23 | 0.85 | 5929.31 | 0.004 |
| HolPZ05 | TS15VLR062 | 2015/07/16 | 13:00 | | < 0.6 | 367.12 | 0.23 | < 0.6 | 1574.67 | 0.002 |
| | TS15VLR089 | 2015/09/09 | 15:53 | 0.8 | 10.17 | 272.37 | 0.43 | 0.72 | 2228.24 | 0.002 |
| HolPZ04 | TS15VLR061 | 2015/07/16 | 12:25 | | 1.88 | 644.67 | 6.39 | 5.49 | 660.77 | 0.061 |
| | TS15VLR090 | 2015/09/09 | 16:20 | 0.82 | 5.39 | 723.02 | 5.83 | 1.22 | 3308.74 | 0.010 |
| | TS15VLR0116 | 2015/11/25 | 15:56 | 1.72 | 1.88 | 523.02 | 5.67 | 2.54 | 970.89 | 0.014 |
| | T16VLSR0131 | 2016/06/15 | 16:11 | | 5.00 | 621.15 | 10.06 | 16.10 | 1137.64 | 0.016 |
| HolPZ03 | TS15VLR059 | 2015/07/16 | 11:35 | | 604.32 | 54.51 | 0.19 | < 0.6 | 1243.25 | < 0.002 |
| | TS15VLR091 | 2015/09/09 | 17:24 | 1.78 | 92.05 | 55.62 | 0.24 | 0.36 | 1107.91 | 0.003 |
| | TS15VLR0112 | 2015/11/25 | 11:00 | 1.75 | 302.91 | 47.99 | 0.26 | 0.35 | 905.98 | 0.003 |
| | T16VLSR0134 | 2016/06/15 | 17:27 | 1.565 | 83.62 | 54.13 | 0.15 | 0.05 | 408.62 | 0.003 |
| HolPZ02 | TS15VLR058 | 2015/07/16 | 11:00 | | 2.24 | 328.81 | 1.70 | 4.18 | 996.03 | 0.024 |
| | TS15VLR092 | 2015/09/09 | 17:58 | 0.66 | 0.87 | 239.72 | 0.93 | 3.94 | 931.77 | 0.005 |
| | TS15VLR0114 | 2015/11/25 | 11:51 | 1.25 | 2.49 | 267.18 | 1.00 | 6.40 | 972.33 | 0.004 |
| HolPZ01 | TS15VLR075 | 2015/07/17 | 13:45 | | < 0.6 | 1639.91 | 4.44 | 1.91 | 978.90 | 0.092 |
| | TS15VLR085 | 2015/09/09 | 10:23 | 0.92 | 9.99 | 1763.21 | 4.14 | 6.34 | 1407.04 | 0.016 |
| | TS16VLR0127 | 2015/03/02 | 10:26 | 2.463 | 8.86 | 1848.07 | 3.70 | 1.19 | 1300.63 | 0.057 |
| Average | | | | 1.33 | 67.56 | 594.37 | 4.61 | 3.10 | 1754.23 | 0.018 |
| Standard Deviation | | | | 0.50 | 152.49 | 547.60 | 8.73 | 3.87 | 1372.33 | 0.025 |
| Kruismans Piezometer | Sample ID | Date | Time | DW (m) | Al [1] [µg/L] | B [1] [µg/L] | As [1] [µg/L] | Se [1] [µg/L] | Sr [1] [µg/L] | W [1] [µg/L] |
| KRPZ01 | TS15VLR045 | 2015/06/17 | 10:32 | | 6.97 | 767.12 | 1.97 | 1.59 | 1614.64 | 0.009 |
| | TS15VLR081 | 2015/07/17 | 15:13 | | < 0.6 | 632.35 | 0.62 | 1.22 | 1094.70 | 0.018 |
| | TS15VLR0105 | 2015/09/11 | 14:14 | 0.25 | 2.42 | 619.85 | 0.49 | 0.60 | 1272.51 | 0.012 |
| | TS15VLR0121 | 2015/11/25 | 18:48 | 1.36 | 8.12 | 516.81 | 1.66 | 0.43 | 700.56 | 0.006 |
| | T16VLSR0139 | 2016/06/16 | 11:32 | 0.825 | 4.84 | 513.52 | 0.21 | 0.68 | 979.74 | 0.004 |
| KRPZ02 | TS15VLR082 | 2015/07/17 | 15:55 | | 0.96 | 452.73 | 0.28 | 1.90 | 1901.25 | 0.003 |
| | TS15VLR0104 | 2015/09/11 | 13:54 | 1.39 | 4.90 | 391.77 | 0.23 | 0.70 | 1839.48 | 0.003 |
| | TS15VLR0119 | 2015/11/25 | 18:08 | 1.48 | 1.97 | 422.48 | 0.33 | 0.54 | 1805.47 | 0.006 |
| | T16VLSR0136 | 2016/06/16 | 11:03 | 1.38 | 15.58 | 426.12 | 0.26 | 1.34 | 1718.92 | 0.004 |
| KRPZ03 | TS15VLR065 | 2015/07/16 | 15:05 | | < 0.6 | 593.87 | 0.75 | < 0.6 | 1803.36 | 0.017 |
| | TS15VLR095 | 2015/09/10 | 9:35 | 0.46 | 5.20 | 418.34 | 1.38 | 0.97 | 1563.93 | 0.004 |
| | T16VLSR0141 | 2016/06/16 | 11:57 | 0.62 | 7.82 | 553.56 | 0.55 | 0.80 | 2752.88 | 0.006 |
| KRPZ04 (LL) | TS15VLR035 | 2015/06/13 | 16:07 | | 3.56 | 402.28 | 0.44 | 1.07 | 2576.73 | 0.003 |
| | TS15VLR048 | 2015/06/17 | 13:30 | | 3.61 | 699.25 | 0.72 | 3.95 | 2006.03 | 0.005 |
| | TS15VLR079 | 2015/07/17 | 14:33 | | < 0.6 | 434.04 | 0.55 | 0.70 | 2231.71 | 0.037 |
| | TS15VLR093 | 2015/09/10 | 8:52 | 0.9 | 4.59 | 434.54 | 0.67 | 0.80 | 2658.52 | 0.021 |
| | TS15VLR0117 | 2015/11/25 | 16:52 | 1.66 | 1.42 | 421.44 | 0.77 | 0.58 | 2468.79 | 0.012 |
| | T16VLSR0128 | 2016/06/15 | 11:05 | | 1.42 | 421.44 | 0.77 | 0.58 | 2468.79 | 0.012 |
| KRPZ05 | TS15VLR050 | 2015/06/17 | 14:19 | | 3.51 | 427.64 | 0.65 | 1.20 | 3143.40 | 0.012 |
| | TS15VLR080 | 2015/07/17 | 14:40 | | < 0.6 | 486.72 | 0.27 | 0.89 | 3122.90 | 0.014 |
| | TS15VLR094 | 2015/09/10 | 9:12 | 0.75 | 8.66 | 463.24 | 0.41 | 2.36 | 4759.56 | 0.006 |
| | TS15VLR0118 | 2015/11/25 | 17:15 | 1.5 | 3.00 | 499.66 | 0.50 | 0.77 | 5443.42 | 0.006 |
| Average | | | | 1.05 | 4.92 | 499.94 | 0.66 | 1.13 | 2269.42 | 0.01 |
| Standard Deviation | | | | 0.45 | 3.46 | 101.01 | 0.45 | 0.79 | 1105.32 | 0.01 |
| Notes: Superscripts :(1 ) Stellenbosch University Central Alalytical Faculty, South Africa | | | | | | | | | | |
| Bergvallei | | | | | | | | | | |
| BVPZ01 | TS15VLR083 | 2015/07/17 | 15:01 | | < 0.6 | 329.41 | 0.52 | 0.56 | 888.09 | < 0.002 |
| | TS15VLR0103 | 2015/09/11 | 13:42 | 1.26 | < 0.6 | 312.37 | 0.39 | < 0.6 | 886.12 | 0.002 |
| | TS15VLR0120 | 2015/11/25 | 18:20 | 1.68 | 2.89 | 313.35 | 4.00 | 1.02 | 952.87 | 0.006 |
| | T16VLR0137 | 2016/06/16 | 11:13 | 1.30 | 4.62 | 353.65 | 2.48 | 0.63 | 1870.05 | 0.005 |
| Average | | | | 1.41 | 3.76 | 327.20 | 1.85 | 0.73 | 1149.28 | 0.004 |
| Standard Deviation | | | | 0.19 | 0.86 | 19.23 | 1.48 | 0.20 | 448.92 | 0.002 |
| Verloren | | | | | | | | | | |
| VLPZ02 | TS15VLR018 | 2015/06/07 | 17:15 | 0.76 | 0.83 | 128.64 | 0.15 | < 0.6 | 363.18 | < 0.002 |
| | TS15VLR074 | 2015/07/17 | 13:35 | 0.57 | 0.51 | 130.23 | 0.44 | 0.87 | 494.79 | 0.021 |
| | TS15VLR086 | 2015/09/09 | 11:15 | | 28.69 | 143.62 | 0.28 | 1.17 | 514.74 | 0.012 |
| VLPZ01 (LL) | TS15VLR022 | 2015/06/09 | 10:25 | | 4.01 | 482.99 | 0.22 | 1.36 | 310.89 | 0.005 |
| | TS15VLR024 | 2015/06/11 | 13:14 | | 13.12 | 242.57 | 0.17 | 0.49 | 155.46 | 0.005 |
| | T15VLSR055 | 2015/06/19 | 11:55 | 1.64 | 2.31 | 256.26 | 0.98 | 0.36 | 1052.04 | 0.004 |
| | TS15VLR076 | 2015/07/17 | 13:55 | | 0.62 | 302.37 | 0.21 | < 0.6 | 125.43 | < 0.002 |
| | TS15VLR084 | 9/9/2015 | 9:56 | 0.91 | 3.18 | 320.99 | 0.08 | < 0.6 | 174.39 | < 0.002 |
| | TS15VLR0106 | 2015/11/24 | 16:46 | 1.61 | 9.49 | 327.61 | 0.13 | 0.20 | 225.23 | 0.001 |
| | T16VLR0126 | 2016/03/02 | 10:02 | | 17.16 | 231.73 | 0.93 | 0.50 | 125.29 | 0.002 |
| | T16VLSR0147 | 2016/06/17 | 11:14 | | 17.16 | 191.65 | 0.10 | | 123.85 | 0.004 |
| Average | | | | 1.10 | 8.83 | 250.79 | 0.34 | 0.71 | 333.21 | 0.007 |
| Standard Deviation | | | | 0.44 | 8.79 | 101.04 | 0.30 | 0.40 | 265.58 | 0.006 |
| Notes: Superscripts :(1 ) Stellenbosch University Central Alalytical Faculty, South Africa | | | | | | | | | | |

## 4.1 Krom Antonies Tributary

### *4.1.1 Physiochemical Parameters*

The pH for surface water in the Krom Antonies ranges between 5.9 and 7.9 with an average value of 6.7 (Table 3). Surface water samples in the same tributary have EC values ranging from 4.71 to 233mS/m, for samples collected in June 2015 and 2016. In both these years, the EC increases downstream towards the confluence although the magnitude of this increase is variable between sampling trips (Table 3). This contrasts with the variation in EC seen in the shallow groundwater described below.

The pH for shallow groundwater samples range from 5.3 to 7.6 with an average value of 6.6. The lowest pH values are found downstream for the months June and July 2015 (Figure 10B). Shallow groundwater samples have a wide range of EC values from 26 to 321mS/m, with the highest EC values measured during the month of July 2015 (Figure 10A). Piezometer KAPZ07, which is the highest point sampled upstream along the tributary, consistently had low EC values of 181.8 to 539mS/m. Thereafter, the EC fluctuated significantly down the tributary, with high values recorded in the winter season of June and July 2015, and then lower values during the summer season of November 2015 as well as the winter season of June 2016 (Figure 10A). Piezometers KAPZ01 and KAPZ02 are the furthest down the tributary and hence are closest to the confluence. These two piezometers are more or less the same distance down the tributary (~13.1km from KAPZ07) but are 300 m apart on a transect across the tributary. Samples collected from these two piezometers show surprisingly variable EC values given they are the same distance down the tributary. Shallow groundwater samples from piezometer KAPZ01, which has a depth of 1.2m, had EC values between 26 and 54.3mS/m, whilst shallow groundwater samples from piezometer KAPZ02, which has a depth of 1.65m, have EC values ranging from 132.9 to 210mS/m.

### *4.1.2 Major and Trace Element Hydrochemistry*

#### *4.1.2.1 Surface water*

Surface water samples in the Krom Antonies have $Ca^{2+}$ concentrations ranging between 1.8 and 72.9mg/L. Concentrations of $Na^{+}$, $Mg^{2+}$ and $Ca^{2+}$ increased down the tributary towards the Verloren confluence in June 2015 and June 2016, with the lowest concentrations of the three cations recorded during the wet season of June 2016 (Table 3). Potassium concentrations increased down the tributary for surface water samples collected in June 2016 and for surface water samples collected in June 2015. Potassium concentrations decreased down the tributary closer to the Verloren confluence. The highest concentrations for $Na^{+}$, $Mg^{2+}$,

$Ca^{2+}$ and $K^{+}$ were recorded during the dry season of November 2015, at the lowest sampled point downstream of the tributary (Table 3). Magnesium and sodium concentrations for surface water samples in the Krom Antonies range from 1.6 to 26.67mg/L and from 7.52 to 337.09mg/L, respectively, with sodium representing an average percentage of about 66.6 % of all cations. Potassium concentrations range between 0.3 and 3.1mg/L.

Chloride concentrations for surface water samples range from 15.4 to 641mg/L, while bromide concentrations range between 0.041 and 2.06mg/L. Surface water samples collected in June 2015 show increased $Cl^{-}$, $Br^{-}$, $SO_4^{2-}$ and $HCO_3^{-}$ concentrations down the tributary. The highest concentrations for the four anions were recorded during the dry season of November 2015 down the tributary towards the Verloren confluence (Table 3). Surface water samples show a wide range of $SO_4^{2-}$ and $HCO_3^{-}$ concentrations ranging from 2 to 81mg/L and from 7.4 to 254.4mg/L, respectively. Sample TS15VLR10 show phosphate concentration of 4.5mg/L recorded upstream of the tributary during the month of June 2015 (Table 3).

Surface water samples have lower trace elemental concentrations compared to shallow groundwater samples. Table 5 represents the Krom Antonies tributary reflecting much lower trace elemental concentrations compared to other tributaries.

*4.1.2.2 Shallow groundwater*

Shallow groundwater samples in the Krom Antonies show a wide range of sodium concentrations between 24.51 and 351.10mg/L. Sodium constitutes an average of 63.09% of all cations (Table 4). Potassium concentrations significantly fluctuates down the tributary, with high concentrations recorded downstream closest to the Verloren confluence. Piezometer KAPZ07, which is the highest point sampled upstream along the tributary, consistently had low $Na^{+}$, $Mg^{2+}$ and $Ca^{2+}$ concentrations. Piezometers KAPZ01 and KAPZ02 are the furthest down the tributary and hence are closest to the confluence. Samples collected from piezometer KAPZ02 have higher $Na^{+}$, $Mg^{2+}$, $K^{+}$ and $Ca^{2+}$ concentrations to samples collected from piezometer KAPZ01 (Figures 10C to F). Magnesium and calcium concentrations range from 5.76 to 72.70 mg/L and from 12.3 to 132.8 mg/L, respectively.

Shallow groundwater samples show significant seasonal variation in anion concentrations down the tributary. Samples collected downstream from piezometer KAPZ01, which is approximately 13.1km down the tributary from piezometer KAPZ07, show low $Cl^{-}$, $Br^{-}$, $HCO_3^{-}$ and $SO_4^{2-}$ concentrations during the wet season of June 2016 (Figures 10G to J). Chloride concentrations for shallow groundwater samples range widely from 35mg/L to 910mg/L, with the highest chloride concentration surprisingly found downstream at piezometer KAPZ01 in July 2015. Shallow groundwater samples collected in June 2016 show low $HCO_3^{2-}$ concentrations to samples collected in June, July, September and November 2015.

Bicarbonate and sulphate concentrations for shallow groundwater samples range from 2.8 to 258mg/L and from 6 to 786mg/L, respectively (Table 4). Nitrate concentrations for shallow groundwater samples range from 0.97 to 43mg/L, with the highest $NO_3^-$ and $PO_4^{2-}$ concentrations determined for sample TS15VLR101 collected from piezometer KAPZ05 during the month of November 2015 (Table 4)

Shallow groundwater samples show a simultaneous increase of strontium and boron concentrations, with Se and W concentrations ranging from 0.29 to 3.00 µg/L and from 0.0012 to 0.0295 µg/L. High Al concentrations are found from samples with low pH value, and arsenic concentrations are between 0.21 and 31.40 µg/L (Table 5).

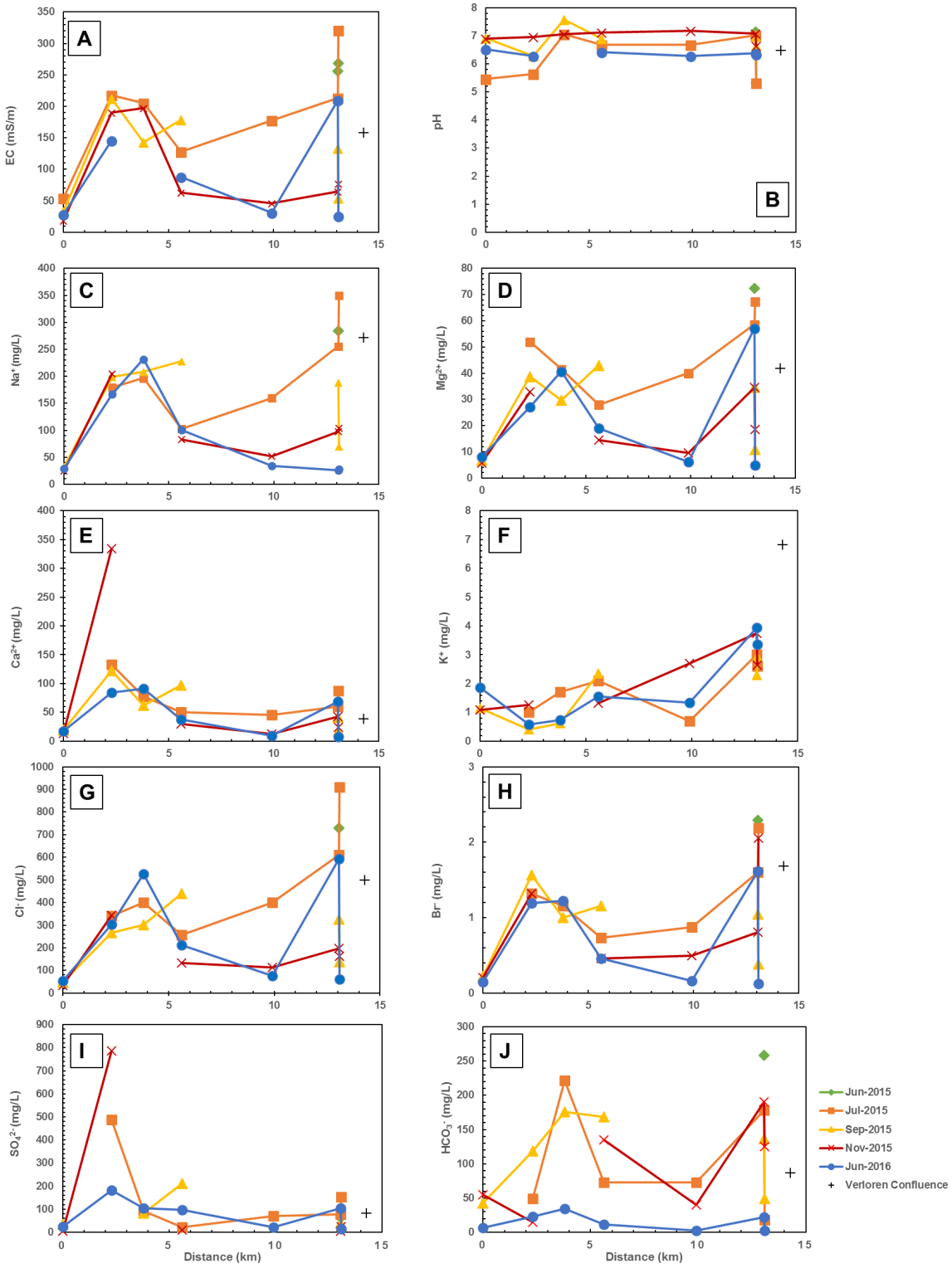


**Figure 10:** *Relationship between A) EC; B) pH; C) $Na^{+}$; D) $Mg^{2+}$; E) $Ca^{2+}$; F) $K^{+}$; G) $Cl^{-}$; H) $Br^{-}$; I) $SO_4^{2-}$; J) $HCO_3^{-}$ and the relative distance for shallow groundwater in the Krom Antonies tributary during 5 sampling months (2015-2016). Zero km distance representing upstream and 15km representing the lower reaches of the tributary close to the Verloren Confluence. Units for the ionic concentrations have been mentioned in each figure and units of the relative distances are in kilometres.*

### *4.1.3 Isotope Geochemistry*

Surface water samples have $\delta^{18}O$ ratios ranging from -3.82 to 0.21‰ and $\delta^{2}H$ ratios ranging from -16.3 to 0.7‰ (Table 3). Surface water samples plot scattered with respect to the GMWL and plot below and away from the LMWL (Figure 11A). Surface water samples indicating a wide range of d-excess values between 18.08 and -4.31. Shallow groundwater samples show depleted $\delta^{18}O$ ratios to surface water samples with enriched $\delta^{18}O$ ratios. Shallow groundwater samples in the Krom Antonies have $\delta^{18}O$ ratios ranging from -3.9 to -1.4‰ and $\delta^{2}H$ ratio ranging from -15.9 to -5.4‰, and plot between the LMWL and the GMWL. Shallow groundwater samples show a slope of 3.4, which is lower than that of the LMWL of 6.8 (Figure 11B) The d-excess value of shallow groundwater samples range from 17.61 to -5.80 with an average value of 8.12 which is lower than the global average of 10. Samples collected from piezometer KAPZ02 show a constant $^{87}Sr/^{86}Sr$ value of 0.71528 with increasing Sr concentration ranging from 300.8 µg/L for sample TS15VLR0109 to 412 µg/L for sample TS15VLR077. Samples TS15VLR0102 and TS15VLR088 collected upstream and downstream respectively, have tritium values of 1.5 TU.

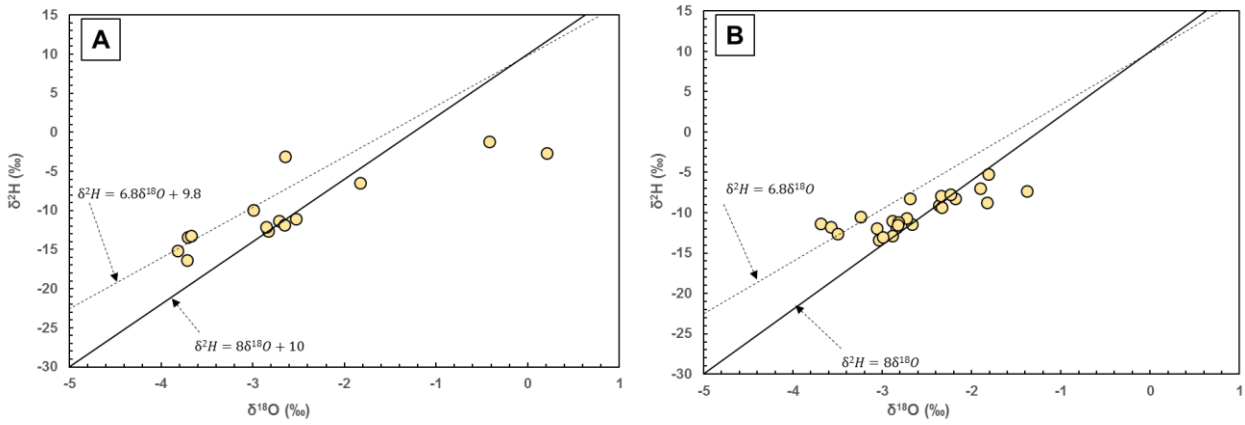


**Figure 11:** *Relationship between $\delta^{18}O$ and $\delta^{2}H$ for A) surface water samples; B) shallow groundwater samples in the Krom Antonies tributary. Dotted line: Local Meteoric Line (LMWL= ($\delta^{2}H$ = 6.8 $\delta^{18}O$ + 9.8), solid line: Global Meteoric Water Line (GMWL: $\delta^{2}H$ = 8 $\delta^{18}O$ + 10) (Craig, 1961).*

## 4.2 Bergvallei Tributary

### *4.2.1 Physiochemical Parameter*

Surface water and shallow groundwater in the Bergvallei depict a narrow range of pH values from 6.3 to 6.8 and between 6.5 and 6.6, respectively. Comparing the EC values of both surface water and shallow groundwater in the Bergvallei tributary, shallow groundwater has higher EC values to surface water. The highest EC values in both surface water and shallow groundwater were measured during the month of June 2016. Surface water EC values in the

Bergvallei range from 165.8 to 183.4mS/m, whilst shallow groundwater EC values in the same tributary range between 520 and1020mS/m (Tables 3 and 4).

### *4.2.2 Major and Trace Element Hydrochemistry*

#### *4.2.2.1 Surface water*

Surface water samples in the Bergvallei tributary show a narrow range of $Na^+$, $Mg^{2+}$ and $Ca^{2+}$ concentrations. Sodium concentrations for surface water samples range from 243.2mg/L 261.74mg/L, with sodium constituting an average of 75% of all cations (Table 3). Potassium concentrations increased from 5.9mg/L to 15.35mg/L during the months of June 2015 and June 2016, respectively. Anion concentrations of $Cl^-$, $Br^-$, $SO_4^{2-}$ and $HCO_3^-$ determined for surface water samples in the Bergvallei are 518 and 580mg/L, 1.70 and 1.83mg/L, 55 and 73.2mg/L and 5.8 and 43mg/L, respectively. Table 3 shows decreased $HCO_3^-$ concentration for surface water samples during the month of June 2016, whilst $Cl^-$, $SO_4^{2-}$ and $Br^-$ concentrations show slight seasonal variation. Surface water samples show high strontium concentrations ranging from 240.05 to 256.87µg/L, simultaneously increasing with boron concentrations between 124.09 and 126.21µg/L.

#### *4.2.2.2 Shallow Groundwater*

Sodium and calcium concentrations for shallow groundwater samples in the Bergvallei range from 1126.51 to 1291.67mg/L and from 102.7 to 124.1mg/L, respectively. Samples collected in June 2016 depict the highest cation concentrations in the Bergvallei, with an exception $K^+$ concentrations, which shows the lowest $K^+$ concentration during the month of June 2016. Potassium concentrations range from 11.73 to 19.71mg/l and magnesium concentrations range between 188.30 to 383.2mg/L (Table 4). Shallow groundwater samples show slight seasonal variation in cation concentrations for months June, July, September and November 2015.

Shallow groundwater samples collected in June, July, September and November 2015 have uniform $Cl^-$ and $SO_4^{2-}$ concentrations. Chloride and $SO_4^{2-}$ concentrations show a sharp increase in concentrations in June 2016, with $SO_4^{2-}$ concentration increase from 218mg/Lin September to 887mg/L in June 2016. (Figure 12E). Chloride also shows a gradual increase of concentrations of 2612.20mg/L in June 2015 to 2789.9mg/L in November 2015, thereafter an observable increase of $Cl^-$ concentration of 3768mg/L during the month of June 2016. Figure 12J shows a wide variation in $HCO_3^-$ concentrations that range from 57.80 to 229.20mg/L. The highest $HCO_3^-$ concentration is observed in June 2015 and lowest $HCO_3^-$ concentration measured from samples collected in June 2016. Alkalinity and bromide concentrations decreased for shallow groundwater samples collected in June 2016, while concentrations of

$Cl^-$ and $SO_4^{2-}$ in the same month increased. Shallow groundwater sample TS15VLR083 collected in July 2015 shows a nitrate concentration of 6mg/L and sample TS15VLR0103 collected in September 2015 has a phosphate concentration of 14mg/L (Table 4). Shallow groundwater samples show strontium concentrations between 886.12 and 986.33µg/L and narrow boron concentration ranging of between 312.37 to 383.33µg/L. Low concentrations of arsenic, aluminium, selenium and tungsten are found in both surface water and shallow groundwater samples.

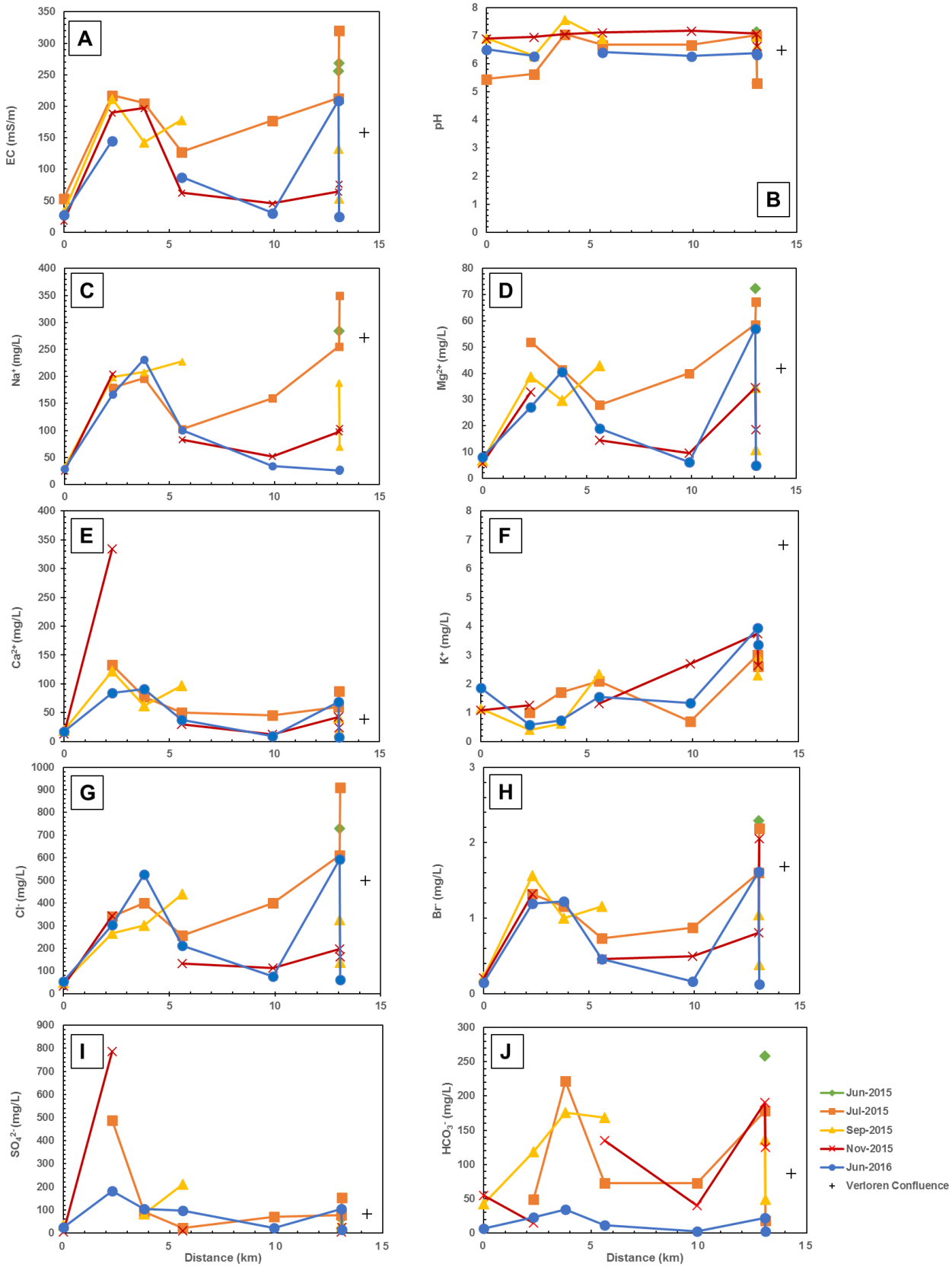


**Figure 12:** *Relationship of between A) EC; B) pH; C) $Na^{+}$; D) $Mg^{2+}$; E) $Ca^{2+}$; F) $K^{+}$ ; G) $Cl^{-}$; H) $Br^{-}$; I) $SO_4^{2-}$; J) $HCO_3^{-}$ and the relative distance for shallow groundwater in the Bergvallei tributary during 5 sampling months (2015-2016). Zero km distance representing upstream and 8km representing the lower reaches of the tributary close to the Verloren Confluence. Units for the ionic concentrations have been mentioned in each figure and units of the relative distances are in kilometres.*

### *4.2.3 Isotope Geochemistry*

Surface water and shallow groundwater samples in the Bergvallei plot below LMWL and the GMWL (Figures 13A and B). Surface water samples have a slope of 4.7 and shallow groundwater samples have a slope of -0.48, and hence both the slopes for surface water and shallow groundwater samples are lower than that of the GMWL of 8. Surface water $\delta^{18}O$ ratios range between -3.28 and -2.38‰ and $\delta^{2}H$ ratios range from -16.5 to -12.3‰. Shallow groundwater samples depict narrow compositions of $\delta^{18}O$ and $\delta^{2}H$ between -2.83 and -2.42‰ and -12.6 and -11.7‰, respectively. The deuterium excess for both surface water and shallow groundwater samples range from 9.7 to 6.8‰ and show decreased values to the global average of 10. Bergvallei shallow groundwater samples have an intermediate $^{87}Sr/^{86}Sr$ ratio of 0.71527, with Sr concentration between 888.1 and 952.9 µg/L. One tritium sample was obtained in the Bergvallei and has a tritium value of 0.5 TU.

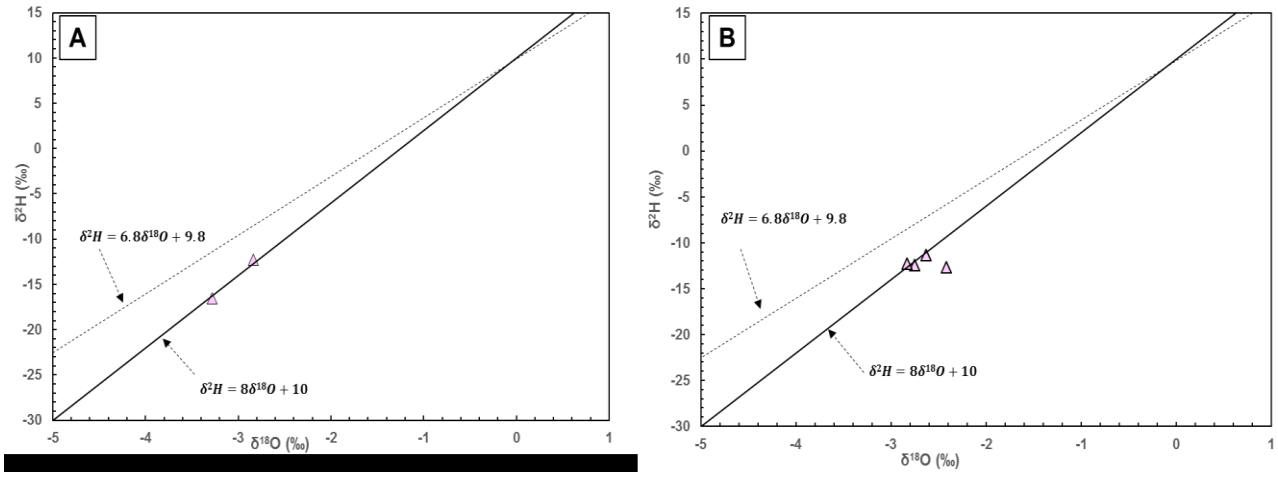


**Figure 13:** *Relationship between $\delta^{18}O$ and $\delta^{2}H$ for A) surface water samples; B) shallow groundwater samples in the Bergvallei tributary. Dotted line: Local Meteoric Line (LMWL= ($\delta^{2}H$ = 6.8 $\delta^{18}O$ + 9.8), solid line: Global Meteoric Water Line (GMWL: $\delta^{2}H$ = 8 $\delta^{18}O$ + 10) (Craig, 1961).*

## 4.3 Kruismans Tributary

### *4.3.1 Physiochemical Parameters*

The pH values for surface water in the Kruismans range from 6.2 to 7.6, the pH of surface water measured in June 2015, increased downstream towards the confluence. Surface water in the same tributary have EC values ranging from 414 to 749mS/m, the EC recorded in June 2015 fluctuates down the tributary with the highest measured EC value in the same month downstream towards the confluence (Table 3).

The pH for shallow groundwater range between 5.3 and 7.6 The highest recorded pH values in shallow groundwater are found upstream at sampling point KRPZ01 which is at the

confluence of the Kruismans and the Bergvallei, during the months of July and September 2015 (Figure 14B). The EC for shallow groundwater fluctuates down the tributary, and range from 102.5mS/m during the wet season of June 2016 to 1988mS/m during the dry season of November 2015. Piezometer KRPZ03 located at 950m downstream from piezometer KRPZ02, depicts the highest EC value for shallow groundwater in June 2016. Piezometers KAPZ04 and KAPZ05 are the furthest down the tributary and hence are closest to the confluence. These two piezometers are more or less the same distance down the tributary (~5.9km from KRPZ02) but are 70m apart on a transect across the tributary. Shallow groundwater samples from these two piezometers show a wide variation in EC values, given they are at the same distance down the tributary (Figure 14A). Shallow groundwater samples from piezometer KAPZ04, which has a depth of 1.6m, had EC values between 102.5 to 953mS/m, whilst shallow groundwater samples from piezometer KAPZ05, which has a depth of 1.66m, had EC values ranging from 551 to 1988mS/m.

### *4.3.2 Major and Trace Element Hydrochemistry*

#### *4.3.2.1 Surface water*

Surface water samples in the Kruismans show slightly increased $Na^+$, $Mg^{2+}$ and $Ca^{2+}$ concentrations at 0.26km, which is the second highest sampled point upstream of the tributary just after the Kruismans and Bergvallei confluence. Thereafter, a significant decrease is observed in $Mg^{2+}$, $Na^+$, $Ca^{2+}$ and $K^+$ concentrations at sampled point 1.24km (near piezometer KRPZ03) down the tributary during the month of June 2015 (Table 3). Surface water samples collected in June 2016 present $Na^+$, $Mg^{2+}$, $Ca^{2+}$ and $K^+$ concentrations, with sodium concentrations ranging from 766.83 to 1295.85mg/L and magnesium concentrations between 185.5 and 248.30mg/L. Surface water samples collected during the month of June 2015 present decreased cation concentrations downstream at the lowest sampled point in the tributary toward the Verloren confluence.

Chloride concentrations for surface water samples in the Kruismans range from 1665 to 2717.6mg/L, surface water of the Kruismans present the highest $Cl^-$ concentrations compared to other tributaries. For surface water samples collected at the highest sampled points upstream the tributary, $Br^-$ and $HCO_3^-$ show variation in concentrations during the months of June 2015 and June 2016. Bromide and alkalinity concentrations are 1.70 and 8.74mg/L and 24.8 and 671.2mg/L, respectively and sulphate concentrations range from 227 to 301mg/L. Nitrate concentrations are between 8 and 10mg/L for samples TS15VLR014 and TS15VLR046, respectively. These concentrations are found at highest sampled points upstream in the tributary (Table 3). Surface water samples show high strontium concentrations between 131.42 and 2064.77µg/L compared to other tributaries. Boron concentrations for

surface water samples in the Kruismans increase proportionally to increasing Sr. Aluminium concentrations vary between from 1.38 and 40.18µg/L for surface water samples (Table 5).

*4.3.2.2 Shallow groundwater*

Piezometer KRPZ02, which is the highest point sampled upstream the Kruismans tributary shows uniform concentrations of $Na^+$, $Mg^{2+}$ and $Ca^{2+}$ for shallow groundwater samples collected during the months of June, July, September, November 2015 and June 2016. Thereafter, a surprisingly slight decrease in $Na^+$, $Mg^{2+}$ and $Ca^{2+}$ concentrations 0.26km from KRPZ02, which is a point sampled just after the Kruismans and Bergvallei confluence (Figure 14C to E). Magnesium and calcium, show a wide range of concentrations from 88.4 to 662.5mg/L and between 69.75 and 472.12mg/L, respectively (Table 4). Sodium constitute an average of 75% of all cations and has concentrations from 268.6 to 3511.32mg/L (Table 4). Potassium concentrations range from 4.20 to 23.37mg/L with lowest concentration from samples collect in June 2015 at piezometer KRPZ04 which is 950m away from piezometer KRPZ02 down the tributary (Figure 14F). Shallow groundwater samples in the Kruismans show the highest concentrations of $Na^+$, $Mg^{2+,}$ $Ca^{2+}$ and $K^+$ found downstream the tributary towards the Verloren confluence during the dry season of November 2015.

Piezometer KRPZ03 located at 950m downstream from piezometer KRPZ02, depicts the highest $Cl^-$, $Br^-$ and $SO_4^{2-}$ concentrations for shallow groundwater samples in June 2016, with the exception of $HCO_3^-$, which shows low $HCO_3^-$ concentrations in the same month (Figure 14G to J). Piezometers KAPZ04 and KAPZ05 are the furthest down the tributary and hence are closest to the confluence. Shallow groundwater samples from these two piezometers show a wide variation in anion concentrations, given they are at the same distance down the tributary. Chloride concentrations for shallow groundwater samples in the Kruismans range from 949 to 9248mg/L, with the highest concentrations observed downstream in the tributary at piezometer KRPZ05 in November 2015. Sulphate and alkalinity concentrations fluctuate down the tributary, with concentrations increased downstream at KRPZ04 and unusually decreased at piezometer KRPZ05 during July 2015 (Figure 14I and J). Alkalinity and sulphate show a wide range of concentrations from 34.60 to 543mg/L and from 136.1 to 692mg/L, respectively. Nitrate concentrations range from 5 to 6 mg/L, with 6mg/L recorded down the tributary near the Verloren confluence (Table 4).

Shallow groundwater samples in the Kruismans have high strontium concentrations ranging from 700.56 to 5443.42µg/L, with the highest value found at piezometer KRPZ05. For shallow groundwater samples, boron concentrations decrease with increasing Sr concentrations and also show higher concentrations to W, Se, As and Al. Aluminium concentrations range from

0.6 to 8.66µg/L for shallow groundwater samples. The Kruismans tributary reflects higher trace elemental concentrations compared to other tributaries

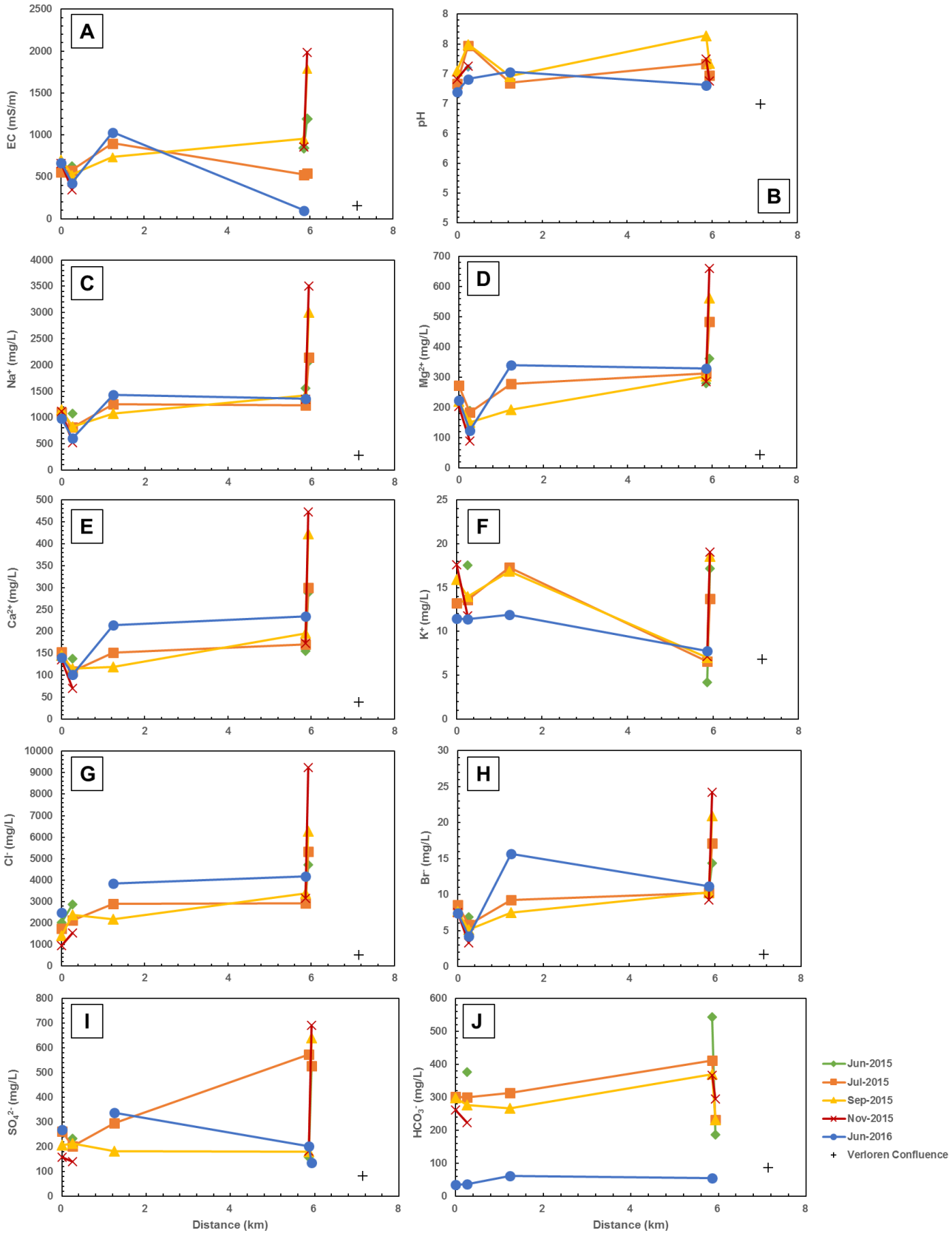


**Figure 14:** *Relationship between A) EC; B) pH; C) $Na^+$; D) $Mg^{2+}$; E) $Ca^{2+}$; F) $K^+$ ; G) $Cl^-$; H) $Br^-$; I) $SO_4^{2-}$; J) $HCO_3^-$ and the relative distance for shallow groundwater in the Kruismans tributary during 5 sampling months (2015-2016). Zero km distance representing upstream and 8km representing the lower reaches of the tributary close to the Verloren Confluence. Units for the ionic concentrations have been mentioned in each figure and units of the relative distances are in kilometres.*

### *4.3.3 Isotope Geochemistry*

Surface water samples cluster below the GMWL and show a linear inclination relationship to the GMWL with equation (not shown on the figure) $\delta^2H$ =6.17 $\delta^{18}O$ +3.39, with sample TS15VLR054 as an outlier showing depleted ratios of $\delta^{18}O$ (Figure 15A). The $\delta^2H$ and $\delta^{18}O$ stable isotope signature for surface water samples range from -19.5 to-12.0‰ and -3.58 to -2.49‰, respectively. Deuterium excess from surface water samples range from 6.6 to 10.2‰ to that of the global average of 10. Shallow groundwater $\delta^{18}O$ ratios range from -3.79 to -0.14‰ and $\delta^2H$ ratios from -16.6 to -0.3‰, samples plot below the GMWL and show a trajectory ($\delta^2H$ = 3.9 $\delta^{18}O$ -1.13, $R^2$=0.90) away from the LMWL and the GMWL (Figure 15B). Shallow groundwater samples show a wide range of d-excess samples from -0.24 to 13.6‰, with one outlier showing a value of 23.8‰. An apparent correlation is observed reflected by high $^{87}Sr/^{86}Sr$ ratios with high Sr concentration. The $^{87}Sr/^{86}Sr$ ratio range from 0.71571 to 0.7197 with the highest signatures observed for samples TS15VLR081 and TS16VLR0121 collected from piezometer KRPZ01, which is located downstream the tributary. Samples TS15VLR093 and TS16VLR0104 are 5.22 km apart and have tritium values of 1.3 and 0.9 TU, respectively.

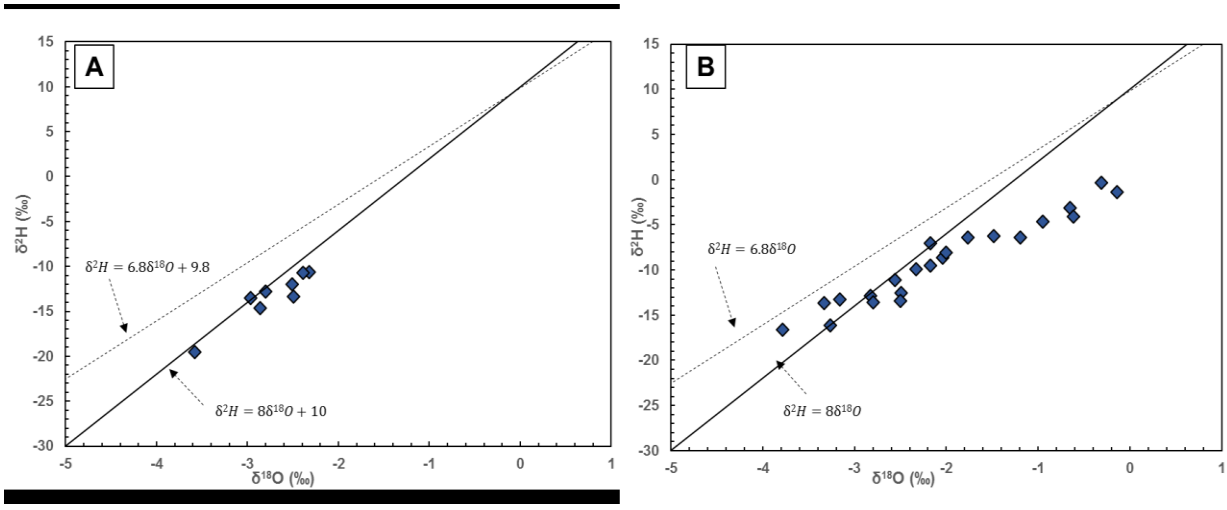


**Figure 15:** *Relationship between $\delta^{18}O$ and $\delta^2H$ for A) surface water samples; B) shallow groundwater samples in the Kruismans tributary. Dotted line: Local Meteoric Line (LMWL= ($\delta^2H$ = 6.8 $\delta^{18}O$ + 9.8), solid line: Global Meteoric Water Line (GMWL: $\delta^2H$ = 8 $\delta^{18}O$ + 10) (Craig, 1961).*

## 4.4 Hol Tributary

### *4.4.1 Physiochemical Parameters*

The pH for surface water in the Hol tributary range from 5.67 to 7.77 with an average value of 7.08. Surface water collected during June 2015, show consistent pH values down the tributary towards to the confluence. Electrical conductivity for surface water in the same tributary range

from 57 to 770mS/m. Surface water sample collected at 2.3km down the highest point sampled upstream in the tributary, shows the highest EC value recorded in June 2016 (Table 3).

The pH for shallow groundwater fluctuates down the Hol tributary and range from 3.8 to 7.69 with an average value of 6.7 (Table 4). Electrical conductivity for shallow groundwater range between 189.4 and 1499mS/m and are variable down the tributary for the months of June, July and November 2015 (Figure 16A). Piezometer HOLPZ06, which is the highest point sampled upstream along the tributary, has the highest EC value of 1893mS/m for shallow groundwater measured in June 2016. Electrical conductivity recorded in the winter season of June 2016 show deceased EC values downstream towards the Verloren confluence. Piezometer HOLPZ01 located at 10.59km, which is the lowest point sampled downstream the tributary, show high EC values recorded in June, September and November 2015 and low EC values recorded in July 2015 and June 2016 (Figure 16A).

### *4.4.2 Major and Trace Element Hydrochemistry*

#### *4.4.2.1 Surface water*

Surface water samples in the Hol collected during the month of June 2015 show increased $Na^+$, $Mg^{2+}$ $Ca^{2+}$ and $K^+$ concentrations down the tributary closer to the Verloren confluence. Surface water samples collected in June 2015 at the highest point sampled upstream the tributary, show increased $Na^+$, $Mg^{2+}$ and $Ca^{2+}$ concentrations, while $K^+$ in the same month and at the same sampling point show decreased concentrations (Table 3). Sodium shows a wide range of concentrations from 70.10 to 1000.5mg/L, and constitutes an average of 74% of all total cations. Calcium concentrations range from 26.7 to 186.7mg/L, whilst, magnesium and potassium have average concentrations of 103.4mg/L and 7.7mg/l, respectively. Cations for surface water samples collected during the wet season of June 2016 show a significant increase with the highest concentrations at downstream the tributary.

Chloride concentrations for surface water samples in the Hol range from 107 to 2062mg/L, with the highest $Cl^-$ concentration of 2703mg/L found at 2.3km upstream the tributary in June 2016. Samples collected in June 2016 show an increase in $Cl^-$ and $SO_4^{2-}$ concentrations, whilst, $Br^-$ and $HCO_3^-$ concentrations decreased down the tributary near the Verloren confluence. Alkalinity concentrations are high during the dry season of November 2015 and low during the wet season of June 2016, $HCO_3^-$ for surface water samples present a wide range of concentrations from 4 to 394mg/L. Sample TS16VLR0132, has the highest sulphate concentration of 391.77mg/L and was collected during the wet season of June 2016. Sulphate concentrations range from 19 to 391.7mg/L and $Br^-$ concentrations range between 0.39 and 7.49mg/L. The Hol tributary has the highest nitrate and phosphate concentrations compared to other tributaries. Sample TS15VLR099 located in cultivated wheat land upstream in the

tributary records $NO_3^-$ of 18mg/L and $PO_4^{2-}$ of 17mg/L (Table 3). Surface water samples have Sr concentrations ranging from 150.91 to1293.94µg/L with the highest concentration from sample TS15VLR0108 and B concentrations between 38.33 and 256.26µg/L. Arsenic has an average concentration of 1.01 µg/L and W has the lowest average concentration of 0.004µg/L (Table 5).

*4.4.2.2 Shallow groundwater*

Piezometer HOLPZ06 is the highest point sampled upstream in the Hol tributary. Shallow groundwater samples show a wide range of $Na^+$ and $Mg^{2+}$ concentrations ranging from 449.8 to 2385mg/L and from 37.13 to 414.4mg/L, respectively. The highest concentration of $Na^+$ and $Mg^{2+}$ observed at HOLPZ06 is during the month of June 2016. Piezometer HOLPZ04 is 6.40km away from HOLPZ06 down the tributary. Figure 16C, shows that $Na^+$ concentrations decreased down the tributary to piezometer HOLPZ04, then significantly increased down the tributary towards the Verloren confluence for samples collected in July, September, and November 2015. Calcium concentrations show a different trend to $Na^+$ concentrations for shallow groundwater samples collected from piezometer HOLPZ04. The $Ca^{2+}$ concentrations increased significantly and the highest $Ca^{2+}$ concentration of 2125.86mg/L were observed during the month of September 2015 (Figure 16E). Shallow groundwater samples collected in September 2015 from piezometer HOLPZ04 present a sharp increase in $Mg^{2+}$, $Ca^{2+}$ and K+ concentrations (Figure 16F). Magnesium and potassium concentrations show seasonal variation, with increased $K^+$ concentrations at the lowest point sampled down the tributary. Calcium and potassium concentrations for shallow groundwater samples in the Hol range from 41.7 to477.5mg/L and from 0.79 to 18.04mg/L, respectively.

Chloride concentrations for shallow groundwater samples in the Hol range between 1053 and 20437mg/L, and gradually increased down the tributary closer to the Verloren confluence. An exception of one sample collected during the dry season of November 2015, show higher $Cl^-$ and $SO_4^{2-}$ concentrations of 20437mg/L and 2616mg/L, respectively. Bromide concentrations for shallow groundwater samples in the same tributary range between 1.49 and 16.84mg/L, with a sharp increase at piezometer HOLPZ04 during September 2015 (Figure 16F). Alkalinity concentrations fluctuate down the tributary, with highest concentration of 1018.2mg/L in September 2015 (Figure 16J). The Hol tributary reflects the highest $NO_3^-$ and $PO_4^{2-}$ concentrations compared to the other three tributaries. Phosphate concentrations of 143mg/L and 106mg/L are found for sample TS15VLR058 and sample TS15VLR0116, respectively. Nitrate concentration of 75mg/L was from sample TS15VLR059 collected from piezometer HOLPZ06 (Table 4). Shallow groundwater reflects a wide variation in the Sr concentrations ranging from 660.7 to 4094.1µg/L, the Sr concentrations increase with boron concentrations which are between 47.9µg/L and 1848.1µg/L. Tungsten has the lowest and least variable

concentration with its highest value being 0.0072µg/L. Aluminium, selenium and arsenic concentrations range from 0.39 to 4.00µg/L (Table 5).

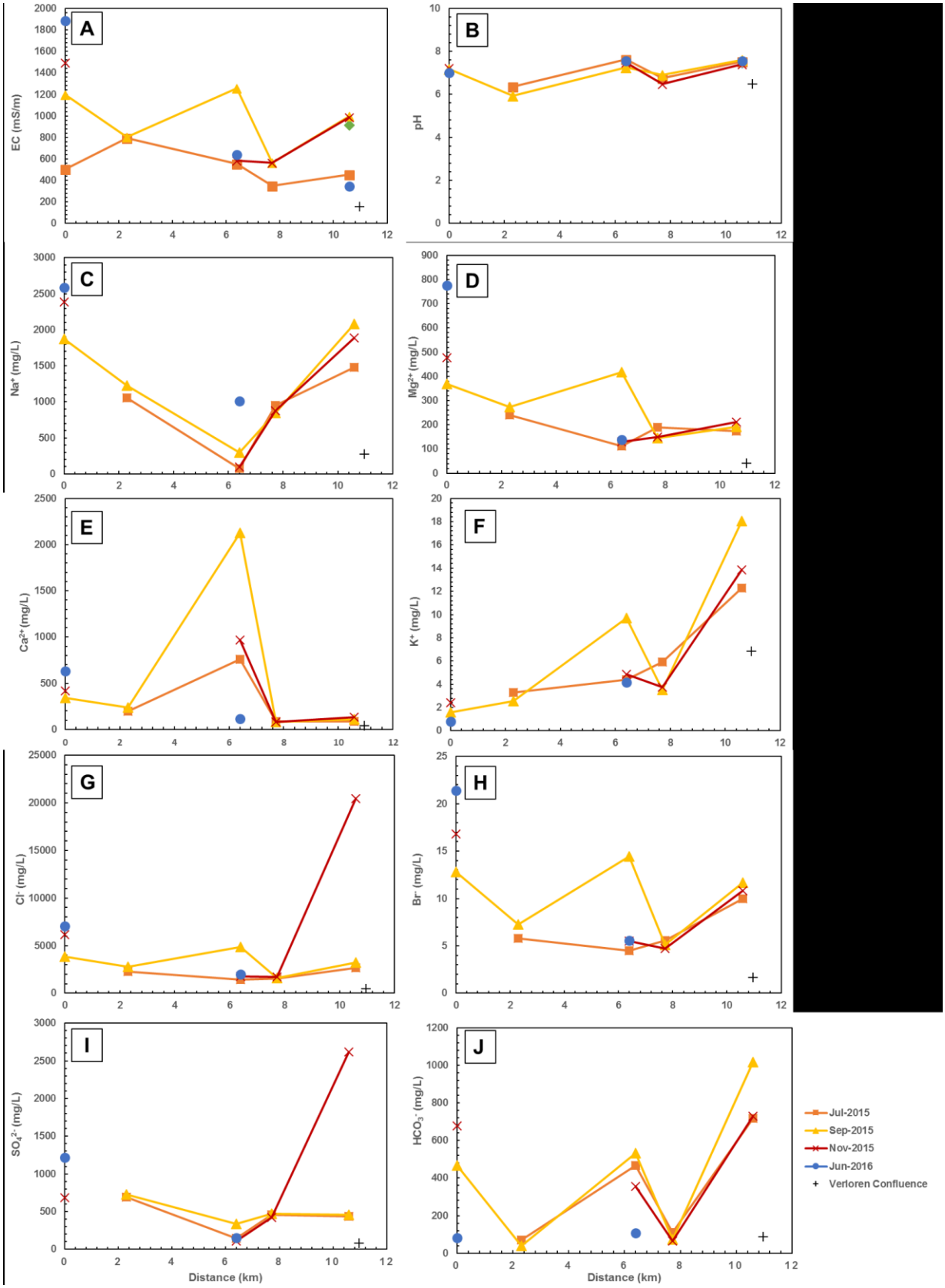


**Figure 16:** *Relationship between A) EC; B) pH; C) $Na^{+}$; D) $Mg^{2+}$; E) $Ca^{2+}$; F) $K^{+}$ ; G) $Cl^{-}$; H) $Br^{-}$; I) $SO_4^{2-}$; J) $HCO_3^{-}$ and the relative distance for shallow groundwater in the Hol tributary, during 4 sampling months (2015-2016). Zero km distance representing upstream and 12km representing the lower reaches of the tributary close to the Verloren Confluence. Units for the ionic concentrations have been mentioned in each figure and units of the relative distances are in kilometres.*

### *4.4.3 Isotope Geochemistry*

Surface water samples in the Hol plot along and above the GMWL (Figure 17A). The isotopic composition of surface water for $\delta^{18}O$ range between -3.68 and -0.51‰ and for $\delta^{2}H$ ratio range between -16.7 and -8.1‰, with an exception of sample TS15VLR0108 ($\delta^{2}H$ = 7.8‰ and $\delta^{18}O$ = 2.85‰) showing heavier isotopic signature (Table 3). Surface water samples show an average d-excess of 7.2 that is lower to the global average, with one outlier showing d-excess of 14.9. Shallow groundwater samples plot above the GMWL, samples that plot below the GMWL diverge from the GMWL, showing a linear relationship to the GMWL with equation (not shown on the figure): $\delta^{2}H = 3.969\delta^{18}O - 0.993$ (Figure 17B). Sample TS15VLR0112 plots as an outlier with $\delta^{2}H$ and $\delta^{18}O$ ratios ranging from 2.0‰ and 0.5‰, respectively. Shallow groundwater samples show deuterium excess with an average of 9.9‰, closer to the global average of 10‰. The two shallow groundwater samples in the Hol have a mean $^{87}Sr/^{86}Sr$ value of 0.71461, with Sr concentrations ranging from 978.90 to 1642.2 µg/L. Tritium concentrations range from 1.0 to 1.3 TU (Table 4).

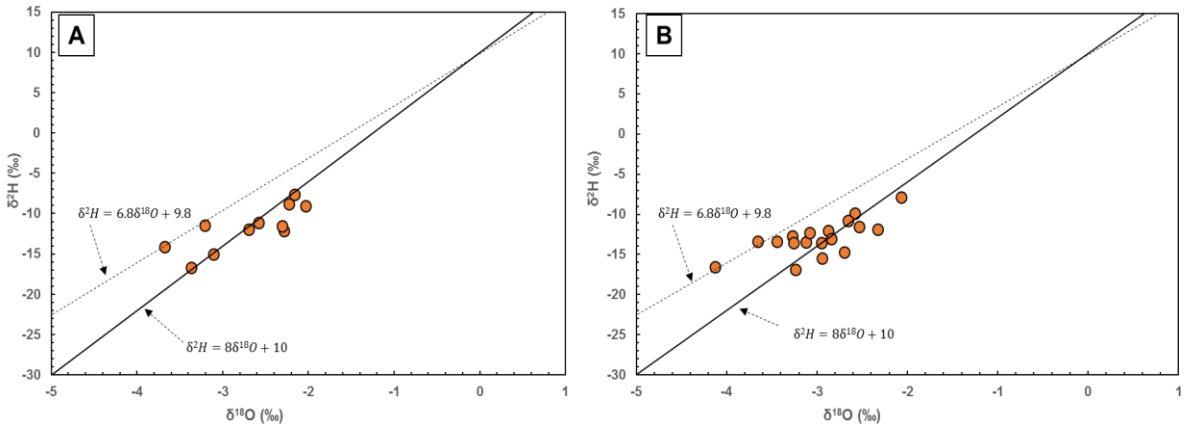


**Figure 17:** *Relationship between $\delta^{18}O$ and $\delta^{2}H$ for A) surface water samples; B) shallow groundwater samples in the Hol tributary. Dotted line: Local Meteoric Line (LMWL= ($\delta^{2}H$ = 6.8 $\delta^{18}O$ + 9.8), solid line: Global Meteoric Water Line (GMWL: $\delta^{2}H$ = 8 $\delta^{18}O$ + 10) (Craig, 1961).*

## 4.5 Verloren Confluence

### *4.5.1 Physiochemical Parameters*

Surface water in the Verloren confluence exhibit pH values ranging from 5.64 to 7.04. The pH values for surface water measured during month of June 2015, show an increase in pH at the Verloren confluence (Table 3). The EC for surface water at the same sampled point range from 22.5 to 414mS/m. Electrical conductivity values for surface water measured during the month of June 2015, show an increase in EC at the Verloren confluence. The lowest EC value measured for surface water was during the winter season of June 2016 (Table 3).

Shallow groundwater in the Verloren confluence have pH values ranging from 5.4 to 7.5 with an average value of 6.5. Given that the Verloren confluence is represented by piezometer VLPZ01, the pH for shallow groundwater samples measured in June, July, September and November 2015 and June 2016 decreased from piezometer VLPZ02 down to the Verloren confluence (VLPZ01). The highest pH value for shallow groundwater was measured during the dry season of November 2015, from piezometer VLPZ01 (Figure 18B). Piezometer VLPZ02, which is the highest sampled point upstream the Verloren river before the Verloren confluence show consistent EC values for shallow groundwater ranging from 235 to 275mS/m. Electrical conductivity for shallow groundwater samples collected at piezometer VLPZ01 range between 85.4 and 179.5mS/m.

### *4.5.2 Major and Trace Element Hydrochemistry*

#### *4.5.2.1 Surface water*

The lowest $Na^+$, $Ca^{2+}$, $Mg^{2+}$ and $K^+$ concentrations for surface water samples from the Verloren were recorded in the month of June 2016. Surface water samples collected in June 2015 show increased Na+, $Ca^{2+}$, $Mg^{2+}$ an $K^+$ concentrations at the Verloren confluence (Table 3). Sodium concentrations for surface water samples range from 24.05 to 1048mg/L and constitutes on average 69.9% of all cations. Calcium and magnesium concentrations range from 3.40 to 107mg/L and from 4.21 to 67.69mg/L, respectively. Potassium concentrations have an average concentration of 4.85mg/L.

Lowest $Cl^-$, $Br^-$and $HCO_3^-$ concentrations for surface water samples in the Verloren confluence are recorded for the month of June 2016, with an exception of $SO_4^{2-}$, which show highest $SO_4^{2-}$ concentration for month June 2016. Surface water samples collected in June 2015 show increased $Cl^-$, $Br^-$and $HCO_3^-$ at the Verloren confluence (Table 3). Sulphate concentrations for surface water samples collected in June 2015 show a decreased trend in concentrations in the Verloren river down to the Verloren confluence. Chloride and bromide concentrations range from 55 to 1620mg/L and from 0.10 to 2.27mg/L, respectively. Sulphate and alkalinity show a wide range of concentrations between 3.34 and 162mg/L and from 2.2 to 137.2mg/L, respectively. Phosphate concentration of 22mg/L and nitrate concentration of 8mg/L were found in sample TS15VLR020.

#### *4.5.2.2 Shallow groundwater*

Sodium for shallow groundwater samples at the Verloren confluence accounts on average 77% of all cations and ranges from 124.6 to 622.87mg/L. Magnesium shows a wide range of concentrations from 13.34 to 123.18mg/L. Calcium concentrations range from 11.92 to 128.76mg/L. Shallow groundwater samples collected in June 2015 show decreased $Na^+$, $Ca^{2+}$

and $Mg^{2+}$ concentrations for samples collected from piezometer VLPZ01 (Figure 18C to F). Samples collected from piezometer VLPZ01 show high Na+, $Ca^{2+}$, $Mg^{2+}$ and $K^{+}$ concentrations during the dry season of November 2015 and low concentrations during the wet season of June 2016. Potassium concentrations for shallow groundwater samples range from 2.34 to 14.40mg/L, and show increased $K^{+}$ concentrations for samples collected from piezometer VLPZ01.

Shallow groundwater samples in the Verloren river (VLPZ02), record decreased concentrations of chloride, bromide, sulphate and alkalinity with an exception of one sample collected in June 2016 which show increased $Cl^{-}$ concentration at VLPZ02 (Figure 18G to J). Chloride concentrations range from 239 to 1057.37mg/L, and the highest concentration of 1753mg/L recorded in June 2016. Bromide concentrations range from 0.72 to 3.97mg/L and alkalinity has concentrations between 13 and 316.2mg/L. Sulphate for shallow groundwater has an average concentration of 90.49mg/L (Table 4). Phosphate concentrations increase with nitrate concentrations for samples collected from piezometer VLPZ01, with the highest concentrations of nitrate and phosphate being 15mg/L and 74mg/L, respectively. Shallow groundwater samples collected from piezometer VLPZ01 show increased phosphate concentrations from June 2015 to November 2015 (Table 4).

Shallow groundwater samples in the Verloren confluence show a simultaneous increase of Sr and B concentrations, with Se and W concentrations ranging from 0.35 to 6.34µg/L and from 0.002 to 0.092µg/L, respectively. Aluminium concentrations range from 03.51 to 28.69µg/L and from 7.67 to 78.02µg/L for shallow groundwater and surface water, respectively. Shallow groundwater samples have a higher and wide range of Sr, W, B, Se and As concentrations compared to surface water samples in the Verloren confluence.

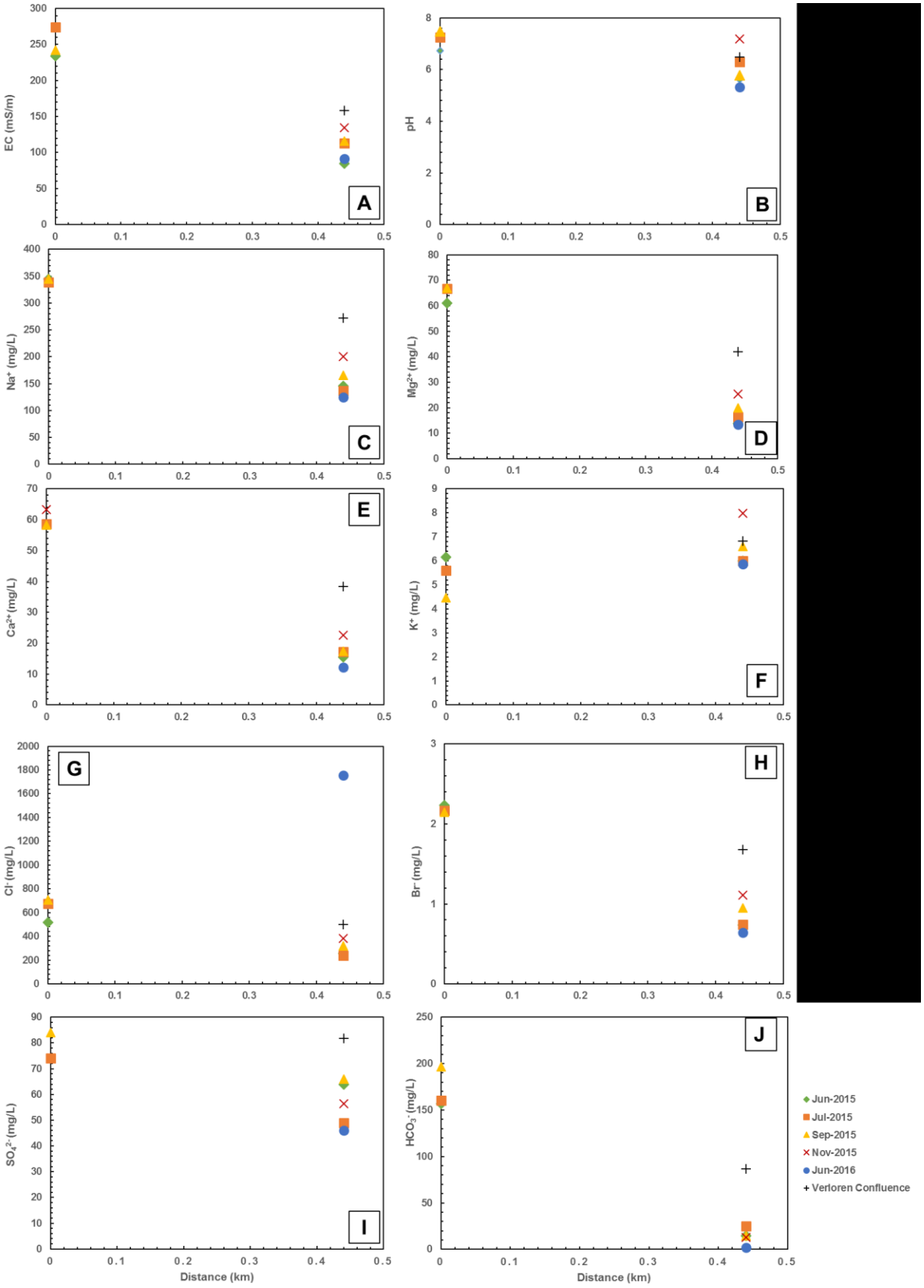


**Figure 18:** *Relationship between A) EC; B) pH; C) $Na^{+}$; D) $Mg^{2+}$; E) $Ca^{2+}$; F) $K^{+}$ ; G) $Cl^{-}$; H) $Br^{-}$; I) $SO_4^{2-}$; J) $HCO_3^{-}$ and the relative distance for shallow groundwater in the Verloren confluence, during 5 sampling months (2015-2016). Zero km distance representing upstream and 0.5km representing lower reaches. Units for the ionic concentrations have been mentioned in each figure and units of the relative distances are in kilometres.*

### *4.5.3 Isotope Geochemistry*

There are two sets of surface water samples, the first set plots above the GMWL showing more depleted ratio of $\delta^{18}O$ and the second set plots below the GMWL showing enrichment in $\delta^{18}O$. The first set of samples was collected near piezometer VLPZ02 and the second set near piezometer VLPZ01 (Figure 19A). Surface water samples $\delta^{18}O$ values range from -3.79 to -1.97‰ and $\delta^{2}H$ ratios between -16.2 and -7.9‰. The d-excess ranges from 6.7 to 15.5. Shallow groundwater samples plot below the GMWL and show a linear trajectory away from the GMWL. Verloren shallow groundwater samples collected from piezometer VLPZ01 (Verloren confluence) plot below the GMWL (Figure 19B), samples TS15VLR022, TS15VLR024, TS15VLR076, TS16VLR0126 have more depleted $^{18}O$ values to samples TS15VLR08, TS15VLR056, TS15VLR074, TS15VLR086 collected from piezometer VLPZ02 and plot above GMWL (Table 4). Stable isotopes of $\delta^{18}O$ and $\delta^{2}H$ range from -3.83 to -1.03‰ and from -20.6 to -1.6‰, respectively. The deuterium excess for shallow groundwater samples range from 16.9 to -0.6, showing a wide deviation from the global average of 10‰. The $^{87}Sr/^{86}Sr$ ratio for shallow ground water samples range from 0.71418 to 0.71556 and increases with increasing strontium concentrations which has values between 125.4 and 514.7µg/L. Tritium range from 0.5 to 1.5 TU, with sample TS15VLR086 reflecting tritium concentration of 1.3 TU.

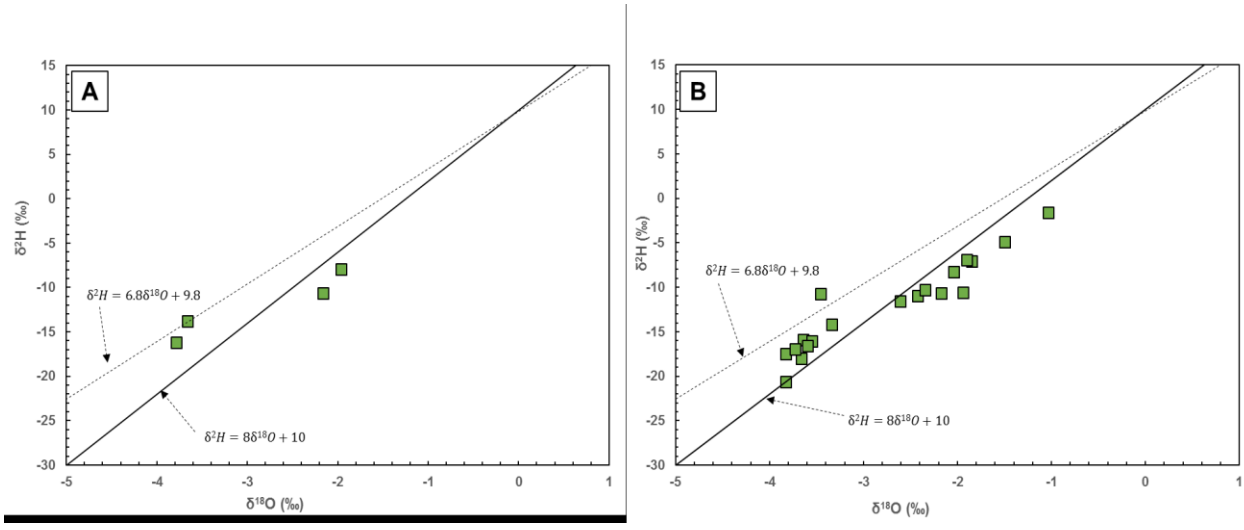


**Figure 19:** *Relationship between $\delta^{18}O$ and $\delta^{2}H$ for A) surface water samples; B) shallow groundwater samples in the Verloren river and confluence. Dotted line: Local Meteoric Line (LMWL= ($\delta^{2}H$ = 6.8 $\delta^{18}O$ + 9.8), solid line: Global Meteoric Water Line (GMWL: $\delta$ $^{2}H$ = 8 $\delta^{18}O$ + 10) (Craig, 1961).*

## 4.6 Discharge

Figure 20 shows discharge ($m^3/s$) in the Hol, Kruismans, Krom Antonies and Bergvallei during the years of 2012 to 2016. The discharge for each tributary includes baseflow, surface runoff and subsurface runoff from soil and weathering zone as interflow, in each tributary. The discharge was simulated using the J2000 rainfall/runoff model. The JAMS/ J2000 model was developed by Krause (2001) at Hamburg, Germany. The J2000 model is a distributive hydrological model that can be used to stimulate various components of the hydrological cycle by calibration of parameters using streamflow, climate and rainfall data (Krause, 2001). Streamflow was simulated by calibration with a gauging station G3H3001, using data from 1989 to 1991 for model calibration to optimise parameters and data from 1992 to 1998 for model initialisation. Data from 1999 to 2006 was used for validation. Discharge is runoff, baseflow and interflow after subtraction of evapotranspiration (ET) (Fleischer et al., unpublished data).

The Bergvallei has average discharge values ranging from 0.0102 to 10.162$m^3/s$, and is the highest discharge of all the tributaries. The Kruismans has an average discharge that ranges from 0.01 to 6.15$m^3/s$, with the highest discharge during the wet season of 2016. The Krom Antonies and the Hol tributaries have average discharge of 0.39 and 0.08$m^3/s$, respectively (Figure 20). The discharge of all four tributaries coincide with the rainfall amounts shown in Figure 21A and 21B, and both the discharge and the rainfall follow the same trend. In 2010 and 2011 (Figure 20A) a decrease in rainfall coincided with a decrease in discharge in the same years, and again in 2015 there was a decrease in the amount of rainfall, which also led a decrease in discharge. This shows that the discharge in each tributary is dependent on rainfall events.

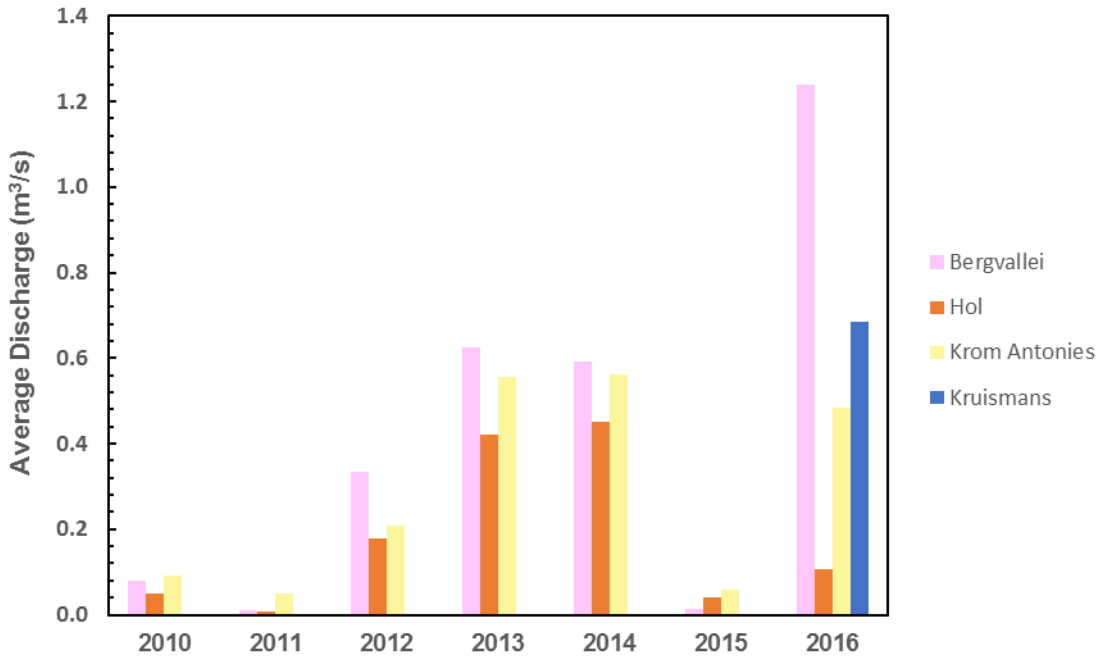


**Figure 20:** *Calculated average discharge from 2010 to 2016 for each tributary (Fleischer et al. unpublished data).*

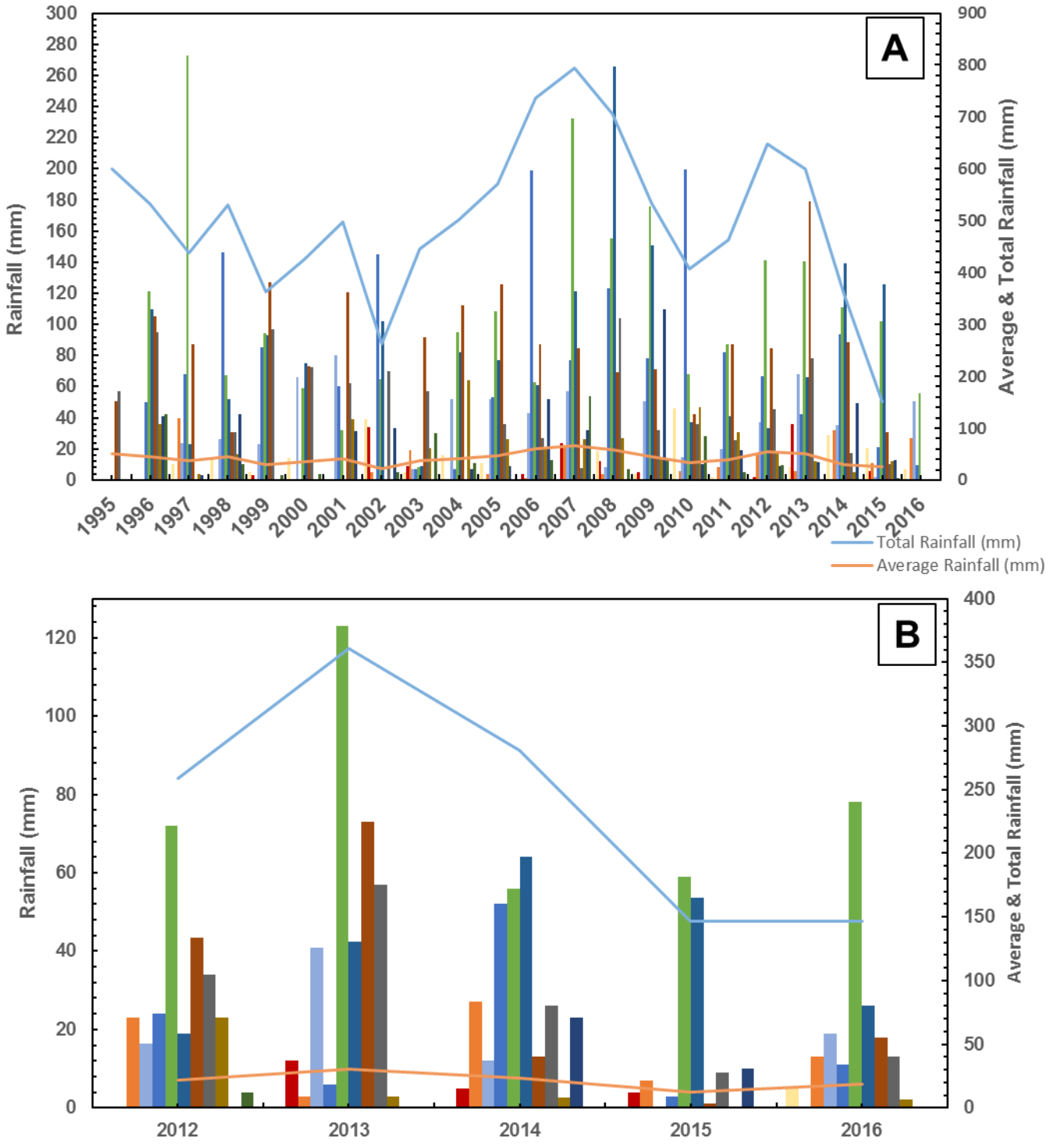


**Figure 21:** *Rainfall data records from A) Namaquasfontein farm near the Krom Antonies tributary; B) Middelpos farm near the Kruismans tributary (Eilers, 2018). The different colours show rainfall events from January to December.*

# 5. DISCUSSION

In this section, water quality of surface water and shallow groundwater in the study area is evaluated using physiochemical parameters such as EC and pH and comparing concentrations of major ions and trace elements with values acceptable as water quality guidelines values. Characterisation of surface water and shallow groundwater in each tributary is the presented based on major ion chemistry in a form of Stiff Diagrams and Piper Diagrams. Thereafter, potential explanations for the water chemistry based on collective geochemical data (physiochemical parameters, major ions and isotopes) and graphic representations are used to effectively discriminate among multiple sources of salinity and processes salinisation throughout the catchment. Finally, discharge data, TDS and strontium isotopes are used to identify the relative contribution of salt load from each tributary to the Verloren confluence and the implications of this for the Verlorenvlei estuarine lake are discussed.

## 5.1 Water Characterisation

### *5.1.1 Water Quality*

Understanding of the water quality is important before its supply for domestic, agricultural or industrial purposes (Kumar, et al., 2014). In order to ascertain the potability of surface water and shallow groundwater quality, parameters such as EC and pH recorded during each sampling trip have been compared with the standard guidelines values recommended by the World Health Organisation (WHO, 2011) and those provided and accepted by the South African Water Quality guidelines (SAWQ, 1999). According to the drinking water standards recommended by WHO and SAWQ, the acceptable pH values for surface water and groundwater should range between 6.5 and 8.5. The average pH value for surface water and shallow groundwater samples in the Krom Antonies, Hol, Kruismans and Bergvallei tributaries and the Verloren confluence range from 6.5 to 7.2, suggesting slightly acidic to neutral nature of water. The pH for surface water and shallow groundwater samples in the four tributaries and the Verloren confluence indicate that samples are well within the safe limit of 6.5 to 8.5 for water.

EC and pH are used in conjunction with other parameters as indicators for water quality. Based on Freeze and Cherry (1979) and WHO (2011) classification (Table 6) water can be categorised as freshwater, brackish, saline and brine. In South Africa, EC values less than 70 mS/m is generally regarded as good. Surface water and shallow groundwater of the Kruismans, Hol and Bergvallei can be classified as being brackish water, having EC values

between 150 and 1500mS/m. In contrast, surface water and shallow groundwater samples of the Verloren confluence and the Krom Antonies classified as freshwater, hence the preferred use of Krom Antonies surface water for irrigation purposes.

**Table 6:** *Classification of inland water salinity (Freeze & Cherry, 1979).*

| **Class Name** | **Class Limits (EC range, in mS/m)** |
|---|---|
| Freshwater | <150 |
| Brackish water | 150-1500 |
| Saline | 1500-15000 |
| Brine | >15000 |

Chloride inputs to surface waters can arise from irrigation return flows, sewage effluent discharges and various industrial processes (DWAF,1996). According to South African Water Use Guideline (1996) 0-100 mg/l of $Cl^-$ would not cause health effects, and is below the corrosion acceleration threshold. For sulphate, which is associated with dissolution of minerals such as gypsum in South Africa, 0-200 mg/l sulphate does not have human health effects. Sodium is omnipresent in the environment and usually occurs as sodium chloride, sometimes as sodium sulphate or sodium bicarbonate (DWAF, 1996). The South Africa Water Use Guideline (1996) indicates that a content of 0-100 mg/l of sodium has no health effects on humans. Potassium is everywhere in the environment. According to DWAF (1996) typically the concentration of potassium in freshwater is within the range of 2-5 mg/l; but there are no effects to human health when $K^+$ is present in the range of 0-50 mg/l in the water. In the South Africa Water Use Guideline (1996) the average concentration of calcium in freshwater is 15 mg/l. and the concentration of $Mg^{2+}$ in fresh water is between 4-10 mg/l; 0-30 mg/l of $Mg^{2+}$ in the water would not cause bitter taste, scaling problems and health effects.

Based on the South Africa Water Use Guideline mentioned above, the majority of surface water and shallow groundwater samples in the Kruismans, Hol and Bergvallei show elevated $Na^+$ and $Cl^-$ concentrations greater than the drinking water guideline value of 200 mg/L for $Na^+$ and 250mg/L for $Cl^-$. Surface water and shallow groundwater samples of the Krom Antonies and Verloren confluence exhibit major cation concentrations below the recommended standards. Chloride concentrations for surface water samples in the Verloren confluence and Krom Antonies are within the accepted standard of 250mg/L, compared to shallow groundwater samples depicting greater than 250mg/L $Cl^-$ concentrations. Shallow groundwater samples TS15VLR068 and TS16VLR0124 collected in piezometer KAPZ06 in

the Krom Antonies exceed permissible $SO_4^{2-}$ concentrations of 250mg/L, ranging from 489mg/L to 786mg/L, respectively (Table 4). Nitrate values for both surface water and shallow groundwater samples in all four tributaries and Verloren confluence fall within the maximum permissible limit of 50 mg/L. There is an exception for samples TS15VLR085 and TS15VLR092 collected in piezometer HOLPZ02 which exhibit values higher than 60 mg/L. Most surface water and shallow groundwater samples exceed the maximum permissible $K^+$ concentrations of 5mg/L set by WHO (2013).

Surface and shallow groundwater samples are well within the acceptable limits for As (10µg/l), B (30µg/L), Se (10µg/l) and Al (0.2mg/L) recommended by the World Health Origination.

### *5.1.2 Water Type*

Major cations and anions expressed as meq/L were used to plot Piper diagrams (Figures 23 and 24) and absolute values for Stiff diagrams (Figures 25 and 26) to characterise the geochemical facies of the different waters. The dominant cations and anions for surface water and shallow groundwater samples in the Kruismans, Hol, Bergvallei, Krom Antonies and Verloren confluence are, $Na^+ > Mg^{2+} > Ca^{2+} > K^+$ and $Cl^- > SO_4^{2-} > HCO_3^- > NO_3^- > PO_4^{3-}$, respectively. An exception of surface water and shallow groundwater samples in the Krom Antonies depict dominant cations as $Na^+ > Ca^{2+} > Mg^{2+} > K^+$ and surface water and shallow groundwater samples in the Verloren confluence showing dominant anions as $Cl^- > HCO_3^- > SO_4^{2-} > NO_3^- > PO_4^{3-}$. It is evident that from the piper plots and stiff diagrams, that $Na^+$ represents the dominant cation, whilst $Cl^-$ is the dominant anion in both surface water and shallow groundwater. Therefore, Na-Cl water type is the predominant water type for surface water and shallow groundwater samples in the Krom Antonies, Hol, Kruismans, Bergvallei and Verloren confluence. The dominancy of $Na^+$ and $Cl^-$ in both surface water and shallow groundwater samples is defined by the 'Y' shaped stiff diagrams (Figures 24 and 25) and may originate from several sources such as sea-salt aerosol due to the proximity (~60km) of study area to the sea, halite dissolution, or from interaction with aquifer matrix and anthropogenic activities. These are evaluated in section 5.2.

The dominant trace elements for surface water and shallow groundwater samples in the Kruismans, Hol, Bergvallei, Krom Antonies and Verloren confluence are, Sr > B > Al > Se > As > W (Figure 22). Strontium is the dominant trace element in all four tributaries and is likely derived from host lithologies. Boron is the second dominant trace element and increases with increasing salinity levels, boron may be derived from host lithologies and has been documented to be rich in marine shales (Curtis, 1964). Elevated aluminium concentrations are associated with low pH values and the increased solubility of metals at lower pH levels.

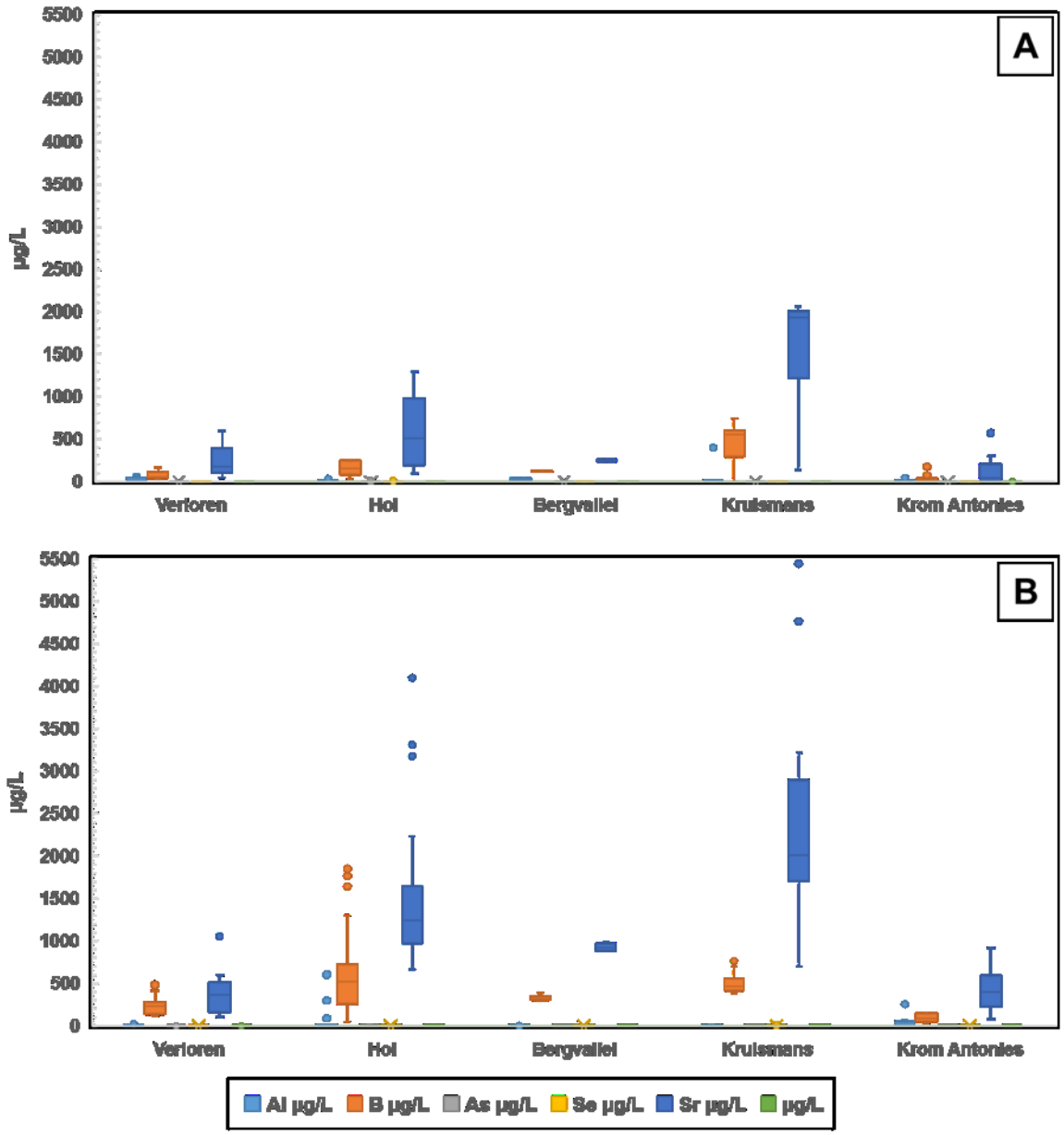


***Figure 22:*** *Box and Whisker plot showing trace elemental concentrations in the four tributaries and Verloren confluence; A) Surface water samples and B) Shallow groundwater samples.*

Surface water samples TS15VLR012 and TS15VLR067 collected upstream in the Krom Antonies tributary (Figure 23) show enrichment in $HCO_3^-$ and reflect a Ca-$HCO_3$ water type, which suggests infiltration of recent freshwater, rich in Ca and $HCO_3^-$. Samples TS15VLR069, TS15VLR110 and TS16VLR0123 indicate a Mg-Ca-SO4-Cl water type and may represent mixing of different waters or dissolution of evaporites and this water type is shown by an overturned "Y" shaped Stiff diagram. Surface water sample TS16VLR0145 in the Krom Antonies reflects a Na-HCO3 water type and may indicate ion exchange processes (Al-Khatib and Al-Najar, 2011). Ion exchange is a common process during re-freshening conditions, when fresh water flushes a salty or brackish water, $Ca^{2+}$ is transferred from the water to the

binding sites of the exchanger and $Na^+$ is dissolved in return, resulting in Na-$HCO_3$ water type (Elgettafi et al., 2012). Focusing on the ternary diagram of cations, a clear migration tendency from the calcium pole to the sodium pole is evident, which may indicate that cation exchange is one of the processes of salinisation for surface water in the Krom Antonies tributary (Figure 23A).

The Krom Antonies shallow groundwater samples TS16VLR0122 and TS16VLR0144 collected from piezometer KAPZ07 show a Ca-Mg-Cl water type. Samples TS15VLR068 and TS16VLR0124 collected from piezometer KAPZ06 reflect a Ca-Na-Cl-SO4 water type and a Ca-Mg-Cl-SO4 water type, respectively (Figure 24A) and is shown by ambiguous shaped stiff diagram (Figure 28A and C). Calcium-magnesium and chloride water types rich in Ca, Mg and Cl may reflect mixing with water of different origins. Sample TS16VLR0109 from KAPZ02 indicate Ca-Mg-Cl water type, whilst sample TS16VLR0152 from piezometer KAPZ03 show Ca-Cl-SO4 water type. The dominant water type in the study area is Na-Cl water type, with minor samples in the Krom Antonies showing dominance of $Ca^{2+}$, creating Ca-Mg-Cl-SO4 water type.

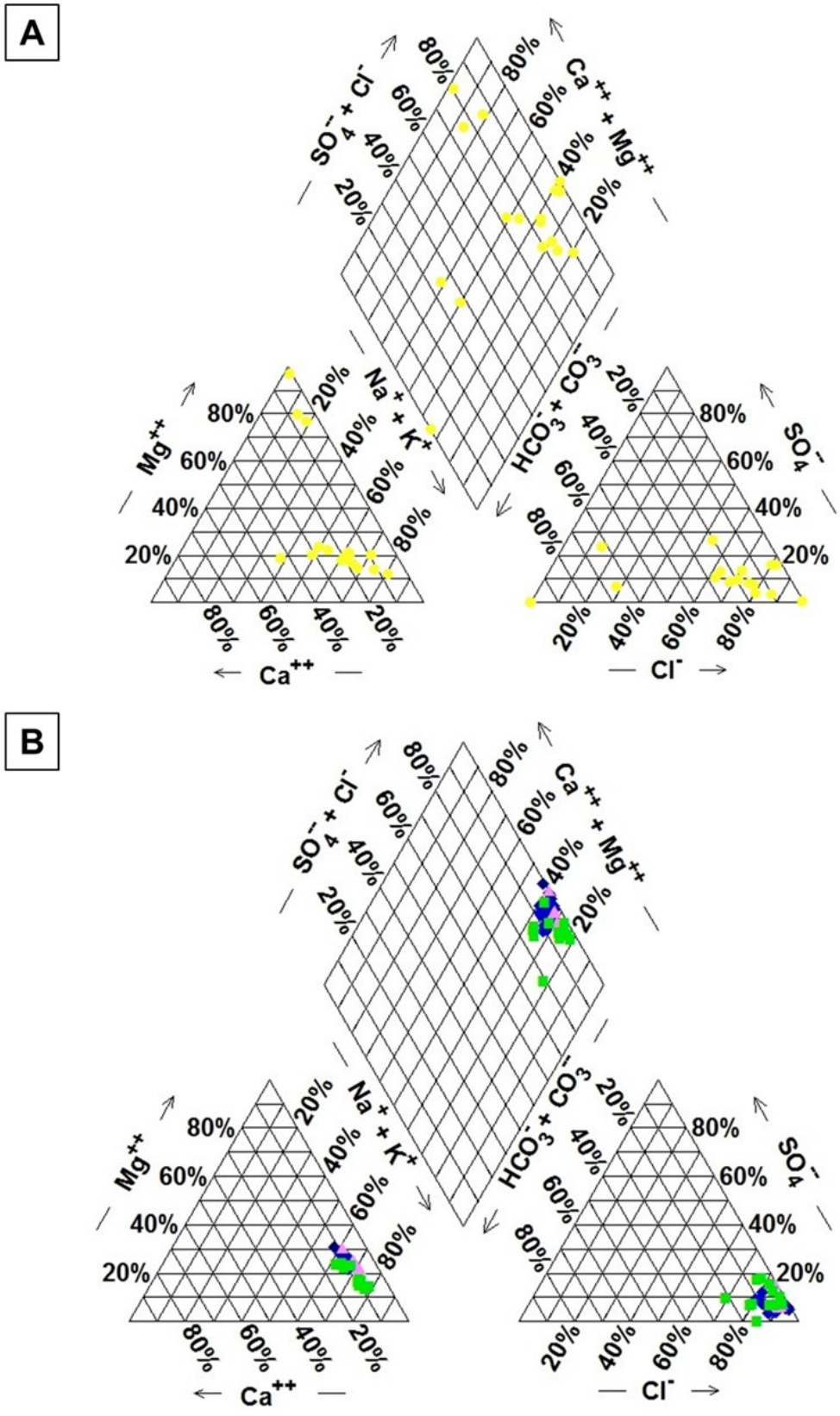


**Figure 23:** *Piper diagrams of surface water samples showing their respective surface water types/facies depending on where they plot on the piper diagram. A) Krom Antonies tributary; B) Hol, Kruismans, Bergvallei tributaries and Verloren confluence. Orange circles = Hol, yellow circles = Krom Antonies, blue diamonds = Kruismans, pink triangles = Bergvallei, green squares = Verloren confluence.*

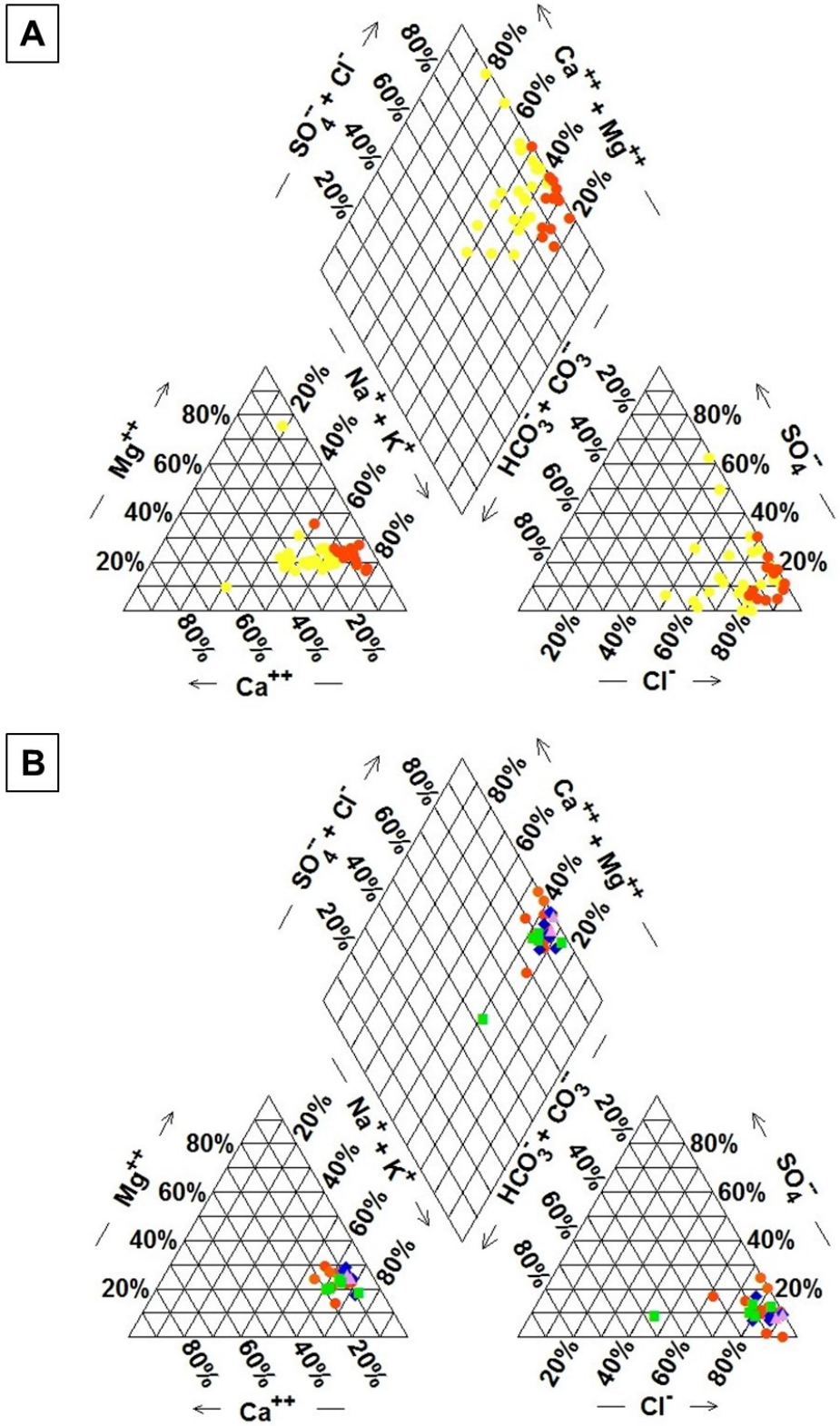


**Figure 24:** *Piper diagrams showing shallow groundwater samples and their respective shallow groundwater water types/facies depending on where they plot on the piper. A) Hol and Krom Antonies tributaries; B) Kruismans, Bergvallei tributaries and Verloren confluence. Orange circles = Hol, yellow circles = Krom Antonies, blue diamonds = Kruismans, pink triangles = Bergvallei, green squares = Verloren confluence.*

### *5.1.3 Spatial and Seasonal Variation*

The spatial distribution of salinity provides valuable information about different salinisation processes in each tributary. Stiff diagrams were used to differentiate surface water and shallow groundwater compositions during the wet and dry seasons. Therefore, Stiff maps for surface water were created for June, July and November 2015 and June 2016 (Figure 25A to D), and for shallow groundwater for July, September and November 2015 and June 2016 (Figure 26A to D). The high standard deviation (Table 3 and 4) of EC and major ion concentrations for surface water and shallow groundwater samples in the Krom Antonies, Kruismans, Hol, Bergvallei and Verloren confluence verify spatial and seasonal variability within the study catchment. The widespread occurrence of Na-Cl water types and the occurrence of fresh and brackish of surface water and shallow groundwater in the area, is indicative of a clear lack of hydro-chemical evolution. The drought conditions experienced in 2015 and 2016 during field sampling may contribute to the complexity of chemical composition and concentrations for both surface water and shallow groundwater. The same lack of a hydro-chemical trend with dominant Na-Cl water types has been recorded for groundwater samples in the Berg River Basin (Demlie et al., 2011)

Surface water samples TS15VLR0123 and TS15VLR0108 were collected during the dry season of November 2015 (Figure 25C). Due to drought conditions which impacted on surface runoff, sample TS15VLR0123 show high Mg content and may result from baseflow. Sample TS15VLR0108 in the lower reaches of the Hol, has high major ion concentrations, the observed chemical composition may be a result of stagnant water that came from the dams upstream the tributary that had undergone evaporation and show enrichment in $\delta^{2}H$ (7.8‰) and $\delta^{18}O$ (2.80‰) (Figure 17A). Surface water samples collected during June 2015 and 2016 in the Krom Antonies show an increasing gradient in major ion concentrations down the tributary and this may be due to salts being flushed down the tributary during the wet season after a rainfall event (Figures 10A and 25A and D). Surface water for the Kruismans and Bergvallei show “Y” Stiffed diagrams for June, July 2015 and June 2016 (Figure 25A, B and D).

Shallow groundwater collected from piezometer HOLPZ06 in the Hol tributary show “Y” shaped Stiff diagram and have high ion concentrations irrespective of the season. The observed high EC and ion concentrations may result from weathering of the Malmesbury shales which contain high concentrations of salts. (Sinclair et al., 1986), Piezometers KAPZ02 is 0.45m deeper than piezometer KAPZ01 (Table 1) and are located in the lower reaches of the Krom Antonies tributary. Piezometer KRPZ05 is 0.06m (Table 1) deeper than piezometer KRPZ04 and are situated in the lower reaches of the Kruismans near the Verloren confluence. It was observed that during the wet season associated with surface runoff, piezometer

KAPZ01 would be susceptible to infiltration by surface runoff, therefore low ion concentrations in this piezometer. Shallow groundwater samples collected in piezometer KRPZ05 shows high EC and major ion concentrations compared to piezometer KRPZ04 during both the wet and dry season (Figure 26A to D). The high EC and major ion concentrations recorded for shallow groundwater samples from piezometer KAPZ02 and KAPZ05 suggests interaction of shallow groundwater with weathered aquifer matrix, which is the weathered observed Malmesbury shale in the vicinity of the piezometers.

High $NO_3^-$ concentrations were recorded during the winter season of months June, September 2015 and June 2016, in each tributary. Shallow groundwater in the Hol tributary (HOLPZ02) show a significant $NO_3^-$ concentration up to 70mg/L. Nitrate is easily dissolved and washed off as runoff but its concentration or enrichment in surface water and shallow groundwater is a common finding in agricultural areas. The application of ammonium fertilizers for winter crops, results in ammonium ($NH_4^+$) being oxidized to $NO_3^-$ through the process of nitrification (Kim et al., 2003).

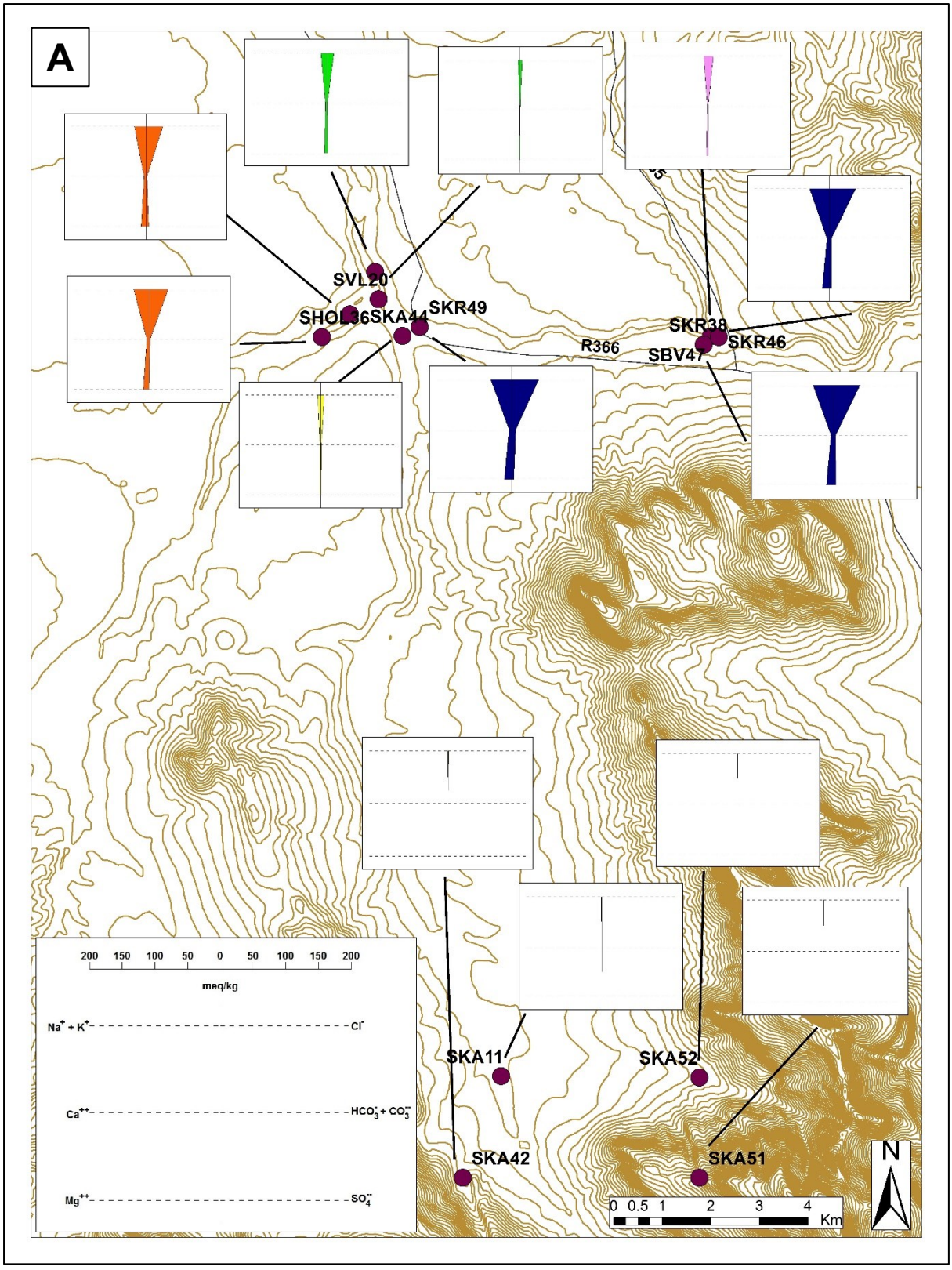


**Figure 25:** *Stiff Diagram maps for surface water depicting spatial and seasonal variation. A) June 2015; B) July 2015; C) November 2015; D) June 2016. SKA, SHol, SKR, SBV, SVL representing surface water samples and sample numbers collected in the Krom Antonies, Hol, Kruismans, Bergvallei and Verloren confluence, respectively. The scale is the same for each stiff diagram in each tributary.*

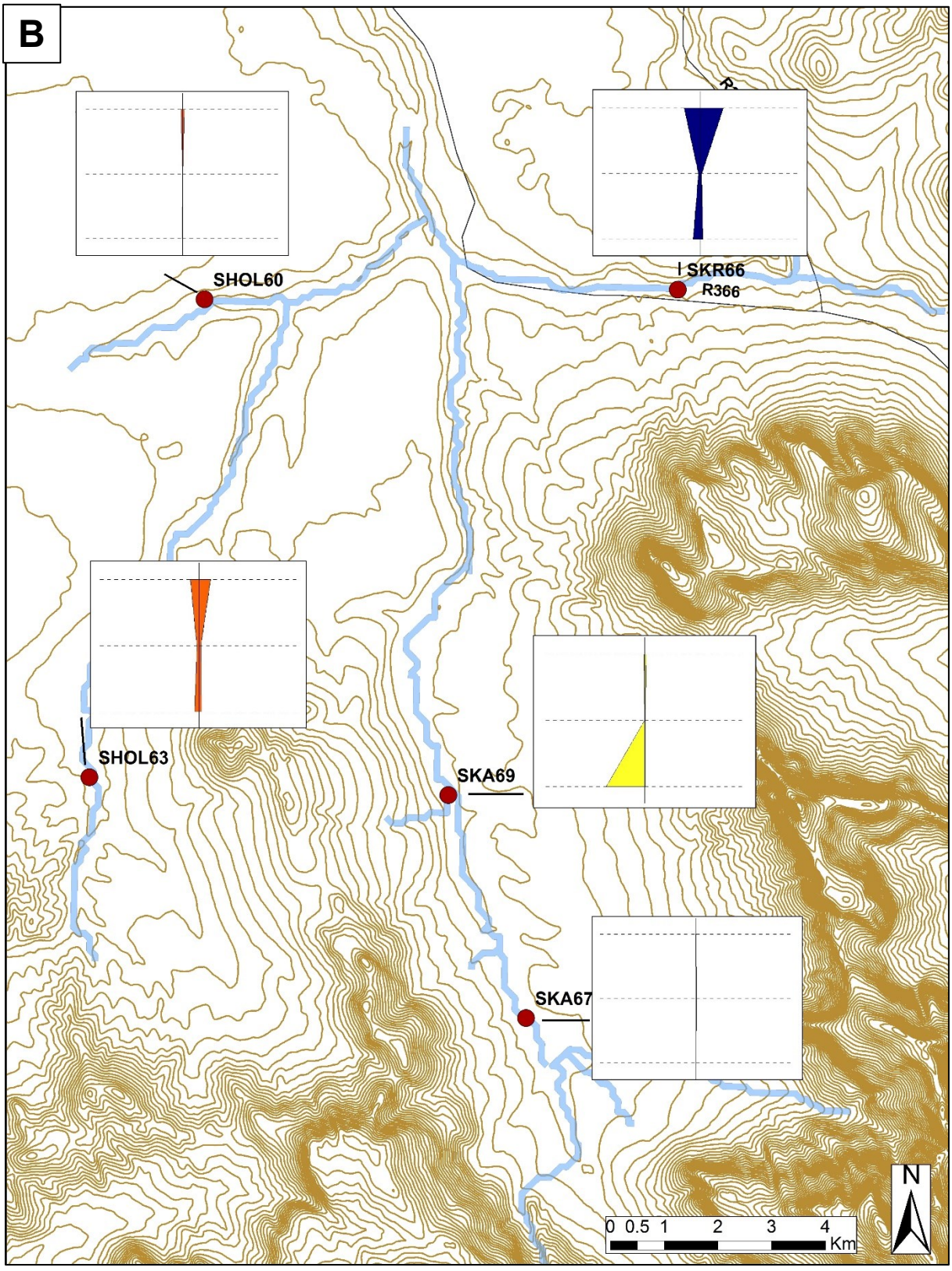


*Figure 25…… continued*

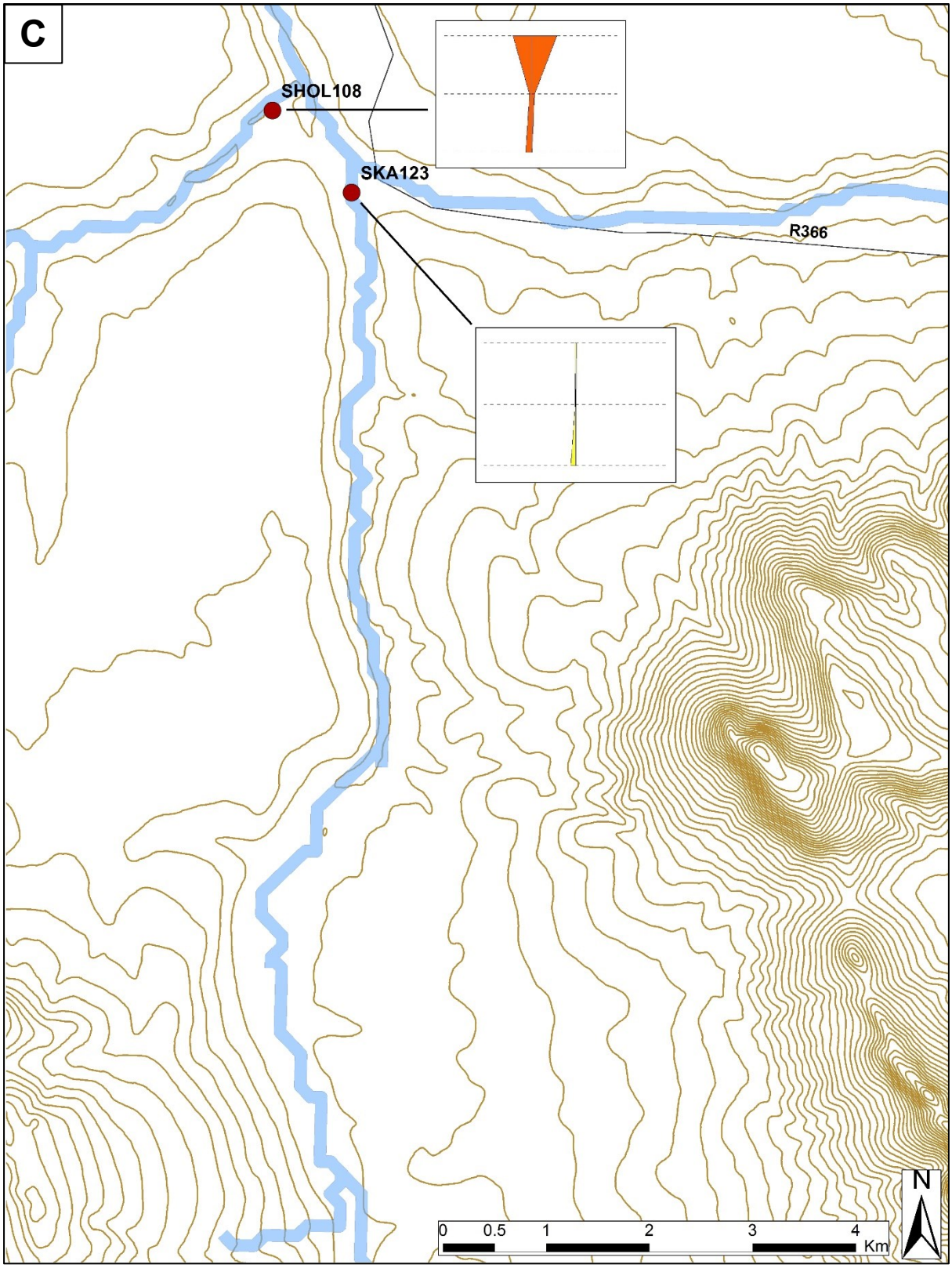


*Figure 25……continued*

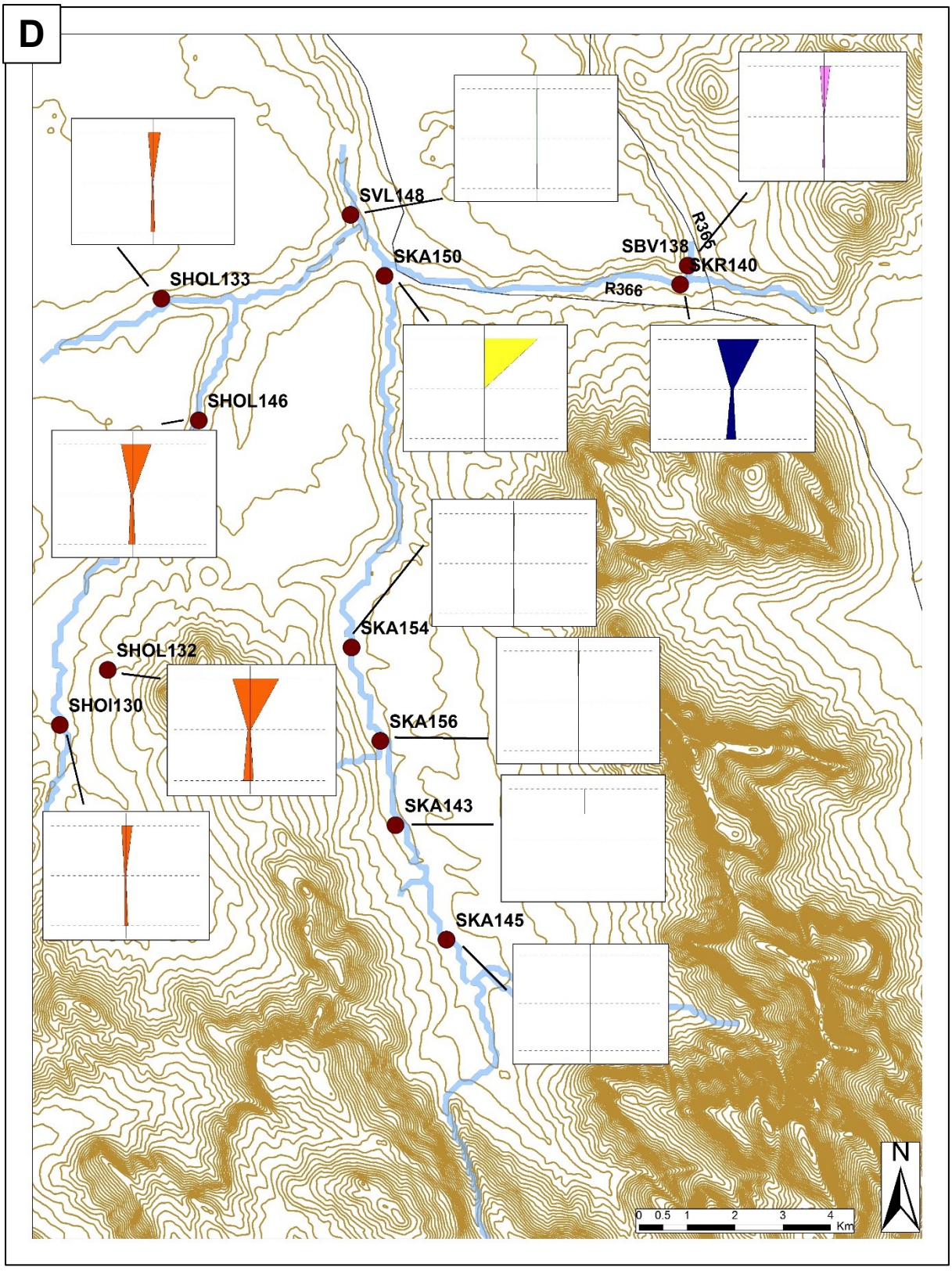


*Figure 25……continued*

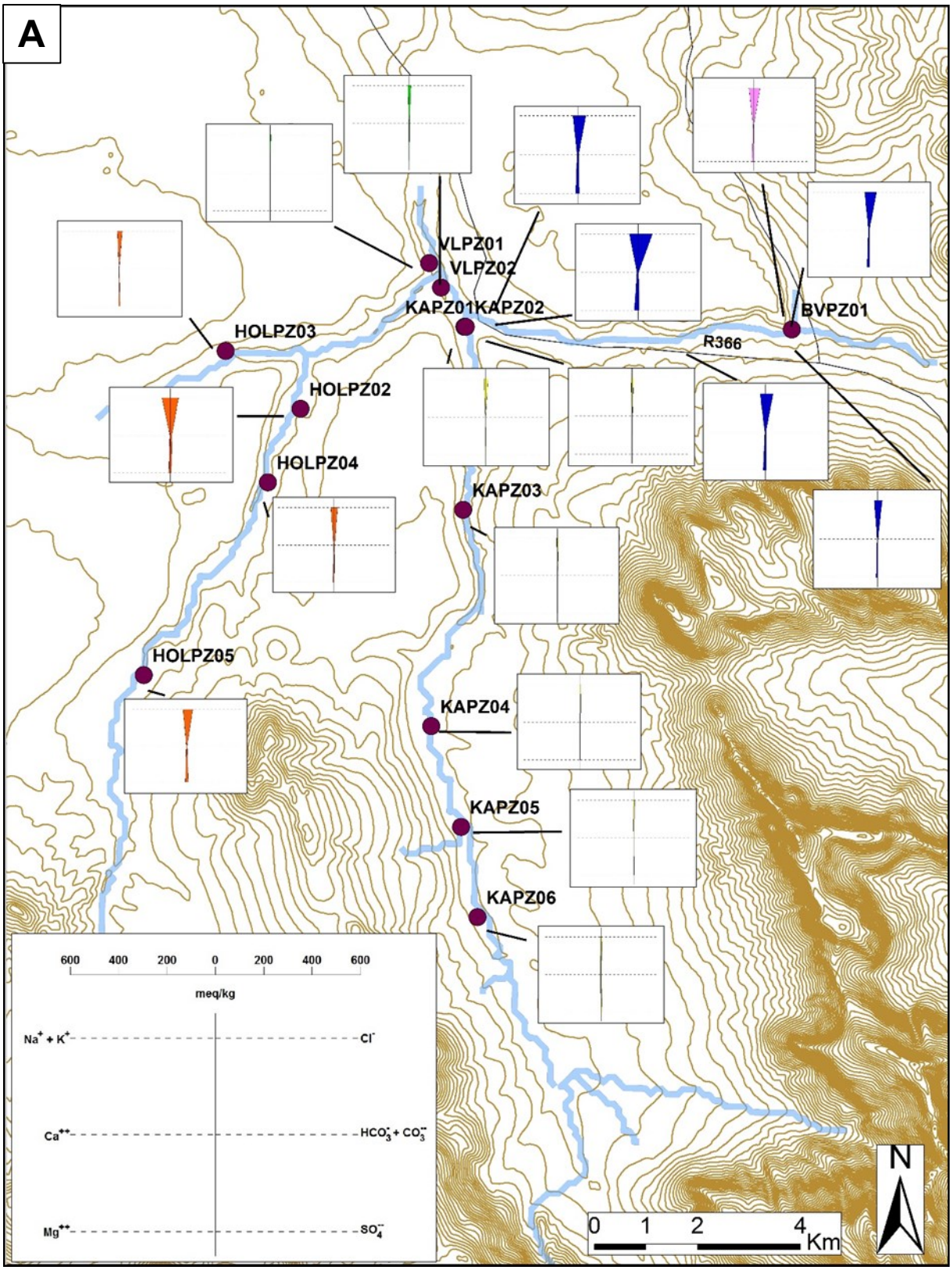


**Figure 26**: *Stiff Diagram maps for shallow groundwater depicting spatial and seasonal variation. A) July 2015; B) September 2015; C) November 2015; D) June 2016. KAPZ, HolPZ, KRPZ, BVPZ, VLPZ representing piezometers located in the Krom Antonies, Hol, Kruismans, Bergvallei and Verloren confluence, respectively. The scale is the same for each stiff diagram in each tributary.*

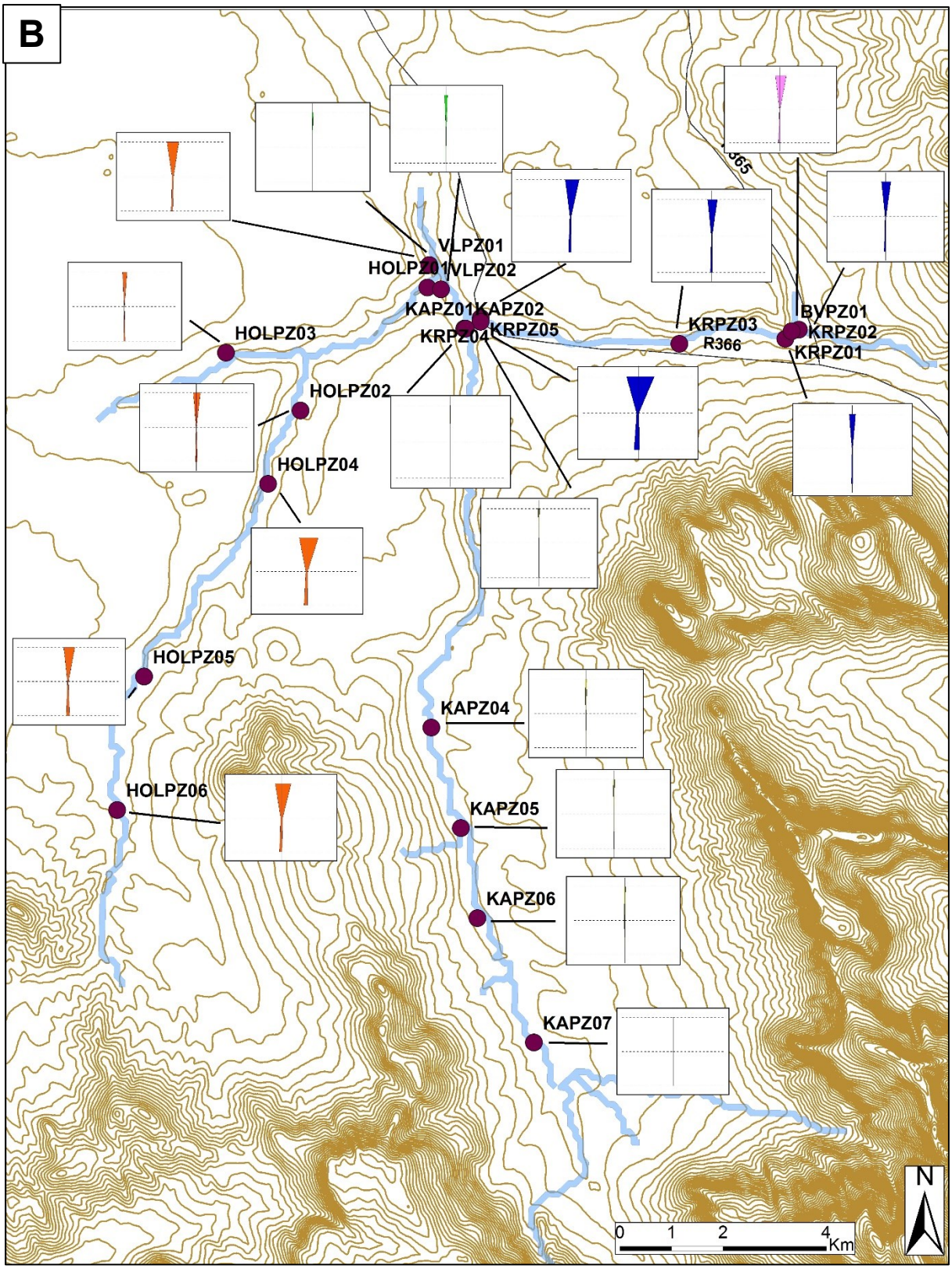


*Figure 26……continued*

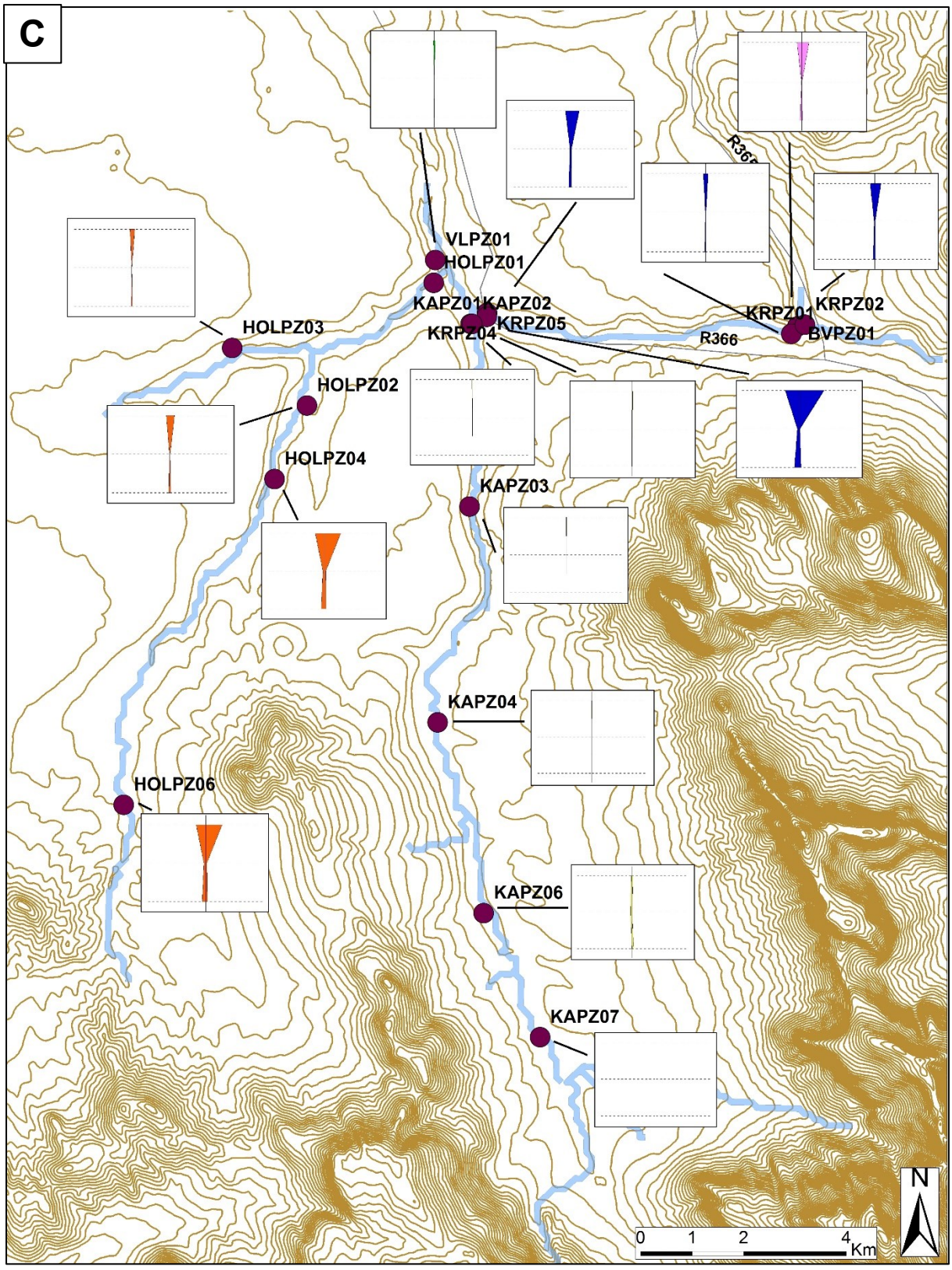


*Figure 26……. continued*

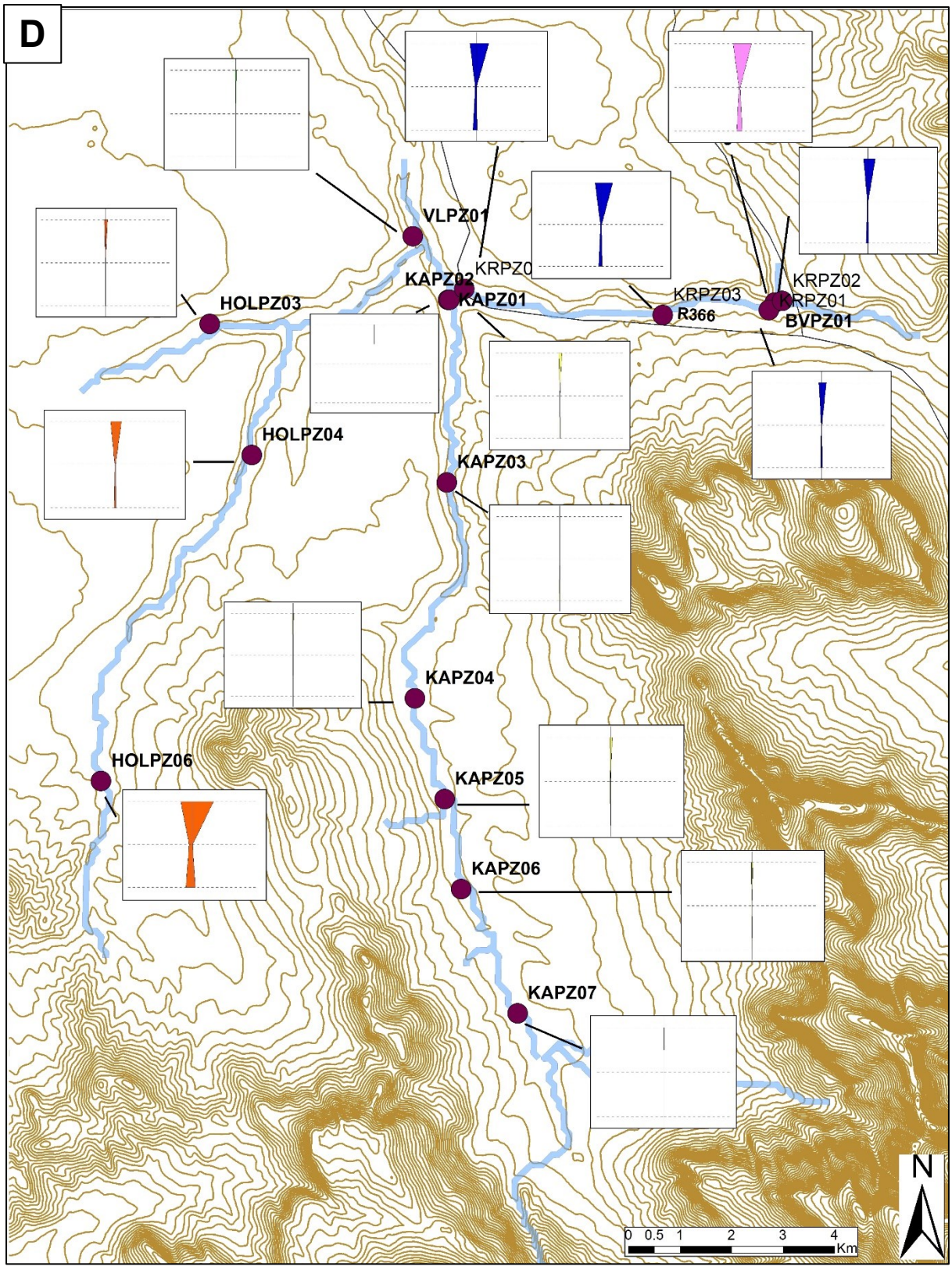


*Figure 26……continued*

## 5.2 Salt Sources

Scatter plots of various major elements as a function of $Cl^-$ were drawn to determine the contributing ions to surface water and shallow groundwater mineralisation. (Figure 27 and 28). Surface water samples in all tributaries and the Verloren confluence plot below the 1:1 line of halite dissolution and show a strong positive correlation between $Na^+$ and $Cl^-$ ($r^2$ between 0.93 and 0.99) (Figure 27A). Surface water samples of the Krom Antonies have a slope of 0.52 which is closer to the slope of the sea water line (0.55) (Figure 27A). There is a strong positive linear correlation that exists between $Mg^{2+}$, $Ca^{2+}$, $Br^-$, EC and $Cl^-$ (Figure 27B, C, E and G)$^-$, and this suggests a single salinity source (Marie & Vengosh, 2001).

Shallow groundwater samples in all tributaries and the Verloren confluence plot below the 1:1 line of halite dissolution, and show a strong positive correlation for $Na^+$ versus $Cl^-$ ($r^2$ ranging from 0.86 to 0.94), except for shallow groundwater samples in the Hol tributary with a correlation coefficient of $r^2$= 0.31 (Figure 28A). There is a strong positive linear correlation that exists between $Mg^{2+}$, $Ca^{2+}$, $Br^-$, EC and $Cl^-$ for shallow groundwater samples, suggesting a common salt source (Figure 28B, C, E and G). The deviation of surface water and shallow groundwater from the sea water line, in Figure 27A to C and Figure 28A to C, implies that seawater may not be the contributing factor for the observed ion concentrations.

Chloride can be regarded as geochemically inert and its concentrations and variations should be entirely source-related and a function of atmospheric (modern or ancient) inputs, anthropogenic inputs or mixing with formation waters or evaporates within the aquifer. Other possible sources of the excess $Cl^-$ in the waters could be saline water from interaction with aquifer matrix, evapo-transpiration, atmospheric input or anthropogenic input (Ekwere et al., 2010; Cartwright et al., 2008).

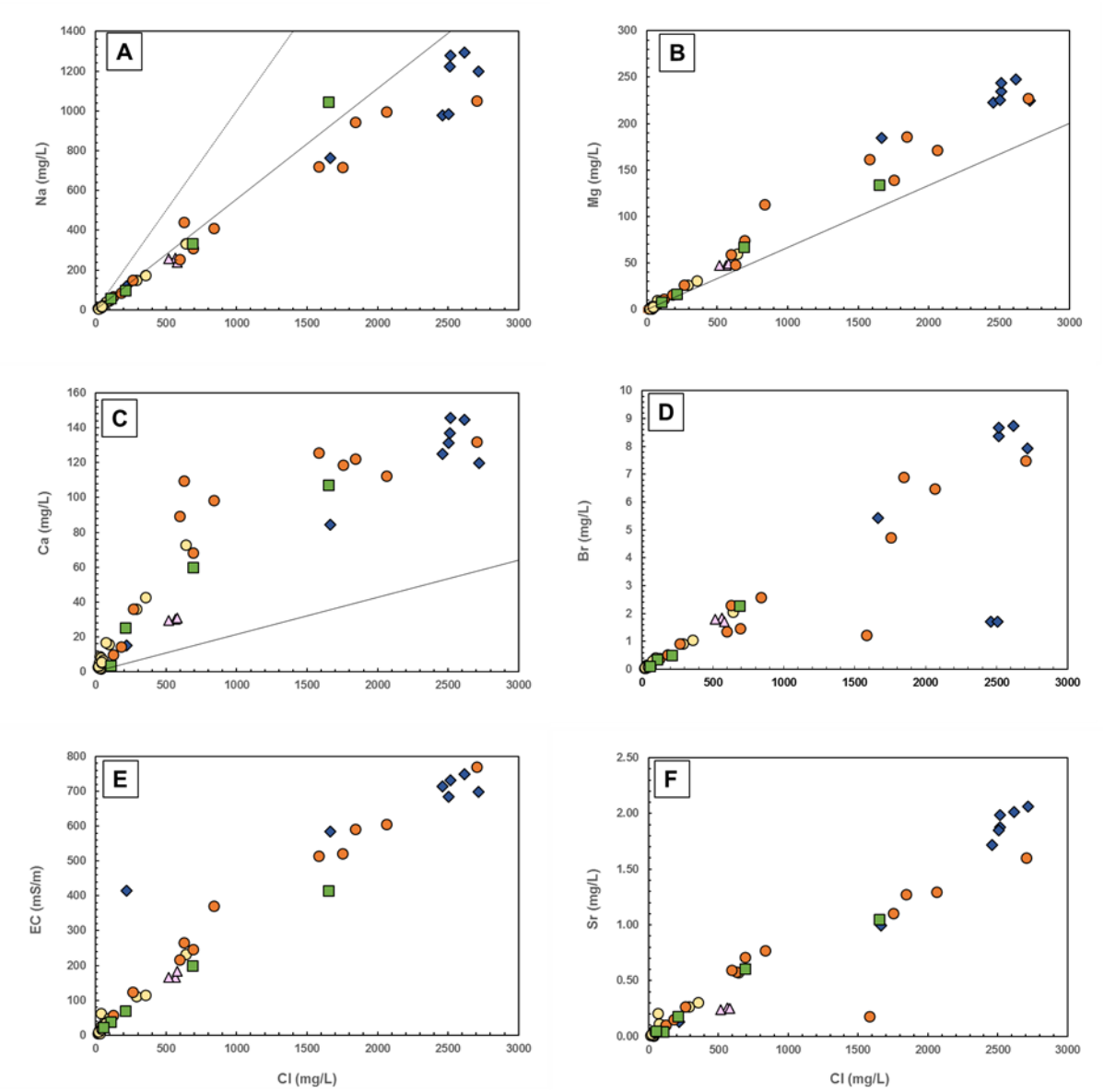


**Figure 27:** *Surface water scatter plots depicting a relationship between A) Na; B) Mg; C) Ca; D) Br; E) EC Br; F) Sr and Cl. The solid line represents seawater line and the dashed line represent a line of halite dissolution. Units for the ionic concentrations have been mentioned in each figure. Blue diamonds = Kruismans, green squares = Verloren confluence, orange circles = Hol, pink triangles = Bergvallei, yellow circles = Krom Antonies.*

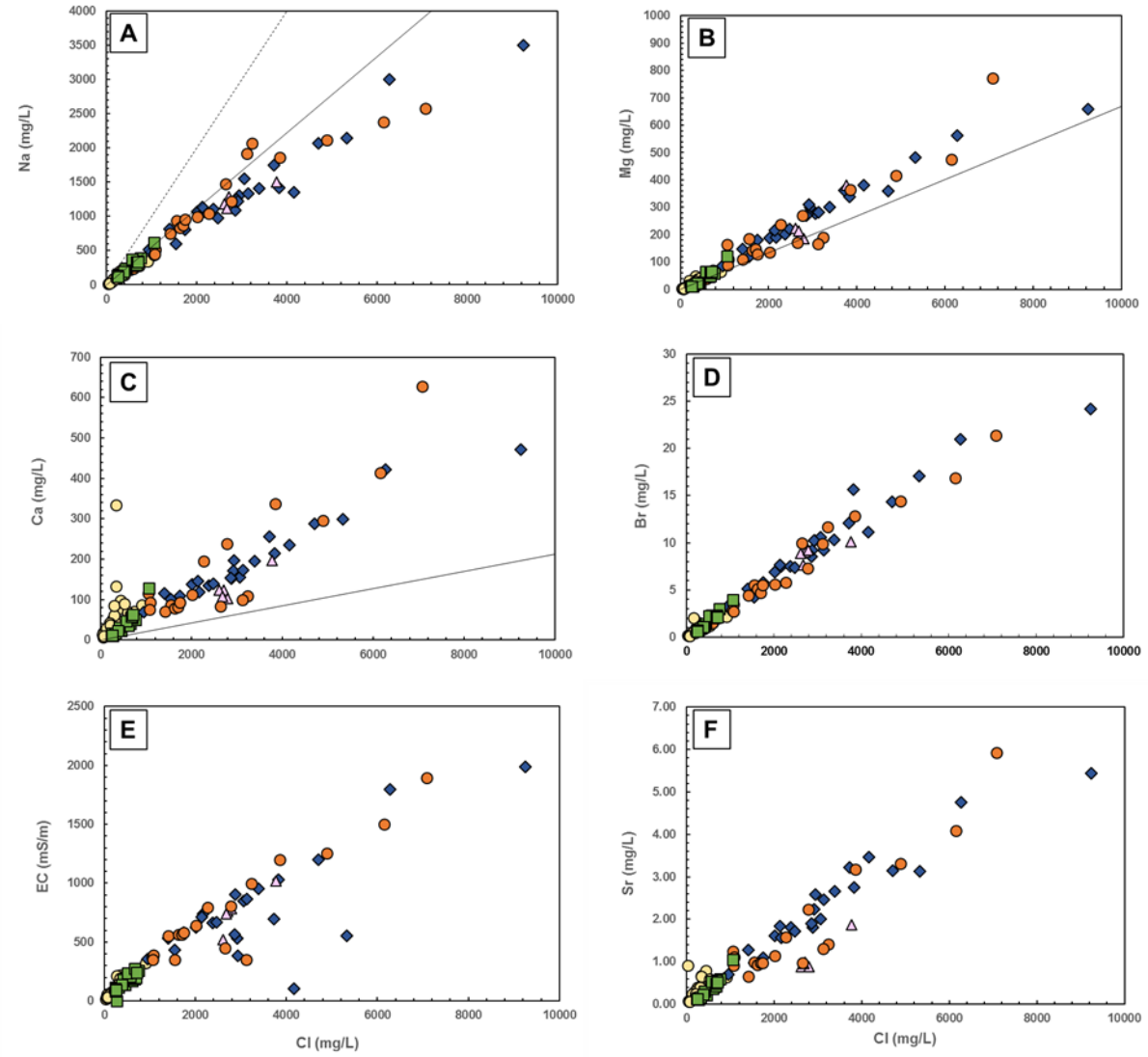


**Figure 28:** *Shallow groundwater scatter plots depicting a relationship between A) Na; B) Mg; C) Ca; D) Br; E) EC; F) Sr and Cl. The solid line represents seawater line and the dashed line represent a line of halite dissolution. Units for the ionic concentrations have been mentioned in each figure. Blue diamonds = Kruismans, green squares = Verloren confluence, orange circles = Hol, pink triangles = Bergvallei, yellow circles = Krom Antonies.*

Several factors control groundwater chemistry, which can be related to the physical situation of the aquifer, bedrock mineralogy and weathering conditions. Gibbs (1970) suggested TDS versus $Na^+/Na^+ + Ca^{2+}$ for cations and TDS versus $Cl^-/ (Cl^- + HCO_3^-)$ for anions to illustrate the natural mechanism controlling groundwater chemistry, including the rainfall dominance, rock weathering dominance, and evaporation and participation dominance. In the present study, the majority of surface water and shallow groundwater samples in the Krom Antonies and Verloren confluence plot in the rock dominance zone on the Gibbs diagram (Figure 29). The majority of the surface and shallow groundwater samples of the Kruismans, Hol and Bergvallei plot in the zone of evaporation crystallisation dominance. The Gibbs diagram suggests that the rock dominance zone indicates the dissolution of silicate-bearing rocks with water (Sheikhy

Narany et al., 2014). The evaporation crystallisation dominance zone is associated with calcite ($CaCO_3$) being the first mineral to precipitate out of solution with evaporation, which may support the over-saturation (SI>0.1) of calcite and minerals of surface and shallow groundwater samples in the Hol and Kruismans.

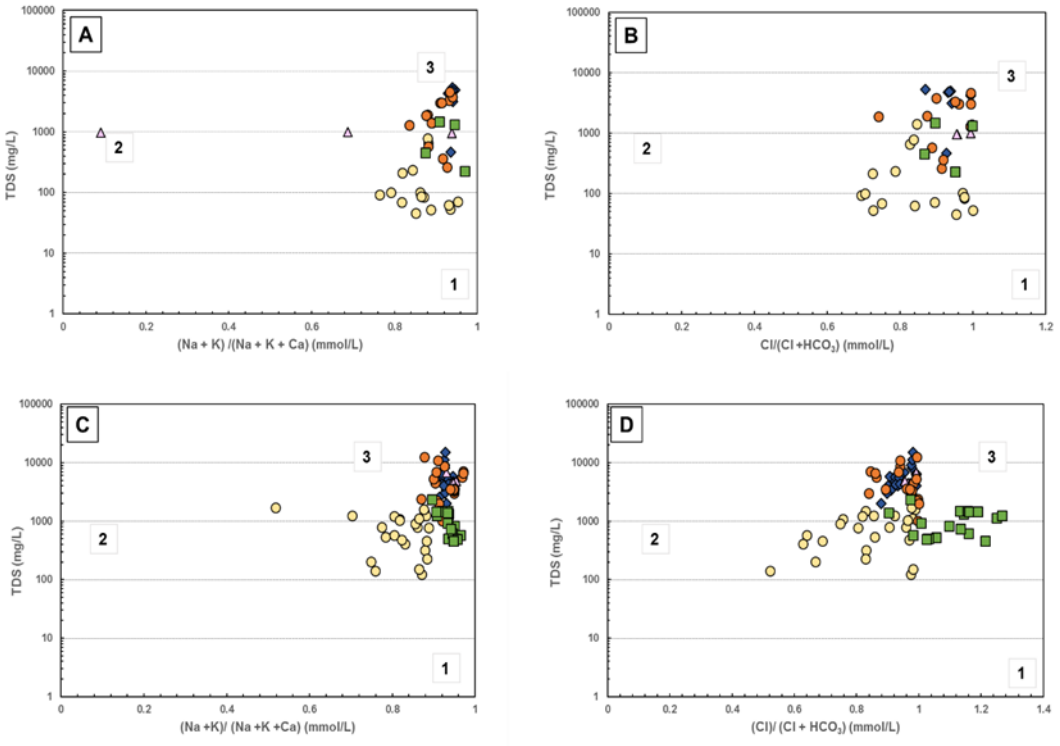


**Figure 29:** *Gibbs diagram plotting the TDS concentration as a function of the ratios of A) Na+/(Na++ Ca2+) for surface water, B) Cl−/(Cl−+ HCO3-) for surface water; C) Na+/(Na++ Ca2+) for shallow groundwater ;D) ) Cl−/(Cl−+ HCO3-) for shallow groundwater. Label 1 = precipitation dominance zone, label 2 = rock dominance zone and label 3 = evaporation crystallisation dominance zone. Blue diamonds = Kruismans, green squares = Verloren confluence, orange circles = Hol, pink triangles = Bergvallei, yellow circles = Krom Antonies.*

The following sections expands on the geochemical processes controlling salinity observed in Krom Antonies, Kruismans, Hol, Bergvallei tributaries and the Verloren confluence. The geochemical processes identified as important are: (1) Evaporation and evapotranspiration; (2) rock-water interactions; (3) precipitation and dissolution of minerals and (3) mixing of waters of different origins.

### *5.2.1. Wet and Dry Atmospheric Deposition*

The atmosphere is an important source of particulate matter and associated pollutants found in oceans and large lakes. Atmospheric deposition comes in two forms: wet and dry deposition. Wet deposition is the process whereby dissolved solutes and insoluble particles are carried to the ground by rainfall and dry deposition is the settling of particulate and aerosols

from the atmosphere without rain as a transport medium (Williams, 1982). In addition to salts related to rainfall, salt transported by atmospheric dry deposition, such as aerosol and dust, is another well-known global phenomenon (Goudie & Middleton, 2006). Marine aerosols consist predominantly of chlorides (88.7%) and sulphates (10.8%), whereas other chemical substances make up only 0.5% of the total mass. Eighty-five percent of sodium and chloride in the atmosphere is derived from sea (Gustafsson & Franz´en, 2000).

A study conducted by Soderberg and Compton (2007) in the Olifants River near Citrusdal, Cape Western, recorded rainfall that was dominated by Na, Cl, Mg and $SO_4$ ions, whose ratios to chloride were similar to that of seawater and chloride concentrations ranging from 0.4 to 10.9 mg/L. Chloride concentrations for rainwater samples by Eilers (2018) in this study area range from 0.49 to 19.55mg/L. Due to the low contribution of $Na^+$ and $Cl^-$ from wet deposition, it can be suggested that $Na^+$ and $Cl^-$ has to be derived from sources other than direct precipitation. Surface water and shallow groundwater samples in tributaries vary in Cl, Na concentrations, with the majority of the samples depicting major ion concentrations more than 50mg/L (Tables 3 and 4). However, Davies et al. (1998) identified that Cl/Br ratios of precipitation samples were ~50, at the lower end of the range of Cl/Br ratios (50 to 150), the latter low Cl/Br ratios might explain the low Cl/Br ratios (<200) observed in the Krom Antonies.

### *5.2.2 Evaporation and Evapotranspiration*

In semi-arid environments, the isotopic composition of $\delta^2H$ and $\delta^{18}O$ in shallow groundwater can be significantly modified from that of local precipitation, as a result of evaporative isotopic enrichment during infiltration (Clark and Fritz, 1997). The stable isotope composition of water in each tributary is quite variable with $\delta\ ^{18}O$ and $\delta\ ^{2}H$ values for shallow groundwater and surface waters ranging from -3.68 to 2.85‰ and -16.9 to 7.8‰ and from -5.8 to 2.24‰ and -16.8 to 2.1‰, respectively. The relationship between $\delta^{18}O$ and $\delta^2H$ for surface water and shallow groundwater does not fall on a mixing line with seawater, as the y intercept of the relationship does not intersect the composition of seawater (Sami, 1992). The isotopic character of surface water indicates displacement from that of the LMWL and GMWL. Plotting on a line with a slope of 3.57 for the Verloren confluence and Hol tributary and 3.71 and 4.75 for the Krom Antonies and Bergvallei, respectively, indicate that variable evaporation occurred during or prior to recharge (Figure 30A). Surface water in the Kruismans seem to plot parallel to the LWML and plot on a line with a slope of 6.44 which is closer to the LMWL slope of 6.8 (Figure 30A). Shallow groundwater samples of the Kruismans, Krom Antonies and Hol tributaries plot diverging away from the LMWL and GMWL with slopes less than 4.0, showing an evaporative trend. The Verloren confluence plots on a line with a slope of 5.2 indicating a

weak evaporative trend (Figure 30B). Some of surface and shallow groundwater samples in the Krom Antonies plot on the LMWL suggesting water is from rainfall.

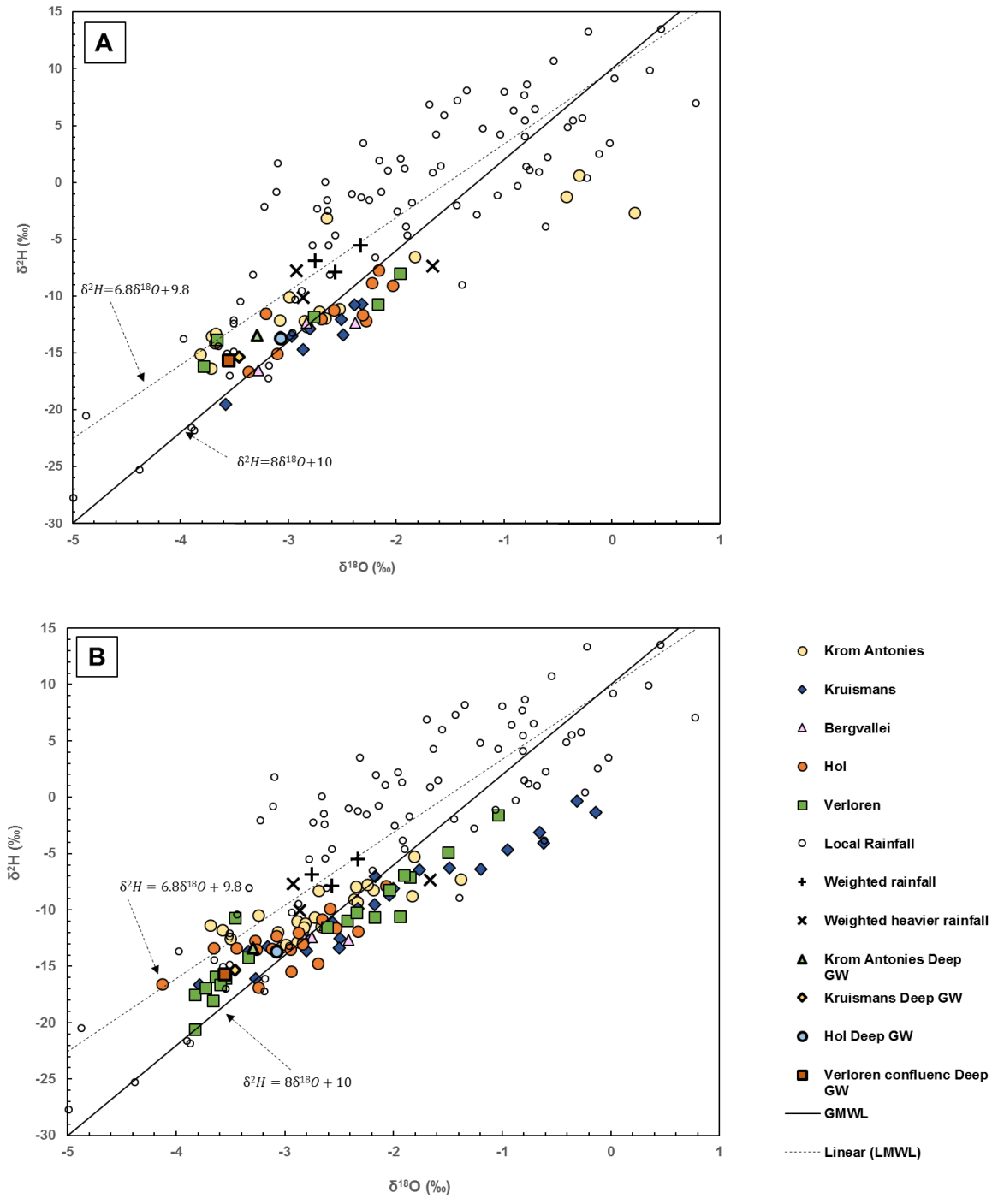


**Figure 30:** *Relationship between $\delta^{18}O$ and $\delta^{2}H$ for A) surface water samples; B) shallow groundwater samples in all four tributaries and the Verloren Confluence. Local Meteoric Line (LMWL= ($\delta^{2}H$ = 6.8 $\delta^{18}O$ + 9.8) represented by a dotted line and the Global Meteoric Water Line (GMWL: $\delta^{2}H$ = 8 $\delta^{18}O$ + 10) (Craig, 1961), represented by a solid line.*

Deuterium excess (*d*-excess) is used as a proxy for identifying secondary processes that influence atmospheric vapour content in the evaporation-condensation cycle in nature (Bodag, et al 2016) and indicates the evaporation effect on physiochemical characteristics of water. To better understand the processes affecting the isotopic signatures of oxygen and hydrogen, chloride versus d-excess have been plotted for both surface water and shallow groundwater samples (Figure 31A and B). If the cause of salinity is evaporation, d-excess should decline with increasing Cl concentration (Cheiken et al., 2012). Therefore, it is evident that evaporation is not the dominant process for $Cl^-$ concentration for surface and shallow groundwater samples in the Krom Antonies.This is evident by inconsistent d-excess values with increasing chloride. Surface water and shallow groundwater samples of the Verloren confluence show a linear correlation ($R^2$ = 0.59) between d-excess and $Cl^-$, suggesting evaporation as a source for salt. Surface water samples of the Kruismans and Hol show two groups in Figure 31A and B. The first group shows a decrease in d-excess relative to an increase in Cl- concentration. The second group depicts almost constant Cl- concentration and variation of d-excess, implying other sources than evaporation are at play.

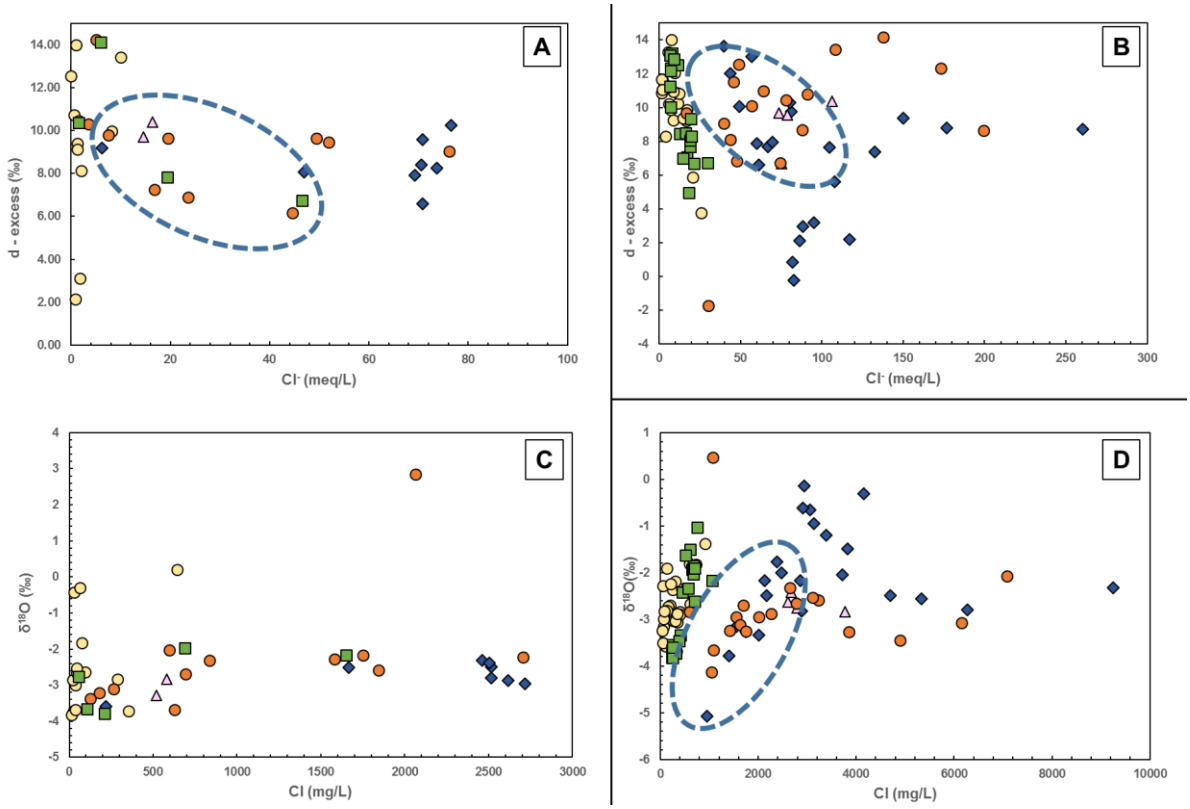


**Figure 31:** *Surface water relationship between A) d-excess; B) $\delta^{18}$OBlue and $Cl^-$ concentrations. Shallow groundwater relationship between C) d-excess; D) $\delta^{18}$O and $Cl^-$ concentrations Dotted ocal showing a group of samples depicting evaporation. Blue and $Cl^-$ concentrations. Diamonds = Kruismans, green squares = Verloren confluence, orange circles = Hol, pink triangles = Bergvallei, yellow circles = Krom Antonies.*

It can be further confirmed by plotting $Cl^-$ concentration of surface water and shallow groundwater samples as a function of the $\delta^{18}O$ isotopic composition (Fig 31C and D), that evaporation is not a dominant process for salinisation for surface water and shallow groundwater samples in the Krom Antonies. It seems that the increase of salt concentration is not accompanied by an isotopic effect. However, if there is a prevailing mechanism that is causing surface water and shallow groundwater salinization in all four tributaries, this heterogeneous arrangement may be due to weathering of silicate minerals (Moussa et al., 2011). Shallow groundwater samples in the Verloren confluence show correlation ($R^2$ =0.66) between $Cl^-$ and $\delta^{18}O$ suggesting evaporation as a source for salt concentration.

### *5.2.3 Exchange with Aquifer Matrix*

#### *5.2.3.1. Precipitation and dissolution of minerals*

Mineral saturation indices (SI) indicate the degree of saturation in a particular mineral phase compared to the aqueous solution with which it is in contact. Based on this SI value, the trend of precipitation or dilution of the mineral phases can be deduced. The simulation was performed using the thermodynamic software PHREEQC. The calculation of the saturation index was performed by the formula:

$$SI = [\log(Q)]/[\log(Ksp)]$$

Where $Q$ is defined as the ion activity product and $Ksp$ is defined as solubility product.

The values of the saturation indices for halite, calcite, anhydrite, dolomite, and gypsum are highlighted in Table 7. It is postulated that mineral phases that are under-saturated (SI ≤ −0.1) will tend to dissolve, and mineral phases that are oversaturated (SI ≥ 0.1) will precipitate these mineral phases out of solution. Equilibrium is taken to be between SI = −0.1 and SI = 0.1 (Bouderbala, 2015).

All surface water and shallow groundwater samples are under-saturated with respect to gypsum and halite, likely to be driving dissolution of the two minerals from the aquifer matrix. Surface water samples in the Verloren confluence and Bergvallei show under-saturation in calcite and dolomite. Surface water sample TS15VLR0110 in the Krom Antonies is oversaturated with respect to calcite ($CaCO_3$) and dolomite $CaMg(CO_3)_2$. Fifty percent and 83% of surface water samples in the Hol and Kruismans, respectively are supersaturated in calcite and dolomite, favouring the possibility of precipitation of these two minerals. Fifty-nine percent and 56% of shallow groundwater samples in the Kruismans and Hol, respectively are supersaturated with respect to calcite and dolomite.

**Table 7**: *Statistical summary of saturation indexes of minerals for A) surface water; B) shallow groundwater. using PHREEQC.*

| A | Calcite | Dolomite | Gypsum | Halite | B | Anhydrite | Calcite | Dolomite | Gypsum | Halite |
|---|---|---|---|---|---|---|---|---|---|---|
| **Verloren confluence** | | | | | | | | | | |
| Min | -4.28 | -7.81 | -3.97 | -6.74 | | -2.86 | -3.49 | -7.24 | -2.64 | -6.07 |
| Max | -0.67 | -0.93 | -1.39 | -4.45 | | -1.46 | -0.02 | -0.21 | -1.24 | -4.85 |
| Mean | -1.93 | -3.42 | -2.38 | -5.68 | | -2.40 | -1.98 | -4.14 | -2.18 | -5.58 |
| SD | 1.67 | 3.19 | 1.15 | 1.02 | | 0.40 | 1.32 | 2.64 | 0.40 | 0.39 |
| **Bergvallei** | | | | | | | | | | |
| Min | -2.06 | -3.57 | -1.65 | -4.23 | | -1.87 | -1.54 | -2.98 | -1.65 | -4.23 |
| Max | -1.66 | -2.77 | -1.57 | -4.17 | | -1.78 | -1.04 | -2.01 | -1.57 | -4.17 |
| Mean | -1.86 | -3.17 | -1.60 | -4.20 | | -1.82 | -1.24 | -2.40 | -1.60 | -4.20 |
| SD | 0.28 | 0.57 | 0.03 | 0.02 | | 0.05 | 0.27 | 0.51 | 0.05 | 0.03 |
| **Krom Antonies** | | | | | | | | | | |
| Min | -4.29 | -8.28 | -4.60 | -8.26 | | -3.54 | -3.10 | -6.52 | -3.32 | -7.61 |
| Max | 0.52 | 1.32 | -1.90 | -5.30 | | -0.65 | 0.03 | -0.45 | -0.43 | -5.14 |
| Mean | -1.60 | -3.63 | -3.24 | -7.19 | | -2.33 | -1.12 | -2.70 | -2.11 | -6.07 |
| SD | 1.49 | 3.09 | 0.87 | 0.95 | | 0.76 | 0.81 | 1.66 | 0.76 | 0.67 |
| **Kruismans** | | | | | | | | | | |
| Min | -2.60 | -4.85 | -2.43 | -6.15 | | -2.00 | -0.33 | -0.75 | -1.78 | -4.95 |
| Max | 0.34 | 2.01 | -1.44 | -4.18 | | -1.11 | 0.65 | 1.31 | -0.90 | -3.28 |
| Mean | -0.35 | 0.19 | -1.66 | -4.59 | | -1.64 | 0.02 | 0.03 | -1.42 | -4.14 |
| SD | 1.11 | 2.51 | 0.39 | 0.78 | | 0.28 | 0.28 | 0.57 | 0.28 | 0.40 |
| **Hol** | | | | | | | | | | |
| Min | -2.84 | -5.28 | -3.06 | -6.62 | | -2.14 | -4.13 | -8.31 | -1.92 | -5.00 |
| Max | 1.03 | 2.61 | -1.32 | -4.38 | | -1.08 | 0.76 | 1.58 | -0.86 | -3.22 |
| Mean | -0.75 | -1.04 | -2.08 | -5.34 | | -1.50 | -0.71 | -1.43 | -1.29 | -4.24 |
| SD | 1.43 | 2.94 | 0.71 | 0.88 | | 0.33 | 1.54 | 3.12 | 0.33 | 0.49 |

The dissolution of halite is represented by negative halite saturation indices for surface water and shallow groundwater samples indicating thus an under-saturated state (Table 7). Scatter plots for surface water and shallow groundwater samples show that these samples do not plot along the 1:1 line of halite dissolution (Figure 27A and 28A) and surface water and shallow groundwater samples depict varying Na/Cl molar ratios (Na/Cl <1) less than that of halite dissolution (Na/Cl = 1). Therefore, this confirms that surface water and shallow groundwater do not reflect inputs of halite dissolution as a major source for $Na^+$ and $Cl^-$ and as a major source for salinity (Sami, 1992).

However, there is significant variation in Cl/Br ratios for surface water and shallow groundwater in the Krom Antonies and Verloren confluence indicative of different sources with higher or lower Cl/Br ratios that are being added to achieve the observed Cl/Br ratios (Moore et al., 2008). There is a possibility that halite dissolution from dry deposition may contribute to the higher Cl/Br ratio of more than 1000 observed for surface water sample TS16VLR0150,154 and 156 in the Krom Antonies collected during the wet season of June 2016. This may also explain the high Cl/Br values of up to 3000 for the two surface water samples TS16VLR0135 and TS16VLR0140 in the Kruismans, which were collected also during the wet season of June 2016 (Table 3).

Figure 32A and C show surface water and shallow groundwater samples in the Krom Antonies, Hol, Kruismans, Bergvallei and Verloren confluence plot below the 1:1 line of gypsum dissolution. Two surface water samples TS15VLR055 and TS15VLR0108 in the Verloren confluence and the Hol, respectively, plot above the 1:1 line of gypsum dissolution, indicating excess $Ca^{2+}$ relative to $SO_4^{2-}$ (Figure 32A). Shallow groundwater samples in all four tributaries show a strong positive linear relationship ($r^2$ ranging from 0.63 to 0.81) of $Ca^{2+}$ versus $SO_4^{2-}$, suggesting a common source, with the exception for Verloren confluence surface water samples that show a weak correlation ($r^2$ = 0.027) between $Ca^{2+}$ and $SO_4^{2-}$ (Figure 32A).

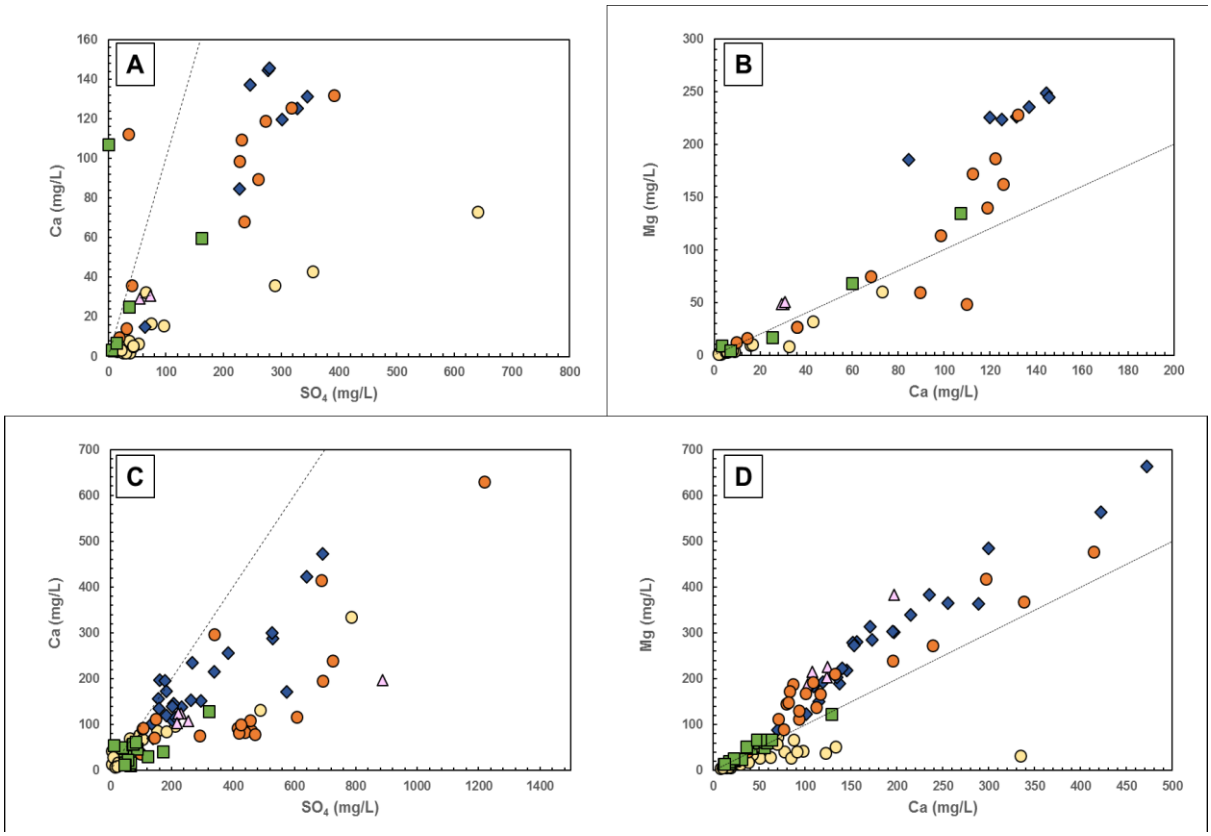


**Figure 32:** *Surface water scatter plots showing relationship between A) $Ca^{2+}$ and $SO_4^{2+}$;B) $Mg^{2+}$ and $Ca^{2+}$. Shallow groundwater scatter plots showing relationship between C) $Ca^{2+}$ and $SO_4^{2+}$; D) $Mg^{2+}$ and $Ca^{2+}$. Line: A) and C) = line of gypsum dissolution and line for B) and D) = line of dolomite dissolution. Blue diamonds = Kruismans, green squares = Verloren confluence, orange circles = Hol, pink triangles = Bergvallei, yellow circles = Krom Antonies.*

Sulphate is the second dominant anion after $Cl^-$ in both surface and shallow groundwater samples. High $SO_4^{2-}$ in waters can be accounted for by weathering of soluble sedimentary minerals that release $Ca^{2+}$, $Mg^{2+}$ and $SO_4^{2-}$ such as via dissolution of gypsum ($CaSO_4.H_2O$) or anhydrite ($CaSO_4$). Gypsum dissolution accompanied by calcite and dolomite precipitation is likely to occur in the Hol and Kruismans tributaries (have SI ≤ 0.1 for gypsum and SI ≥ 0.1 for calcite and dolomite), suggesting precipitation of these minerals may limit $Ca^{2+}$ concentration in both surface and shallow groundwater (Bouderbala, 2015; Bozdag & Goćmez, 2016;

Moussa et al., 2011; Benaabidale & Fryar, 2010). As gypsum has a higher solubility than calcite and the conditions are appropriate for gypsum, the dissolution of gypsum is given by equation:

$CaSO_4.H_2O_{(s)} \rightarrow Ca^{2+} + SO_{4(aq)} + H_2O$

Gypsum dissolution can be further supported by the occurrence of pure gypsum that has been found in the catchment, but has not been prospected (Sinclair et al., 1986). In addition, $Ca^{2+}$ and $SO_4^{2-}$ are correlated ($r^2 = 0.8$) (Figure 32A and C). Therefore, gypsum dissolution is favourable for higher sulphate concentrations observed in each tributary.

A study done by Demlie et al (2011) in the Berg River Basin, which is located in the Western Cape Province, showed that groundwater samples depicted similar hydro-chemical observations to this study, where, $Mg^{2+}$ is a dominant cation over $Ca^{2+}$, indicating a typical geological control in the composition of the water. In this study $Mg^{2+}$ is a dominant cation over $Ca^{2+}$ in both surface water and shallow groundwater samples, except for surface water and shallow groundwater samples in the Krom Antonies which show enrichment of $Ca^{2+}$ over $Mg^{2+}$. There is a strong positive correlation between $Mg^{2+}$ and $Ca^{2+}$ for surface and shallow groundwater samples indicating that such ions are derived from a common salt source, except for shallow groundwater samples in the Krom Antonies (Figure 32B and D).

The relationship between $Mg^{2+}$ versus $Ca^{2+}$ is usually investigated to determine the contribution of calcite and dolomite to water composition (Kumar et al., 2006). In this study, surface water samples in the Kruismans plot above the 1:1 line of dolomite dissolution and those of the Krom Antonies plot below the same line. Surface water samples of the Hol, Bergvallei and the Verloren confluence plot along the 1:1 dolomite dissolution line (Figure 32B), indicating contribution from dolomite dissolution. Shallow groundwater samples of the Kruismans, Bergvallei and the Hol tributaries plot above the 1:1 line of dolomite dissolution showing $Mg^{2+}$ enrichment relative to $Ca^{2+}$. Shallow groundwater samples of the Verloren confluence plot along the same line for both wet and dry sampling seasons. The excess $Mg^{2+}$ may indicate dolomite dissolution or dolomite-rich minerals (Ettazarini 2005; Kumar et al., 2006).

The Mg/Ca molar ratio is often used to explain the sources of $Ca^{2+}$ and $Mg^{2+}$ in groundwater. If the ratio Mg/Ca = 1, dissolution of dolomite should occur. Higher Mg/Ca molar ratio (> 2), indicates the dissolution of silicate minerals which contribute more $Mg^{2+}$ to the groundwater (Xiao et al., 2012). Surface water samples in all tributaries and the Verloren confluence show enrichment in $Mg^{2+}$ relative to $Ca^{2+}$ and high average Mg/Ca molar ratios between 2.99 and 1.46. Surface water and shallow ground water samples show Mg/Ca ratios varying between 1.71 and 0.16 with an average of 0.98 in the Krom Antonies. Shallow groundwater samples in

the Bergvallei, Hol and Verloren confluence depict higher Mg/Ca molar ratios ranging from 4.1 to 1.82 over a wide range of salinities (Table 4). Due to the variation of Mg/Ca ratios for surface water and shallow groundwater in all four tributaries it may be suggested that $Mg^{2+}$ enrichment maybe from dolomite dissolution and silicate weathering.

*5.2.3.2. Weathering and ion exchange processes*

Edmunds and Smedley (2000) observed that sodium concentrations in the Sherwood Sandstone Aquifer in the East Midlands, UK, were significantly higher in groundwater, which could be the result of dissolution of Na rich plagioclase feldspar present in the host lithologies. Krishnaraj et al. (2011) suggests that low molar ratio (<0.5) of $Ca/HCO_3$ measured in the water is due to the exchange of calcium and magnesium in water by sodium bound in clays. The $Ca/HCO_3$ high ratios (>0.5) suggests other sources for Ca and Mg, such as reverse ion exchange, which is observed in hard rock formations with an increase in salinity. In this study most of the surface and shallow groundwater samples show $Ca/HCO_3$ molar ratios greater than 0.5, suggesting that silicate weathering and dissolution of Ca and Mg rich carbonates are the predominate sources of $Mg^{2+}$ and $Ca^{2+}$.

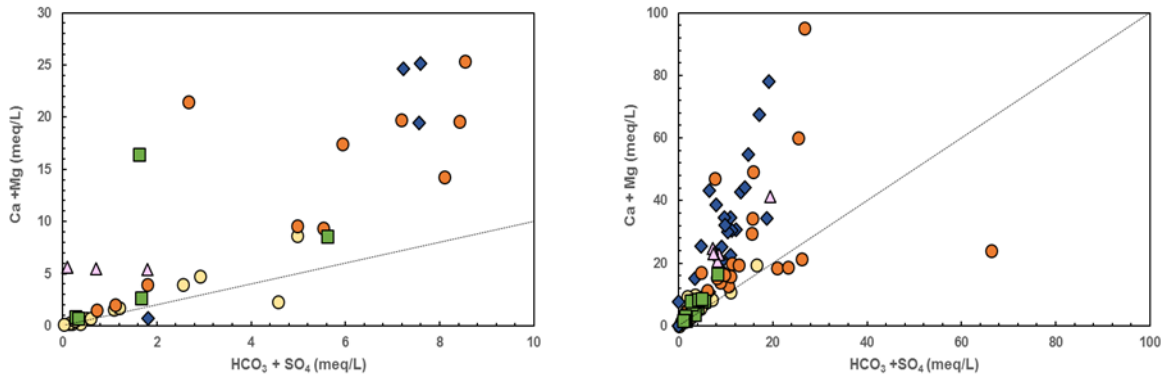


**Figure 33:** *Relationship between $Ca^{2+}$ + Mg2+ and $HCO_3^-$ + $SO_4^{2-}$. A) Surface water samples; B) shallow groundwater samples. Dotted line = 1:1 equiline. Blue diamonds = Kruismans, green squares = Verloren confluence, orange circles = Hol, pink triangles = Bergvallei, yellow circles = Krom Antonies.*

Sodium versus Cl plots (Figure 27A and 28A) shows that there is an overall dominance of $Cl^-$ as compared with $Na^+$, the depletion of $Na^+$ ions can be attributed to reverse ion exchange. However, the excess $Cl^-$ cannot be explained by a simple reverse ion exchange process in which $Na^+$ is replaced by $Mg^{2+}$ and $Ca^{2+}$ in the water. Calcium and magnesium versus $Na^+$ + $K^+$ reveals that overall alkali dominates over alkaline earth elements, supporting that reverse iron exchange is not a dominate process where $Na^+$ replace $Ca^{2+}$ and $Mg^{2+}$. Krom Antonies samples and three shallow groundwater samples of the Hol show that some of the samples show excess of $Ca^{2+}$ + $Mg^{2+}$ is favourable over $Na^+$ + $K^+$, concentrations of $Ca^{2+}$ and $Mg^{2+}$ as compared with $Na^+$ and $K^+$ can be attributed to base ion exchanges. Wherein, the $Na^+$ present

in groundwater is replaced by $Ca^{2+}$ and $Mg^{2+}$ at favourable exchange sights (Zaidi et al., 2015). Samples portraying Na/Cl ratios in excess of 1.0 imply that meteoric $Na^+$ $Cl^-$ is not a source of $Na^+$, but could be due to ion exchange between $Ca^{2+}$, and $Mg^{2+}$, releasing $Na^+$ (Bakari et al 2013). Sodium over chloride molar ratio greater than 1 is an indication of silicate weathering (Meybeck, 1987). This ratio should also decrease due to the cation exchange of $Na^+$ as water moves through the aquifer, which would explain $Cl^-$ enrichment in most water samples (Krishnaraj et al., 2011).

Furthermore, weathering of soda Feldspar (Albite) and Potash Feldspars may contribute $Na^+$ and $K^+$ ions to groundwater. Feldspars are more susceptible for weathering and alteration than quartz in silicate rocks and can be responsible for high concentrations of Na+ (Krishnaraj et al., 2011). The low ratio of K/Na in all waters supports weathering of illite with kaolinite which was observed by Edmunds and Smedley (2000).

Zhu et al. (2008) have shown that low Na/Cl ratios of groundwater probably result from ion exchange of $Na^+$ for $Ca^{2+}$ and $Mg^{2+}$ in clays. Exchange of calcium, magnesium for sodium on clay mineral surfaces and alteration of feldspar may account for low ratios lower than that of seawater (Ekwere, 2010). Clay minerals, such as kaolinte and illite are typically produced by weathering of feldspars and micas, predominant in marine clays and shales and are the most common ion exchangers in the soil and aquifer environments (Lakshmanan et al., 2003). The aquifer matrix of the study area is comprised of weathered feldspars and micas (clays) from micaceous shales, phyllites, schists, and greywackes as host lithologies (Visser &Toerien, 1971). The soils are almost entirely made up of quartzose sand and silt. The elemental composition of Peninsula Formation bedrock indicates high quartz content (98.8 wt% $SiO_2$) with minor amounts of feldspar and mica minerals (0.5 wt% $Al_2O_3$) (Soderberg &Compton, 2007). Albite weathering may be occurring in the sandstones, releasing $Na^+$, $HCO_3^-$ and montmorillonite according to the weathering reaction below (Sami 1990):

Albite: $2NaAlSi_3O_8 + 9H_2O + 2H^+ \rightarrow Al_2Si_2O_5(OH)_4 + 4H_4SiO_4 + 2Na^+$

Therefore, depletion $Ca^{2+}$ relative to $SO_4^{2-}$ (Figure 29 A and C) is probably due to the cation exchange reactions which absorbs $Ca^{2+}$ on the clay fraction as $Na^+$ is released into solution (Cheikh et al., 2012).

This can be accounted for by cation exchange reactions that occur as the water flows through the sands and shale units of the aquifer system. As infiltrating water encounters the sandstone unit, the water acquires small concentrations of $Na^+$ and $Ca^{2+}$ due to calcite (as cement) and feldspar dissolution (Edmunds & Smedley, 2000). On encountering the shale unit (containing some clay minerals), it is to be expected that $Na^+$ would be exchanged for $Ca^{2+}$ according to the generalized reaction equation: (

$2NaAlSi_3O + Ca^{2}+ \rightleftharpoons CaAlSi_3O + 2Na + 2NaAlSi_3O + Ca^{2}+ \rightleftharpoons CaAlSi_3O + 2Na^{+}$

thus, results in a slight increase in $Na^{+}$ concentration and a decrease in $Ca^{2+}$ (Utom et al., 2013).

Potassium is common in many rocks. Many of these rocks are relatively soluble and potassium concentrations in ground water increase with time. Potassium, an important component in fertilisers and is strongly held by clay particles in soil. Potassium increases with sodium concentrations and its concentration in surface water and shallow groundwater is due to silicate weathering of host lithologies

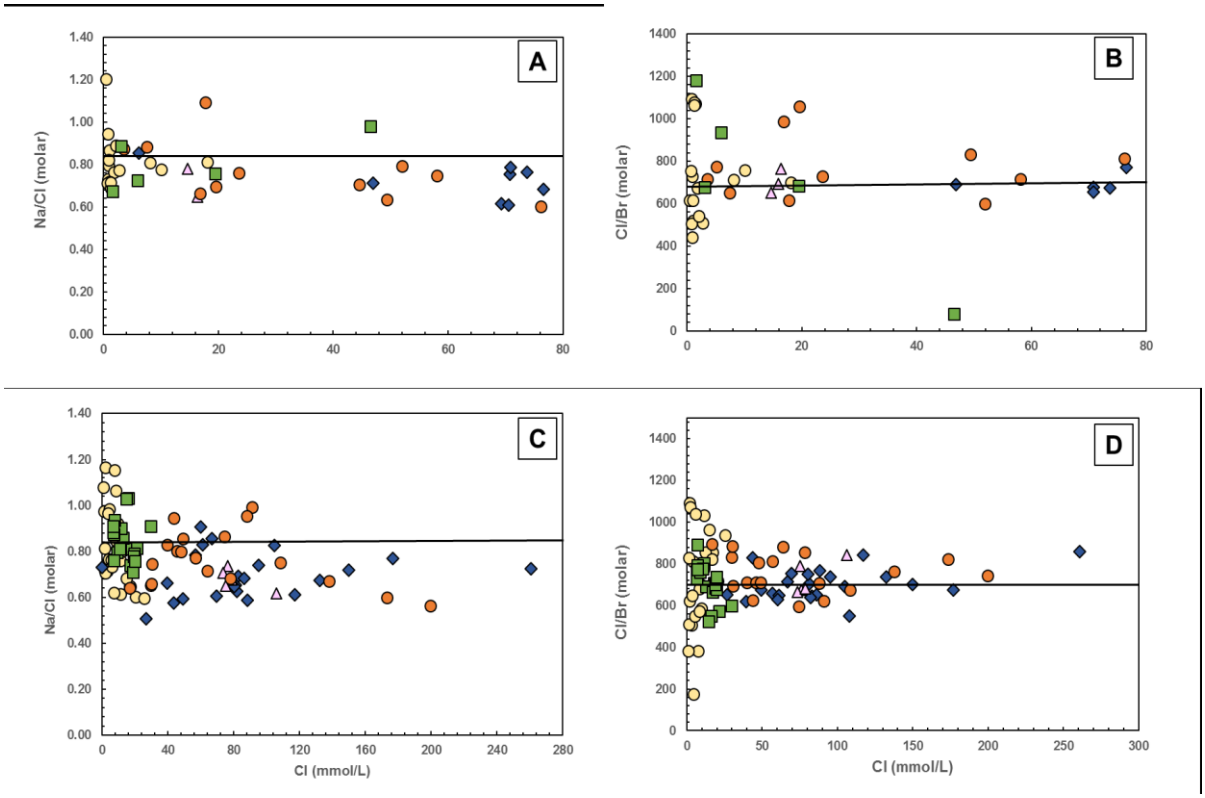


**Figure 34**: *Surface water relationship between A) Na/Cl molar ratios; B) Cl/Br molar ratios and Cl concentrations. Shallow groundwater relationship between C) Na/Cl molar ratios; D) Cl/Br molar ratios and Cl concentrations. Lines indicating sea water molar ratios, Na/Cl = 0.86 and Cl/Br = 655. Blue diamonds = Kruismans, green squares = Verloren confluence, orange circles = Hol, pink triangles = Bergvallei, yellow circles = Krom Antonies*.

Strontium isotopes ratios of the 16 shallow groundwater samples range from 0.7142 ±11.4 to 0.7159 ±9.6 and strontium concentrations ranging from 125.4 to 2468.8µg/L, in the Verloren confluence and Kruismans, respectively. The sixteen shallow groundwater samples have $^{87}Sr/^{86}Sr$ average ratios higher than that of modern seawater (0.709±0.710) and atmospheric deposition, indicating an influence from another $Sr^{2+}$ bearing source (Dagramaci and Skrztpek, 2015).

Other possible sources include observed high $^{87}Sr/^{86}Sr$ ratios, which may be referred to the weathering of silicates such as granite, which deliver $^{87}Sr/^{86}Sr$ ratios higher than 0.710 and up to 0.714 into the water (Brenot et al., 2015; Nègrelet al., 2004). The Riviera Granite of the Cape Granite Suit, intruded the Malmesbury Group rocks around 520 Ma and positioned in the upper-central valley, easterly of the Krom Antonies tributary. The A-type Riviera granite has been exposed due to prolonged erosion processes, this might explain the intermediate strontium ratios (0.7153) of shallow groundwater samples observed in the Krom Antonies. A study conducted by Frost and Toner (2004) in Wyoming, United States showed that samples of the Casper Formation sandstone and limestones displayed radiogenic $^{87}Sr/^{86}Sr$ ratios of 0.7115 to 0.7192 and were similar to the $^{87}Sr/^{86}Sr$ ratios in the groundwater that was interacting with the Casper Formation sandstones and limestones. Soderberg and Compton (2007) found that the $^{87}Sr/^{86}Sr$ ratios of Peninsula Formation (Table Mountain Group) soils, which also comprise soils of this study area ranged from 0.722 to 0.735.

Surface water samples show a strong positive correlation ($r^2$ =0.89) between $Sr^{2+}$ and $Cl^-$ and $Sr^{2+}$ and $Ca^{2+}$ (Figures 27H and 37A). Strontium concentration being proportional to the above mentioned elements reflects that part of the main source of salinity may provide $Sr^{2+}$ input to surface water (Brenot et al., 2015) Shallow groundwater also show a strong correlation between $Sr^{2+}$ and $Cl^-$ and $Sr^{2+}$ and $Ca^{2+}$ (except for Krom Antonies that shows a weak correlation between $Cl^-$, $Ca^{2+}$ and $Sr^{2+}$ (Figures 28H and 34B). This this might reflect a $Sr^{2+}$ input associated with weathering of host lithologies. In addition to the generally good correlation between $Sr^{2+}$ and $Ca^{2+}$ (Figure 37A and B) may be attributed to one or more of the following processes: silicate weathering, dissolution of carbonate or gypsum in the unsaturated zone and/or mineral reactions in the saturated zone (Monjerezi et al., 2011).

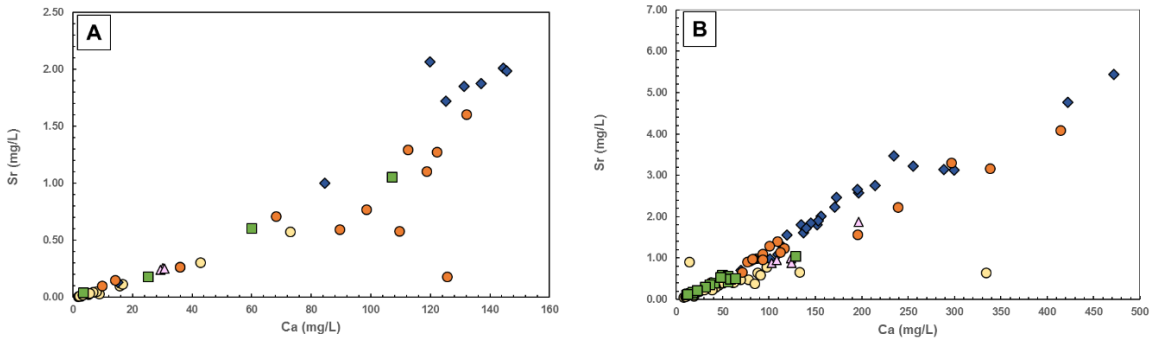


**Figure 35:** *Relationship between A) $Sr^{2+}$ for surface water; B) $Sr^{2+}$ for shallow groundwater and $Ca^{2+}$. Blue diamonds = Kruismans, green squares = Verloren confluence, orange circles = Hol, pink triangles = Bergvallei, yellow circles = Krom Antonies.*

Tritium concentration alone generally cannot be used to quantitatively date shallow groundwater, but can be used to qualitatively determine whether groundwater is modern (less

than 50 years in age) or pre-modern (older than about 50 years in age). All samples fall within a narrow concentration range from 0.5 ±0.2 to 1.5±0.3, with 30% of the samples having tritium concentrations below 1 TU were considered to indicate that the shallow groundwater is at least 50 years old (pre-modern). Tritium values equal to or greater than 1 TU were considered as modern water and comprise 70% of the samples representing recharge of meteoric origin. It is expected that high tritium values correspond to lower EC values and low tritium values to correspond with high EC and high tritium values (Ravikumar et al, 2011, Michel and Schroeder, 1994). Electrical Conductivity against Tritium plotted (Figure 37) to show if there is any relationship between tritium values and EC.

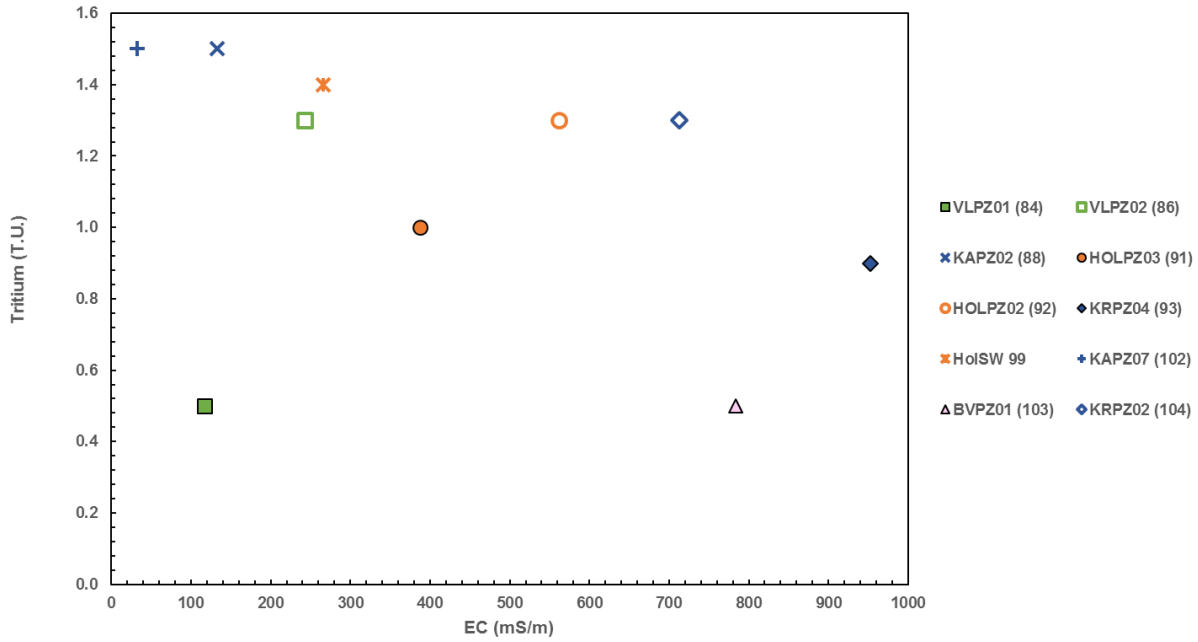


**Figure 36:** *Relationship between tritium and EC for selected shallow groundwater samples.*

Shallow groundwater samples in the Krom Antonies show high tritium values and low EC values, implying circulation of recharge waters. Shallow groundwater in the Kruismans (KAPZ04) show high EC and low tritium values may represent the deep circulating waters. Sample from KRPZ05 may imply evaporation concentrated salts dissolved by modern circulating waters giving and account for high EC and high tritium value. Shallow groundwater sample in the Bergvallei show low tritium value with high EC indicating deep groundwater with high EC percolating shallow groundwater. The fact that tritium concentration had a negative correlation with salinity reiterates that the groundwater is very young, and there is a component of the groundwater that has had more time to interact with the aquifer (Ravikumar et al, 2011).

## 5.3 Salt Load Transfer to Verloren River

The four main tributaries for the upper part of the Verlorenvlei catchment join at the confluence and thereafter form a single river system called the Verloren River, the latter feeding the Verloren estuarine lake (Figure 2). Management of the lake requires an understanding of how much each tributary contributes to the salinity of the Verloren River. In order to understand this, TDS and discharge in each tributary is quantified to obtain the amount of salt load each tributary may contribute into the Verloren confluence.

### *5.3.1 Determining representative TDS values*

High EC and TDS values are observed at the lower reaches of each tributary, during wet and dry seasons. Therefore, to calculate the salt load in each tributary, only TDS at the lowest sampled points in the lower reaches in each tributary close to the Verloren confluence is considered. These are, in the Kruismans TDS from piezometers KRPZ05 and KRPZ04 is considered. In the Krom Antonies TDS from the piezometers KAPZ01 and KAPZ02 is used, in the Hol and Bergvallei TDS from piezometers HOLPZ01 and BVPZ01 are considered, respectively. Figure 38 compares average TDS between tributaries and the Verloren confluence, the Kruismans show the highest average TDS value of 10383.6mg/L, implying that the Kruismans has the highest capacity to contribute to the TDS, whilst the Krom Antonies with the lowest TDS value of 1618.5mg/L, (Table 8) has the smallest capacity.

Verloren confluence show TDS value of 7905.79mg/l and an average TDS of 878.42mg/L. If all four tributaries contribute a certain amount of TDS into the Verloren confluence, it would be expected that the sum of TDS from each tributary be the same as the calculated TDS for the Verloren confluence.

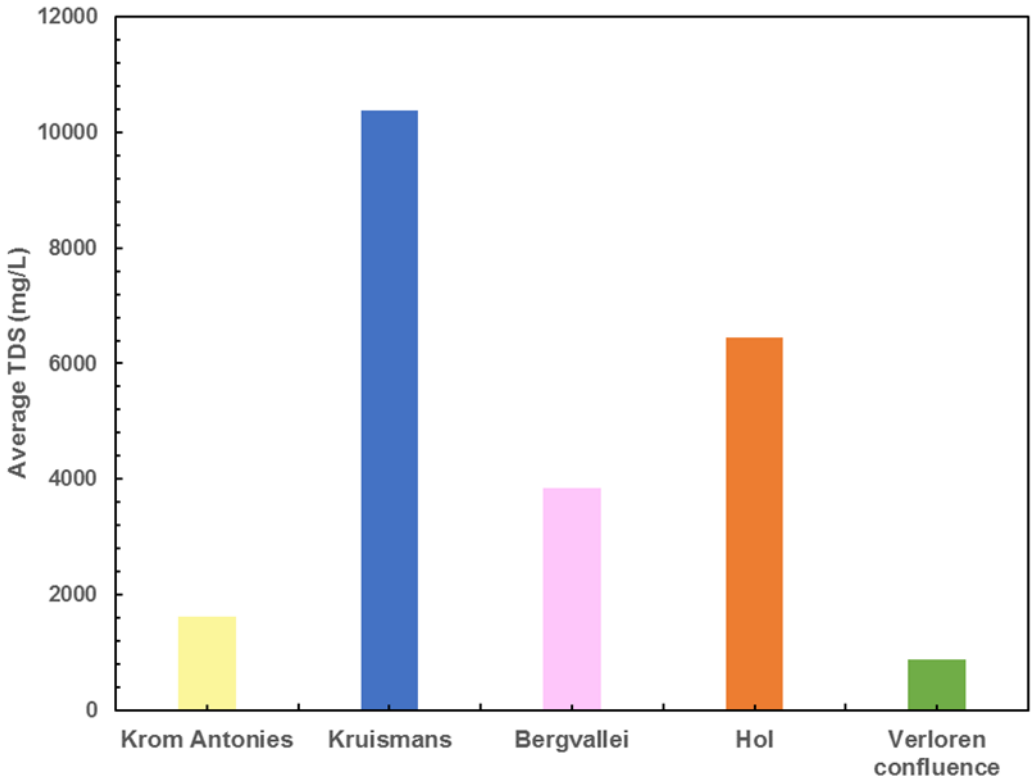


**Figure 37:** *Average TDS for surface and shallow groundwater for samples located at the lower reaches of each tributary near the Verloren confluence. To show how the average TDS in each tributary compare to that of the Verloren confluence.*

### *5.3.2 Determining mixing relationships*

To evaluate the possibility of mixing relationships, the strontium isotopic ratio and strontium concentration of the mixed Verloren Rive and Verloren confluence water is plotted in Figure 40. There are two independent methods that have been used to calculate the relative components for mixing relationship. Method one uses only strontium isotope data and method two uses strontium isotope data and percentage discharge data.

Method 1

This systematic isotope mixing has been described in detail by Faure (1986) and conventionally expressed as follows:

$^{87}Sr/^{86}Sr_m \times [Sr]_m = \alpha\ (^{87}Sr/^{86}Sr_1 \times [Sr]_1 + (1 - \alpha)\ (^{87}Sr/^{86}Sr_2 \times [Sr]_2)$.

Where $^{87}Sr/^{86}Sr_m$ is the measured isotopic ratio in the mixture, $^{87}Sr/^{86}Sr_1$ and $^{87}Sr/^{86}Sr_2$ represent the isotopic ratios of the first and second end-members, respectively, and $[Sr]_m$, $[Sr]_1$, and $[Sr]_2$ are the Sr concentrations of the mixture and the first and second end members, respectively (Frost and Toner, 2004). The mixing parameter α, which is derived from Equation (1), is represented by: $Sr_1/ (Sr_1 + Sr_2)$ and 1-α by $Sr_2/ (Sr_1 + Sr_2)$; α represent the proportions of the two components in the mixture ($0 < \alpha < 1$). When calculated (Appendix 2), α = 0.354,

therefore, $0 < \alpha < 1$. The Kruismans and the Krom Antonies represent their proportions in the mixture, implying that there is a mixture between Kruismans and Krom Antonies shallow groundwater, to give shallow groundwater in the Verloren confluence (VLPZ02 (C1)) its chemical composition. The limitation for this method is that there is no mixing for three component system. The 16m deep borehole in the Bergvallei which is within the primary aquifer has average $^{87}Sr/^{86}Sr$ ratio of 0.00797 and $Sr^{2+}$ concentration of 126.5µg/L. The Hol and the Bergvallei deeper primary aquifer (16m) represent their proportions in the mixture of VLPZ01 (C3), with $\alpha = 1$, this supports the mixing between the two components.

Method 2

Discharge data as a percentage from each tributary was assigned to a component in order to get the mixed strontium isotope and strontium concentration for C1, C2 and C3 (Figure 39). The calculation below has been used to calculate the different mixing components for C1, C2 and C3:

$$^{87}Sr/^{86}Sr_m = \Sigma ((^{87}Sr/^{86}Sr_1 \times Q_1 / 100) + (^{87}Sr/^{86}Sr_2 \times Q_2 / 100) + (^{87}Sr/^{86}Sr_3 \times Q_3 / 100))$$

$$Sr_m = \Sigma ((Sr_1 \times Q_1 / 100) + (Sr_2 \times Q_2 / 100) + (Sr_3 \times Q_3 / 100))$$

Where m is the mixed component (C1, C2, C3); 1,2 and 3 are the mixing components and Q is the percentage discharge of a mixing components.

To obtain $^{87}Sr/^{86}Sr$ and Sr concentration for C1 (0.71550, 0.00207µg/L) a 65% discharge from the Krom Antonies and 35% discharge from the Kruismans has been used to generated C1 mixed strontium isotope ratio and Sr ion concentrations. To obtain $^{87}Sr/^{86}Sr$ and Sr concentration for C2 (0.71454, 0.00444) a 36% discharge from the Krom Antonies, 23% discharge from the Hol and 41% discharge from the Bergvallei has been used to generated C2 mixed strontium isotope ratio and Sr ion concentrations. To obtain $^{87}Sr/^{86}Sr$ and Sr concentration for C3 (0.71418, 0.00797), 3% discharge from the Hol and 97% discharge from the Bergvallei has been used to generated C3 mixed strontium isotope ratio and Sr ion concentrations (Figure 39). The strontium isotope data confirms that the Bergvallei may contribute the most discharge and instead of the Krom Antonies the Bergvallei water alters the chemical composition of water in the Verloren confluence. The EC for the Bergvallei borehole (16m deep) ranges from 38.3 to 111.5mS/m (Eilers, 2018), this may explain the low EC and TDS values in the Verloren confluence.

These two methods indicate a high level of agreement, in which they show mixing between tributaries to obtained mixed components C1, C2 and C3, meaning the two independent methods confirm the robustness of the results.

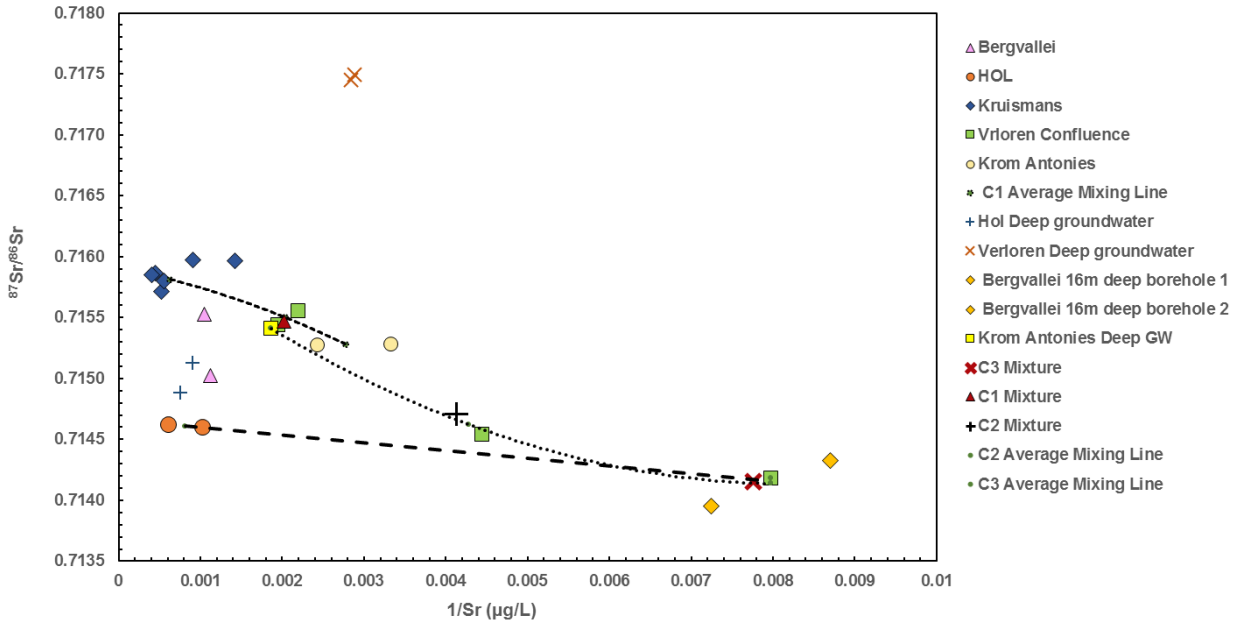


**Figure 38:** *Relationship between $^{87}Sr/^{86}Sr$ ratios and 1/Sr concentration. Dotted lines showing mixing relationships. Square dotted line: C1 mixing line; Round dotted line: C2 mixing line; dash line: C3 mixing line.*

### *5.3.2 Assessing tributary salt loads to total salt flux*

The discharge data shows that from 2010 to 2016 (Figure 44B) 40% of the discharge is from the Krom Antonies, 34% of the discharge is from the Bergvallei, 22% and 4% discharge if from the Hol and the Kruismans, respectively. The discharge from each tributary varies yearly, with the Krom Antonies and the Bergvallei showing the highest discharge values from 2010 to 2016 (Figure 20). Figure 40 and 41 shows that during the dry season months of October 2013 to April 2014, interflow is the dominant output in discharge, and that during the wet season there is an increase in interflow and surface runoff. Most of the discharge is during the wet seasons and the same trend is observed for interflow and surface runoff in all tributaries (Figure 42 and 43).

Figure 42A show that after a rainfall event, surface and interflow increase and leads to a decrease in TDS (9/9/2015). Periods of dry season is associated with high TDS, low interflow, a decrease in the surface runoff and also a decline in the water level (Figure 44). Figure 44 shows that shallow ground water level responds to rainfall, which explains seasonal variation in TDS. After high rainfall TDS will decrease due to dilution and salts that had accumulated during the dry season and are mobilised downstream of each tributary (Figures 42,43 and 44). Figure 42 and 43 show that in July 2015 there was an increase in the interflow and surface runoff with an increase in TDS, this suggests build of salts down the tributary after a rainfall

event. Figure 42A and 43B shows that interflow in the Hol and Krom Antonies is a prominent discharge during dry and wet periods, this might explain the quick response in water level in the Krom Antonies (Figure 44) after rainfall. Figure 45A assesses whether there is a relation between TDs and discharge, there is no observable trend. However, Hol and Kruismans show high TDs associated with low discharge, this may be during the dry season when discharge is low and the main mechanism driving high TDS or salinity is evaporation.

The total salt output from each tributary may be quantified using streamflow quantity and salinity data sets, i.e. the salt load is equal to the product of the discharge (%) and the corresponding stream water salinity (TDS, mg/L).

$$SL = TDS\ x\ Q$$

where SL is the salt load (mg/L), TDS is the total dissolved solids (mg/L) and Q is the discharge (%). The TDS was inferred from the sum of all cation and anions which was previously mentioned in the methods and material section.

Table 8 show salt load contribution from each tributary using the average TDS and average discharge for 2015 and 2016, in which the Kruismans contributes 54% of salt load, 5.3% salt load from the Hol, the Bergvallei and the Krom Antonies contribute 35% and 6.2% of salt load, respectively. Calculations show that from the year 2015 to 2016 which were sampling years for this study, the Kruismans would contribute 192950.9ton/year of salt load, the Hol would contribute 19069.7ton/year of salt load and the Krom Antonies would contribute the least of salt load of 22296.2ton/year into the Verloren confluence. The Bergvallei would contribute about 126320.2ton/year (Figure 45B). The tributary salinity and salt loads would decrease during high flow events, because of the increased dilution capacity; however, large stream flow events can still deliver considerable salt loads. These values are higher compared to those recorded by Bugan et al. (2015) in the Sandspruit catchment, where the salt loads ranged between 12 671 ton/year and 21 409 ton/year, and much larger than that reported by Jolly et al (2001) for the Murrumbidgee catchment (155 $km^2$) in Australia, which had a mean of 2626 ton/year.

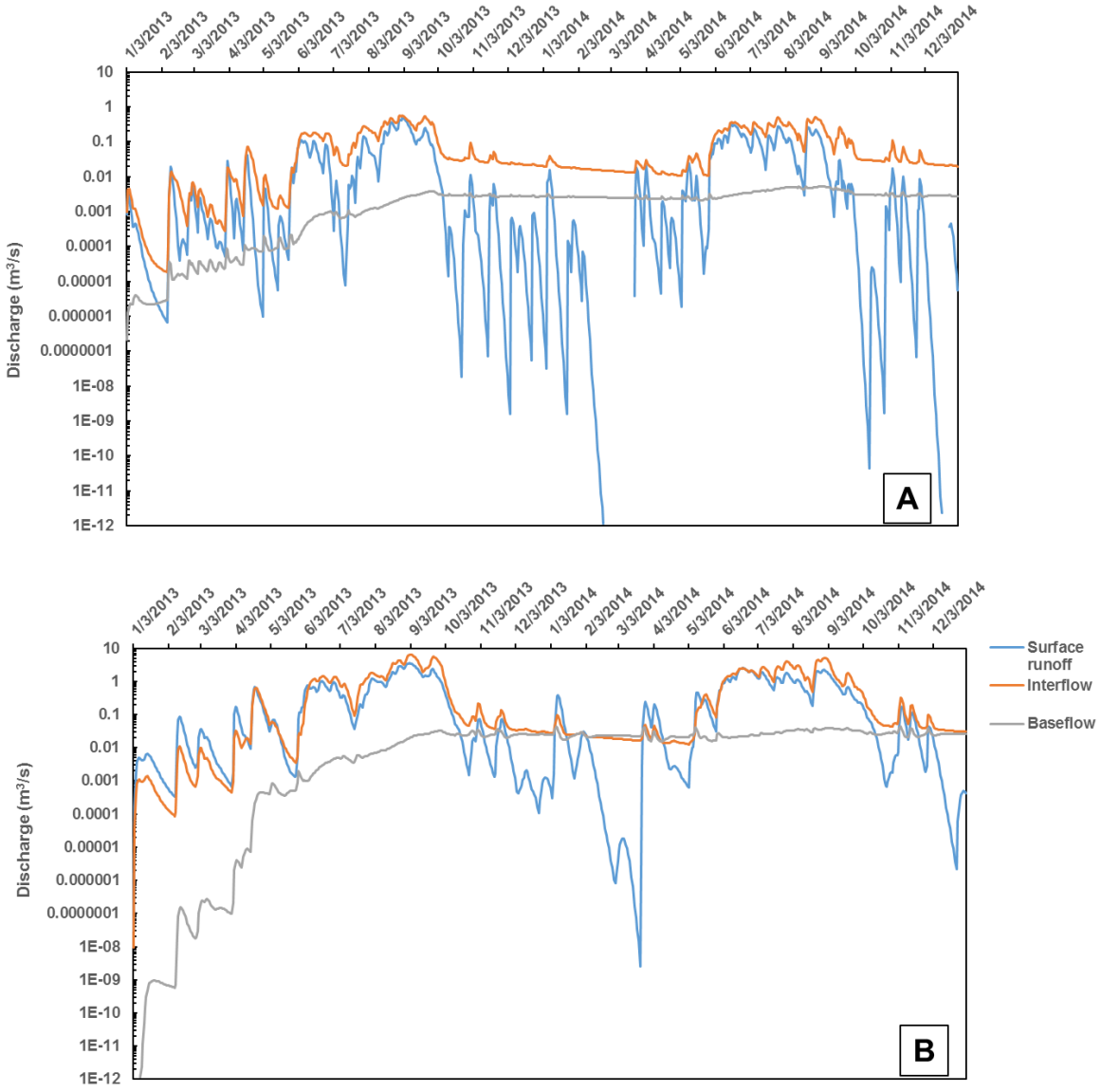


**Figure 39:** *Tributary discharge data: A) HoI discharge data for surface runoff, interflow and baseflow from 2013 to 2014; B) Kruismans discharge of surface runoff, interflow and baseflow from 2013 to 2014. No TDS data from 2013 to 2014. Data obtained from Fleischer et al. unpublished data.*

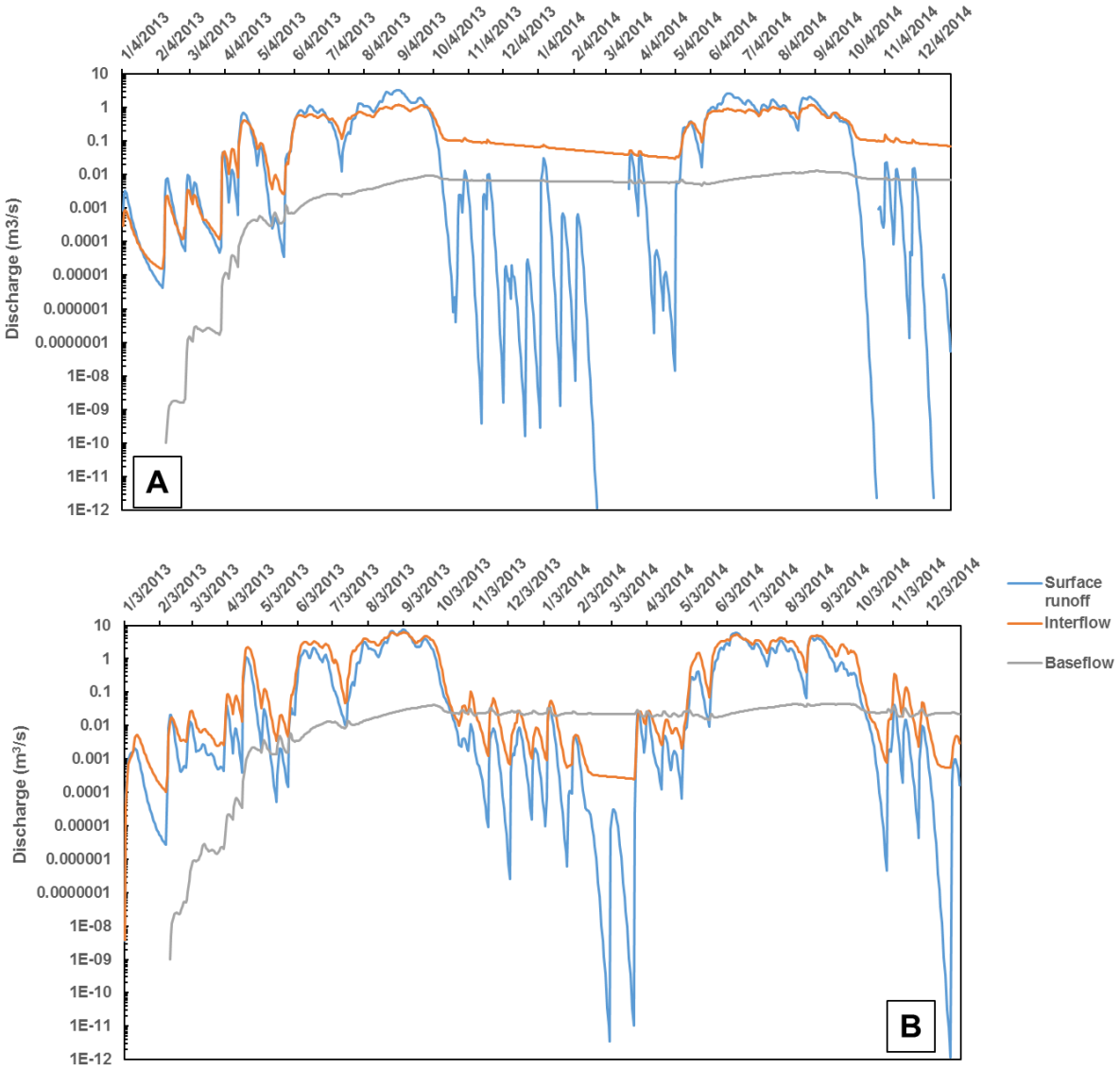


***Figure 40:*** *Tributary discharge data: A) Krom Antonies discharge of surface runoff, interflow and baseflow from 2013 to 2014; B) Bergvallei Depicting discharge of surface runoff, interflow and baseflow from 2013 to 2014. No TDS data from 2013 to 2014. Data obtained from Fleischer et al. unpublished data.*

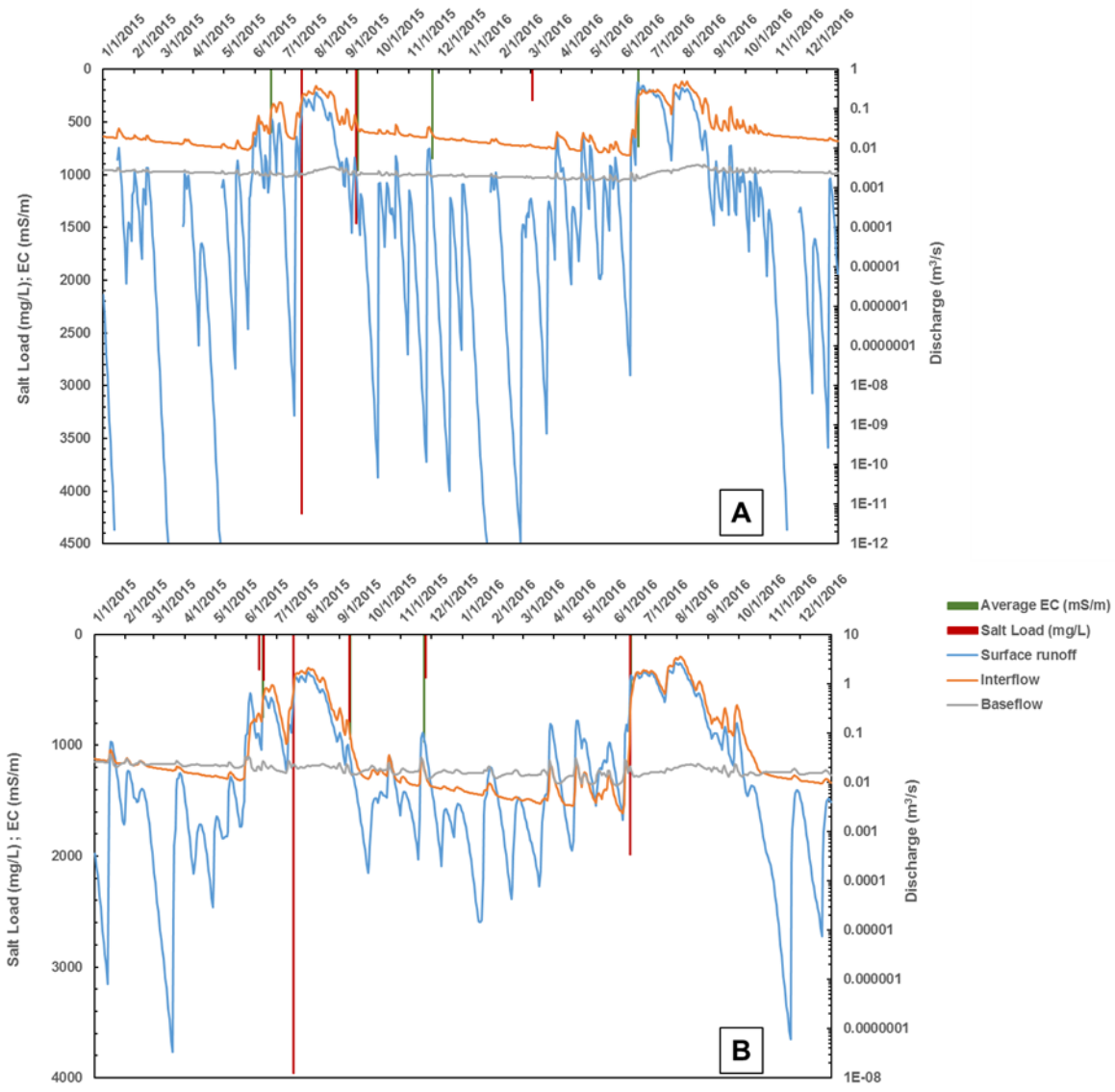


**Figure 41:** *Tributary discharge data: A) Hol discharge data for surface runoff, interflow and baseflow from 2015 to 2016 along with salt load and EC values at each sampled dates; B) Kruismans discharge of surface runoff, interflow and baseflow from 2015 to 2016 and salt load and EC values at each sampled date. Data obtained from Fleischer et al. unpublished data.*

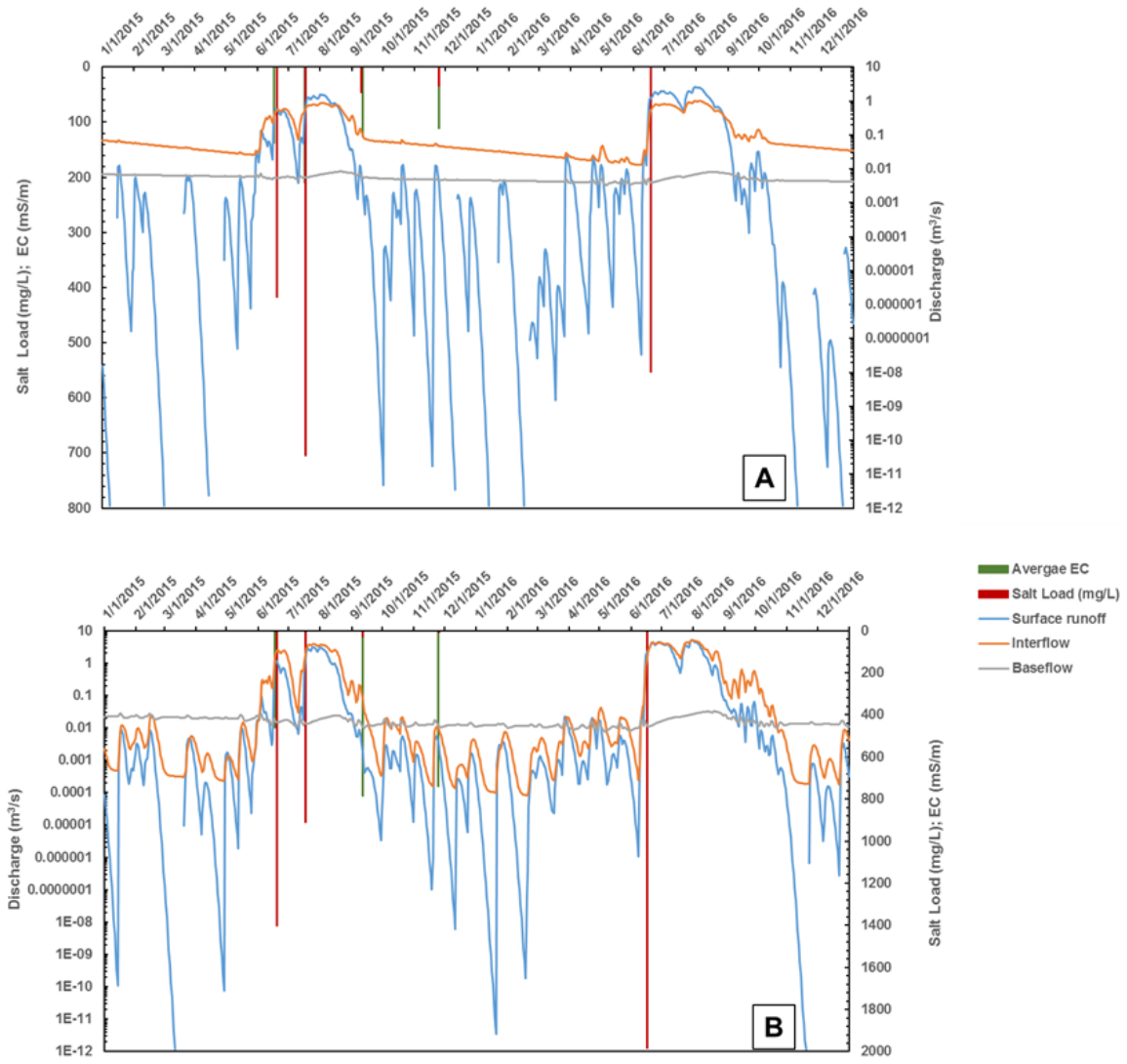


**Figure 42:** *Tributary discharge data: A) Krom Antonies discharge of surface runoff, interflow and baseflow from 2015 to 2016 and salt load and EC values at each sampled date; B) Bergvallei Depicting discharge of surface runoff, interflow and baseflow from 2015 to 2016 and salt load and EC values at each sampled date. Data obtained from Fleischer et al. unpublished data.*

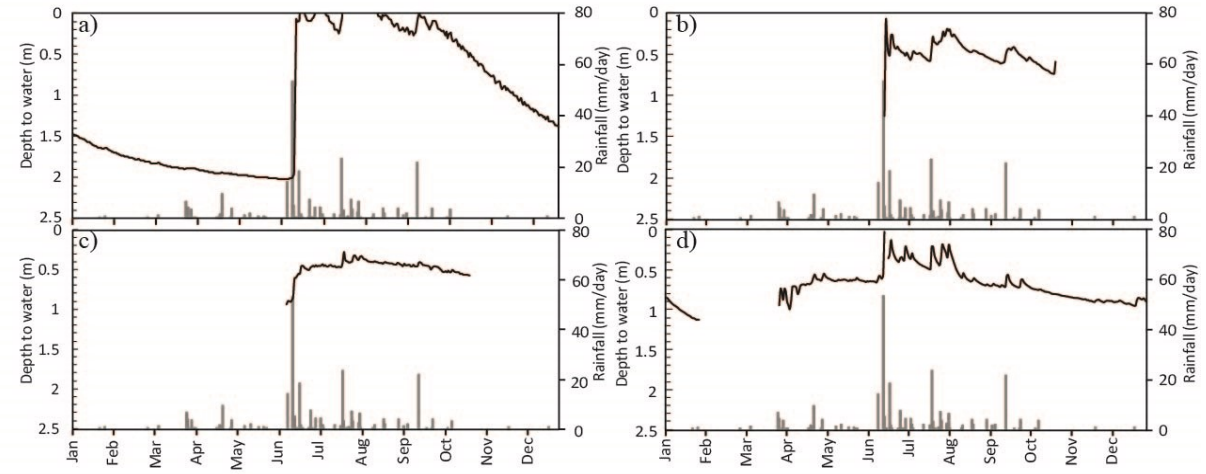


**Figure 43:** *Relationship between shallow groundwater level fluctuations and rainfall for 2016. A) Water level in the Verloren confluence (level logger = VLPZ01); B) Water level in Kruismans (level logger = KRPZ02.; C) water level in the Hol (level logger: HOLPZ03); D) water level in the Krom Antonies (level logger= KAPZ04) (Watson et al., Submitted).*

**Table 8:** *Overall average discharge ( Surface runoff + interflow + base flow) for each tributary during 2015 to 2016.*

| | Krom Antonies | | Kruismans | | Bergavallei | | Hol | |
|---|---|---|---|---|---|---|---|---|
| **TDS (mg/L)** | | | | | | | | |
| | Max | 2842.4 | Max | 20094.8 | Max | 5723.9 | Max | 7120.8 |
| | Min | 1091.7 | Min | 14087.4 | Min | 3008.1 | Min | 5614.4 |
| | Average | 1618.5 | Average | 10383.6 | Average | 3839.2 | Average | 6457.0 |
| | | | | | | | | |
| **Average Discharge ($m^3/s$)** | | 0.396 | | 0.535 | | 0.947 | | 0.085 |
| | | | | | | | | |
| **Salt load (ton/year)** | | 22296.2 | | 192950.6 | | 126320.2 | | 19069.7 |

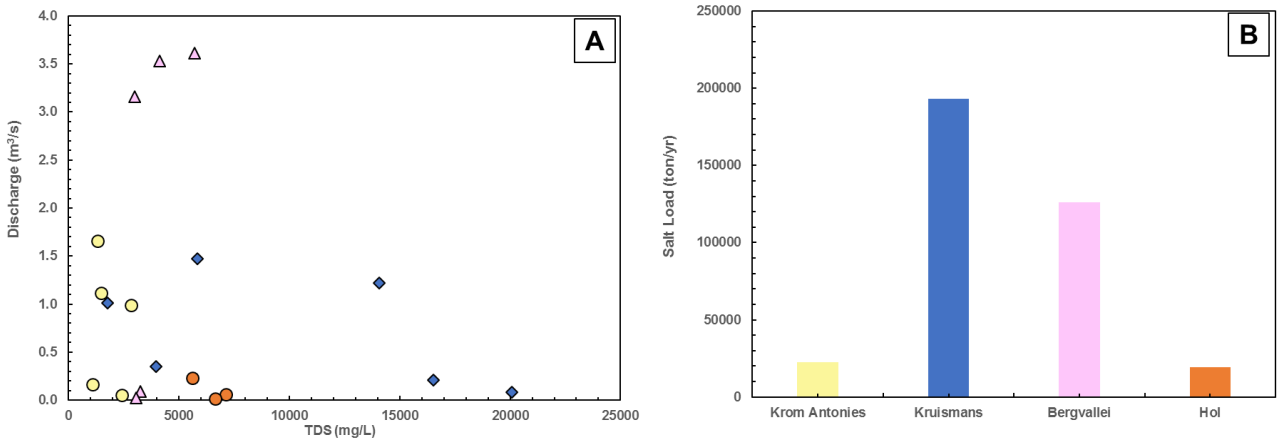


**Figure 44:** *A) Relationship between TDS and average discharge from 2015 to 2016. Blue diamonds = Kruismans, orange circles = Hol, pink triangles = Bergvallei, yellow circles = Krom Antonies. B) the relative contribution of the overall discharge from each tributary from 2010 to 2016. C) The relative salt load contribution for each tributary from 2015 to 2016. Data was obtained from Fleischer et al. unpublished data.*

## 5.4 Implications for the Verlorenvlei Estuarine Lake

The Verlorenvlei estuarine lake is a natural, semi-fresh lake, which hosts a wide diversity of terrestrial and aquatic species. The Verloren River and its tributaries is intermittent, feeding the lake during rainfall months of winter and early summer, providing freshwater into the lake system (Meadows & Baxter, 1996). Therefore, the lake experiences large fluxes in physiochemical characteristics, including fluctuations in salinity both temporally and spatially as a result of several factors. These include ingress and mixing with sea water, evaporation, and salt transported into the lake from terrestrial sources. The EC of the lake has been recorded to range from 204 to 318mS/m, which is lower than that observed in Verloren River tributaries. In normal lake functioning conditions, the salinity declines with increasing distance from the sea and the ionic concentrations of Na, K, Ca and Mg deviate from that of the sea and that of the river water (Sinclair, et al., 1986). The EC and TDS observed in the Verloren confluence in this study shows that the water in the Verloren River can be categorised as freshwater, suggesting that the salt load contributed from the tributaries into the Verloren River may have little impact on lake's salinity increase.

Verlorenvlei estuarine lake normally functions as a freshwater system: the mouth is perched and only allows occasional seawater inflow during high spring tides and stormy conditions at sea. When water levels in the vlei are high, there is a continuous discharge to the sea maintaining freshwater dominated conditions that were observed in September 1985, September 2002 and November 2008 (CSIR, 2009). When the water level in the vlei drops, the outflow to the sea no longer occurs creating a stagnant water body in the lower reaches. During these low water levels, the shallower areas in the lake become more saline, even hypersaline when interchanges of freshwater between the larger vlei and these shallow regions are no longer sufficient to counterbalance salt build-up associated with occasional overwash and evaporation. Such conditions are evident as a result of droughts and marked by a drop in water levels. If the lake were to be hypersaline as a result of prominent factors such as drought, floods and evaporation due to climate change, and secondary salinization, the impact on the flora and fauna of the lake will be significantly threatened (Cyrus et al., 2011).

Climate change is predicted to alter precipitation patterns, which will affect the quality, rate, magnitude and timing of freshwater delivery to estuaries, and will potentially exacerbate human modifications of these flows (Engelbrecht et al., 2011). The Verlorenvlei lake is situated in a semi-arid region, and is subject to high evaporation rates of up to 2400mm/year (Meadows et al 1996), with average rainfall of less than 300mm/per annum, and vulnerable to climatic conditions such as floods and droughts. The water level of the vlei fluctuates as a result of several factors, in 2015 and until mid- summer 2016 the vlei was experiencing very low water

levels, this was also observed in 1981, in which, the lake was completely dry due to drought conditions (Sinclair, et al, 1986). In 2004, 2005 and 2015 a significant drop in the water level was recorded due to drought conditions (Watson et al., Submitted). Consequently, floods and droughts have a strong impact on modifying water quality through dilution or concentration of dissolved salts. (Delpla, et al., 2009). Downscaled regional climate models derived from global climate models indicate the likelihood of increased summer rainfall over the eastern part of South Africa and a slight decrease in wintertime frontal rainfall (during the latter half of winter) in the Western Cape (Engelbrecht et al., 2011). The functioning of estuaries is strongly influenced by the magnitude and timing of freshwater runoff reaching them. Reductions in the amount of freshwater also as runoff (Figure 45) entering the estuarine lake would lead to an increase in the frequency and duration of estuary mouth closures and changes in the extent of seawater intrusion, nutrient levels, suspended particulate matter load, temperature, conductivity, dissolved oxygen and turbidity (Cyrus et al., 2011).

Schulze et al (2005) assessed the impacts of climate change (including rainfall) on South Africa's water resources and predicted that future climate may be characterized by 'hotspots' of hydrological change, one being the present winter rainfall region of the Western Cape. A high change in temperatures is noticeable in southern Africa, with climate change models also predicting an increase in extreme rainfall events which would lead to flooding conditions. Flooding events would allow for a higher mobilisation of salts, which may result in the increase of salinity as high salt loads would be flushed into the Verloren River later into the lake.

The degradation of the Verlorenvlei health is largely attributed to: 1) significant reduction in the freshwater inflow (ground- and surface water) to the system; 2) a decrease in open mouth conditions (i.e. frequency and duration); 3) increase in the nutrient and sediment load to the system; 4) increased coverage by reeds and sedges and changes in the species composition and abundance of fish in the system (CSIR, 2010). The lake is part of the Ramsar listed wetlands, different conservative measures have been taken by the government to improve the health of the wetlands, for example the removal of bridges to obtain better flow in the lake as it used to act as an obstruction for water circulation. Furthermore, increasing the salinity of lake. Continuous monitoring of the key biotic and abiotic components of the lake would help, better understand the functionality of the lake, which will better management implementation strategies (CSIR, 2009).

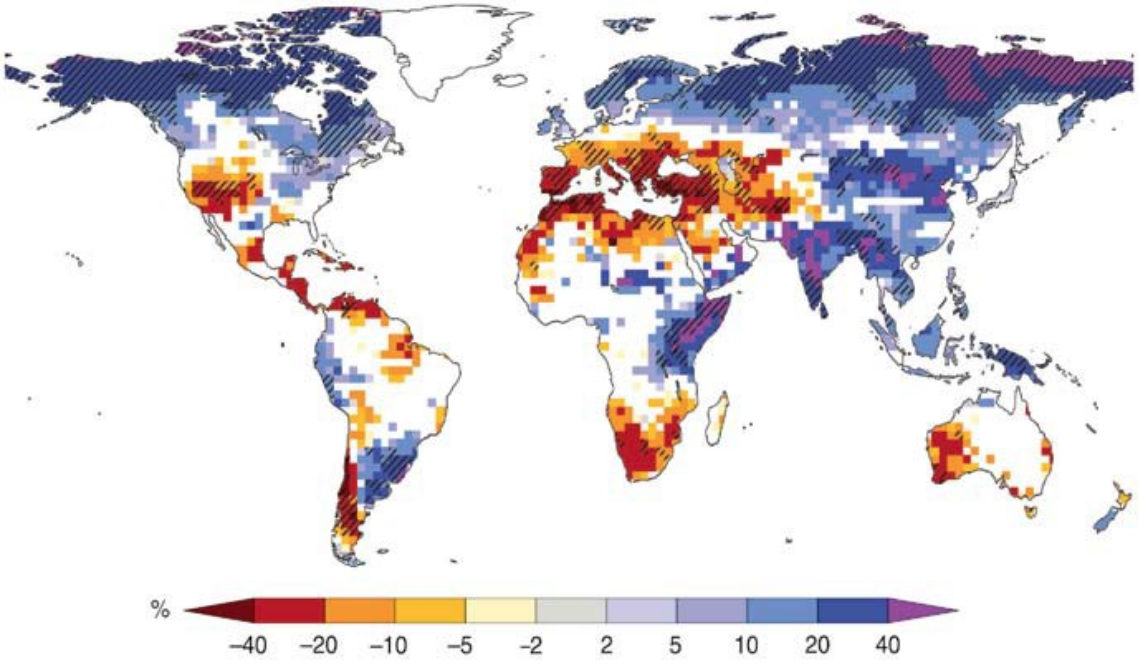


**Figure 45:** *Large-scale relative changes in annual runoff for the period 2090–2099, relative to 1980–1999. White areas are where less than 66% of the ensemble of 12 models agree on the sign of change, and hatched areas are where more than 90%of models agree on the sign of change (Milly et al., 2005; Bates 2009).*

# 6. CONCLUSIONS

## 6.1 General Conclusions

The aim of this study was to characterise the nature of salinity within surface water and shallow groundwater in the catchment to the Verlorenvlei estuarine lake. To achieve this, a number of different geochemical tools have been employed, to achieve the objectives of the study. Surface water samples were collected when the tributaries were flowing and shallow groundwater samples were collected from installed piezometers along each tributary.

In general, surface water had low EC and major ion concentrations compared to that of shallow groundwater, with the highest TDS values in the Kruismans and the least TDS values in the Krom Antonies and Verloren confluence. The average pH ranged from 6.5 to 7.2 suggesting slightly acidic to near neutral nature of water. Based on the physiochemical parameters surface water in the Krom Antonies was classified as freshwater and that of the Bergvallei, Kruismans and Hol were classified as brackish water. Therefore, during the winter season farmers resolve to the use of surface water in the Krom Antonies for irrigation purposes. Analysed trace elements for surface water and shallow groundwater samples in all the tributaries fall within the acceptable limits set by the WHO and SAWG. Spatial and seasonal variation was verified by high standard deviation in EC, major cations and anions concentrations. The EC and ion concentrations for surface water fluctuated down each tributary, with the highest concentrations recorded during the dry season of November 2015 and low ion concentrations during the wet season of June 2016. Shallow groundwater levels decreased during the dry season and increased during the wet season; the rising of water levels was associated with high EC values and the falling of the water level was also associated with high EC values.

The order of most dominant to least dominant cations and anions for surface water and shallow groundwater is, $Na^+ > Mg^{2+} > Ca^{2+} > K^+$ and $Cl^- > SO_4^{2-} > HCO_3^- > NO_3^- > PO_4^{3-}$, respectively. Surface water and shallow groundwater in the Hol, Kruismans, Bergvallei, Krom Antonies and the Verloren confluence can be characterised as Na-Cl water type on the Piper diagrams, which is supported by the “Y” shaped Stiff diagrams. Two surface water samples in the Krom Antonies had $Ca^{2+}$ and $HCO_3^-$ as a dominant ion, which resulted in Ca-$HCO_3$ water type, implying infiltration of recent freshwater in the tributary. One surface water sample in the Krom Antonies reflected Na-HCO3 water type suggesting cation exchange processes of salinisation.

Interaction with the aquifer matrix, evaporation, and precipitation-dissolution control the hydrochemistry of surface water and shallow groundwater. By plotting the major ion as a function of $Cl^-$, imply that $Na^+$, $Mg^{2+}$, $Ca^{2+,}$ $SO_4^{2-}$ $Br^-$ and $Sr^{2+}$ share a common salt with $Cl^-$, as these ions show a strong positive correlation with $Cl^-$. Nitrate concentrations in the study area is probably due to use of fertilisers on the agricultural farms. Phosphate concentrations may also be due to use of fertilisers, although low phosphate concentrations may be accounted for by the presence of phosphate which were observed on sediments of the TMG. Surface water and shallow ground water in the Krom Antonies, Kruismans, Hol, Bergvallei and the Verloren confluence deviate from the seawater line, suggesting that seawater may not be the major source of salinity.

Possible precipitation–dissolution processes were assessed using saturation indices and cation and anion relations. Saturation indices indicated under-saturation with respect to halite, gypsum, anhydrite and in some samples in the Hol, and Kruismans over-saturation in calcite and dolomite. Due to low (Na/Cl<1) ratios and the fact that surface water and shallow groundwater samples did not plot on the 1: 1 line of halite dissolution, halite was not a likely source of salinity. However, the strong positive correlation between Ca and $SO_4$ ions, the dominance of $SO_4^{2-}$ over $Ca^{2+}$and the documented presence of gypsum in the study area, may suggest the possibility of gypsum dissolution in association with calcite precipitation. The presence of limestones and dolomitic limestones have been documented in the study area. The presence of Mg and Ca ions may be due to dissolution of dolomite of the Malmesbury Group, hence the high Ma/Ca molar ratios (1 to 4). In this study most of the surface and shallow groundwater samples show $Ca/HCO_3$ molar ratios greater than 0.5, suggesting that silicate weathering and dissolution of Ca and Mg rich carbonates are the predominate sources of $Mg^{2+}$ and $Ca^{2+}$. Reverse ion exchange process may also explain enrichment of Mg + Ca ions in excess relative to $HCO_3$ + $SO_4$ ions. However, Na + K ions are in excess relative to Mg + Ca ions, implying that the source of $Na^+$ and $K^+$ is due to weathering of feldspars and micas, and $Ca^{2+}$ may be absorbed on clay fraction as $Na^+$ is released. This is shown by low tritium values and high EC values implying longer residence times for interaction.

The Gibbs plot was used to assess the different mechanisms in each tributary and surface water and shallow groundwater of the Kruismans, Hol and Bergvallei plot at the evaporation dominance zone, implying that evaporation is the dominant mechanisms for salt concentration. The evaporation process as a dominant process in these waters can be supported by surface water and shallow groundwater in the Hol and Kruismans being saturated with respect to calcite and dolomite, as these are the first minerals to precipitate during evaporation. Stable isotopes also support evaporation as surface water samples show deviation and lower slopes relative to the LMWL and GMWL and the evaporation trend is

evident from Figure 34. Surface water and shallow groundwater in the Krom Antonies and the Verloren confluence show that majority of the waters plot in the rock dominance zone with some waters in the evaporation dominance zone.

Variation in Cl/Br and Na/Cl molar ratios for surface water and shallow groundwater in the Krom Antonies, suggests different processes. These may be due to atmospheric contribution through precipitation resulting to low Cl/Br ratios and Na/Cl ratios close to that of sea water and high ratios Na/Cl ratios suggesting silicate weathering processes. Verloren confluence Na/Cl and Cl/Br ratios increase with salinity and Cl ion suggesting mixing of different waters with low EC and ion concentration. The support of mixing is explained by strontium isotopes which show mixing of shallow groundwater of Krom Antonies and the Kruismans to give strontium isotope ratios for salinity observed in VLPZ02 and the Bergvallei 16m deep shallow groundwater mixing with the Hol contributes observable salts in the Verloren confluence,

One of the objective in the study was to quantify how much salt load each tributary may contribute to the Verloren confluence. Based on discharge and TDS calculations, the Kruismans would contribute 192950.9 ton/year of salt load, the Hol would contribute 19069.7 ton/year of salt load and the Krom Antonies would contribute the least of salt load of 22296.2 ton/year into the Verloren confluence. The Bergvallei would contribute about 126320.2ton/year. A semi-arid country like South Africa is particularly vulnerable to climate change because less than 9% of annual rainfall ends up in rivers and nationally only 5% reaches aquifer systems as recharge. Furthermore, changing precipitation patterns are most directly observed through the higher frequency of flood and drought events in South Africa in recent years. Consequently, floods and droughts having a strong impact on modifying water quality through dilution or concentration of dissolved salts. This would promote evaporation and evapotranspiration which in turn would elevate concentrations of major ions and salinity. Extreme flooding events are also predicted to increase, which would flush down accumulated salts down to the Verloren River and later into the lake.

## 6.2 Recommendations for Future Work

Short term sampling and drought conditions experienced in the study during sampling, may have contributed to the complexity of the data interpretation. Further investigations and long term monitoring of salinity in the tributaries has to be done, as this would give more insight to source of salinity, the understanding of seasonal and spatial variation and the processes of salinisation in the catchment. Stable isotopes composition of Cl ion that can be integrated with other ions would help elucidate the providence of the excess Cl ions in the catchment. Research studies in the Western Cape have shown that deposition of aerosols can be a contributing factor of major ions for surface water and shallow ground water systems.

Investigation on the amount of maritime aerosols deposition in the area, or investigation on dry and wet deposition in the area would be recommended. To further understand the contribution of terrestrial salt loads into the Verlorenvlei lake and understand the origins of low EC and TDS in the Verloren River, development of salt balance and water balance can be incorporated to estimate net quantity of salt that enters the Verloren River.

## REFERENCES

Aggarwal, P. K., Gat, J. R., & Frohlich, K. F. (2005). Isotopes in the water cycle: Past, present and future of a developing science (1 ed.). Springer Netherlands.

Alcalά, F. J., & Custodio, E. (2008). Using Cl/Br ratio as a tracer to identify the origin of salinity in aquifers in Spain and Portugal. Journal of Hydrology, 359, 189-207.

Al-Khatib, M., & Al-Najar, H. (2011). Hydro-Geochemical characteristics of Groundwater beneath the Gaza Strip. Journal of Water Resources and Protection, 5, 341 - 348.

Amiaz, Y., Sorek, S., Enzel, Y., & Dahan, O. (2011). Solute transport in the vadose zone and groundwater during flash floods. Water Resources Research, 47, W10513, doi:10.1029/2011WR010747.

Anders R., Mendez G.O, Futa K., Danskin W.R., (2013). A Geochemical Approach to Determine Sources and Movement of Saline Groundwater in a Coastal Aquifer. National GroundWater Association, 1-13, doi: 10.1111/gwat.12108.

Bakari, S.S., Aagaard, P., Vogt, R.D., Ruden F., Johansen I., & Vuai S.A. (2013). Strontium isotopes as tracers for quantifying mixing of groundwater in the alluvial plain of a coastal watershed, south-eastern Tanzania. Journal of Geochemical Exploration, 130, 1–14.

Bates, B. (2009). Climate Change and Water: IPCC technical paper VI. World Health Organization.

Baxter, A. J., & Meadows, M. E. (1999). Evidence of Holocene sea level change at the Verlorenvlei, Western Cape, South Africa. Quaternary International, 56, 65-79.

Benaabidate, L., & Fryar, A.E. (2010). Controls on Ground Water Chemistry in the Central Couloir Sud Rifain, Morocco. Ground Water, 48(2), 306-319.

Bing, H., He, P., & Zhang, Y. (2015). Cyclic freeze–thaw as a mechanism for water and salt migration in soil. Environmental Earth Science, 74, 675–681.

Gleeson, T., Befus, K. M., Jasechko, S., Luijendijk, E., & Cardenas, M. B. (2016). The global volume and distribution of modern groundwater. Nature Geoscience, 9(2), 161-167.

Bouderbala A. (2015). Assessment of Groundwater Quality and its Suitability for Agricultural Uses in the Nador Plain, North of Algeria. Water Quality Expo Health. DOI 10.1007/s12403-015-0160-z

Bouzourra, H., Bouhlila, R., Elango, L., Slama, F., & Ouslati, N. (2015). Characterization of mechanisms and processes of groundwater salinization in irrigated coastal area using statistics, GIS, and hydrogeochemical investigations. Environmental Science Pollution Research, 22, 2643–2660.

Bozdag, A., & Göçmez, G. (2016). Hydrogeochemical and isotopic study of groundwater in a semi-arid region: Yeniceoba Plain (Cihanbeyli-Konya) Central Anatolia, Turkey. Acta Geologica Sinica, 90(1), 230-241.

Brenot, A., Negrel, P., Petelet-Giraud, E., Millot, R., & Malcuit, E. (2015). Insights from the salinity origins and interconnection of aquifers in a regional scale sedimentary aquifer system (Adour-Garonne district, SW france): Contributions of $^{34}S$ and $^{18}O$ from dissolved sulfates and the $^{87}Sr/^{86}Sr$ ratio. Applied geochemistry, 53, 27-41.

Bridgman, H., Dragovish, D., and Dodson, J. (2008). The Australian Physical Environment. Oxford University Press, USA.

Bugan, R. D. H., Jovanovic, N. Z., & de Clercq W. P. (2015). Quantifying the catchment salt balance: An important component of salinity assessments. South African Journal of Science,111 (5/6), 1-8.

Conrad, J., Nel, J., Wentzel, J., 2004. The challenges and implications of assessing groundwater 718 recharge: A case study-northern Sandveld, Western Cape, South Africa. Water SA, 30, 75–81.

CSIR (2009) Development of the Verlorenvlei estuarine management plan: Situation assessment. Report prepared for the C.A.P.E. Estuaries Programme. CSIR Report, Stellenbosch

CSIR (2010) Estuary Management Plan: Verlorenvlei (Version 1). Report prepared for the C.A.P.E. Estuaries Programme. CSIR Report CSIR/NRE/CO/ER/2010/0066/B. Stellenbosch

Cartwright, I., Hannam, K., Weaver, T.R. (2007). Constraining flow paths of saline groundwater at basin margins using hydrochemistry and environmental isotopes: Lake Cooper, Murray Basin, Australia. Australian Journal of Earth Sciences, 54,1103 - 1122.

Cartwright, I., Weaver, T. R., & Fifield, L. K. (2006). Cl/Br ratios and environmental isotopes as indicators of recharge variability and groundwater flow: An example from the southeast Murray Basin. Australia Chemical Geology, 231-238.

Chen, J., Wang, F., Xia, X., & Zhang, L. (2002). Major element chemistry of the Changjiang (Yangtze River). Chemical Geology, 187, 231– 255.

Chetelat, B., Liu, C.Q., Zhao, Z.Q., Wang, Q.L., Li, S.L., Li, J., & Wang, B.L. (2008). Geochemistry of the dissolved load of the Changjiang Basin rivers: Anthropogenic impacts and chemical weathering. Geochimica et Cosmochimica Acta ,72, 4254–4277.

Conrad, J., Nel, J., & Wentzel, J. (2004). The challenges and implications of assessing groundwater recharge: A case study - northern Sandveld, Western Cape, South Africa. Cape Town, South Africa: Water of South Africa, 30(5), 75-81.

Craig, H. (1969). Isotopic variation in meteoric waters. Science,133, 1702-1703.

Currell, M. J., Dahlhaus, P., & Li, H. (2015). Stable isotopes as indicators of water and salinity sources in a southeast Australian coastal wetland: identifying relict marine water, and implications for future change. Hydrogeology Journal, 2, 235-248.

Curtis, C.D. (1964). Studies on the use of boron as a paleo-environmental indicator. Geochimica et Cosmochimica Acta, 28(7), 1125-1137.

Cyrus, D., Jerling, H., MacKay, F., & Vivier, L. (2011). Lake St Lucia, Africa's largest estuarine lake in crisis: Combined effects of mouth closure, low levels and hypersalinity. South African Journal of Science, 107(3/4), 1-13.

Dansgaard, W. (19640. Stable Isotopes in precipitation. Tellus, 336-368.

Davis, S. N., Fabryka-Martin, J. T., & Wolfsberg, L. E. (2004). Variations of bromide in potable groundwater in the United States. Groundwater, 42(6), 902-909.

Delpla, I., Jung, A.V., Baures, E., Clement, M., & Thomas, O. (2009). Impacts of climate change on surface water quality in relation to drinking water production. Environment International, 35, 1225-1233.

Demlie, M., Jovanovic, N., & Naicker, S. (2011). Origin of groundwater salinity in the Sandspruit catchment, Berg River basin (South Africa).

Department of Water Affairs and Forestry. (1996). South Africa Water Quality Guidelines. Volume 1.

Edmunds, W. M., & Smedley, P. L. (2000). Residence time indicators in groundwater: The East Midlands Triassic sandstone aquifer. Applied Geochemistry, 737-752.

Eilers. A. (2018). Groundwater characterisation and recharge estimation in the Verlorenvlei catchment. (Masters dissertation, Stellenbosch: Stellenbosch University).

Ekwere, A. S., Edet, A. E., & Ekwere, S. J. (2012) Groundwater chemistry of the Oban Massif, South-Eastern Nigeria. An Interdisciplinary Journal of Applied Science,7(1), 57-66.

Elgettafi, M., Elmandour, A., Himi, M., Casas, A., & Elhaouadi, B. (2012). Messinian salinity crisis impact on the groundwater quality in Kert aquifer NE Morocco: Hydrochemical and statistical approaches. International Journal of Water Resources and Environmental Engineering, 4(11), 339-351.

Engelbrecht, F. A., Landman, W. A., Engelbrecht, C. J., Landman, S., Bopape, M. M., Roux, B., ... & Thatcher, M. (2011). Multi-scale climate modelling over Southern Africa using a variable-resolution global model. Water SA, 37(5), 647-658.

Farbe, R. E., Vengosh, A., Gavriel, I., Marie, A., Bullen, T. D., Mayer, B., Holtzman, R., Segal, M., & Shavitz, U. (2004). The origin and mechanism of salinization of the lower Jordan River. Geochimica et Cosmochica Acta, 68(9), 1989-2006.

Fisher, R.S., & Stueber, A.M. (1976). Strontium Isotopes in Selected streams within the Susquehanna River Basin. Water Resources research,12(5), 1061-1068.

Freeze, R. A. & Cherry, J. A. (1979) Groundwater. Prentice-Hall, Englewood Cliffs.

Fritz, K. M., Fulton, S., Johnson, B. R., Barton, C. D., Jack, J. D., Word, D. A., & Burke, R. A. (2010). Structural and functional characteristics of natural and constructed channels draining a reclaimed mountaintop removal and valley fill coal mine. Journal of the North American Benthological Society, 29(2), 673-689.

Harris, C., Burgers, C., Miller, J. & Rawfoot, F. (2010). O- 18 and H-2 Isotope record of Cape Town Rainfall from 1996 to 2008, and its application to recharge studies of Table Mountain Groundwater, South Africa. South African Journal of Geology,35-56.

Gibbs, R.J, (1970). Mechanisms Controlling World Water Chemistry. Science, New Series, 170, 1088-1090.

Goudie, A., & Middleton, N. J. (2006). Desert dust in the global system. Springer Science & Business Media.

Hamouda, M. F. B., Tarhouni, J., Leduc C., & Zouari, K. (2011). Understanding the origin of salinization of the Plio-quaternary eastern coastal aquifer of Cap Bon (Tunisia) using geochemical and isotope investigations. Environmental Earth Sciences, 63, 889-901.

Han, Z., Tang, C., Wu, P., Zhang, R., & Zhang, C. (2015). Using stable isotopes and major ions to identify hydrological processes and geochemical characteristics in a typical karstic basin, Guizhou, southwest China. Isotope in Environmental and Health Studies, 50(1), 62-73.

Herczeg, A., Dogramaci, S. & Leaney, F. (2001). Origin of dissolved salts in a large, semi-arid groundwater system: Murray Basin, Australia. Marine Freshwater Research, 52, 41-52.

Huang, T., & Pang, Z. (2012). The role of deuterium excess in determining the water salinisation mechanisms: A case study of the arid Tarim River Basin, NW China. Applied Geochemistry, 27,2382-2388.

Hudak, P. F. (2000). Sulfate and chloride concentrations in Texas aquifers. Environment international, 26(1), 55-61.

Issanova, G., Abuduwaili, J., Galayeva, O., Semenov, O., & Bazarbayeva, T. (2015). Aeolian transportation of sand and dust in the Aral Sea Region. International Journal of Environmental Science Technology, 12, 3213–3224.

Jalali, M. (2007). Hydrochemical Identification of Groundwater Resources and Their Changes under the Impacts of Human Activity in the Chah Basin in Western Iran. Environmental Monitoring and Assessment, 130, 347–364.

Jones, C.E., Jenkyns, H.C., & Hesselbo, S.P. (1994). Strontium isotopes in Early Jurassic seawater. Geochem Cosmochim Acta, 58, 1285-1301.

Krause, P., 2001. Das hydrologische Modellsystem J2000. Beschreibung und Anwendung in großen 756 Flussgebieten, in: Umwelt/Environment, Vol. 29. Jülich: Research Centre.

Lakshmanan, L. R., Kannan, R., Kumar, M. S. (2003). Major ion chemistry and identification of hydrogeochemical processes of ground water in a part of Kancheepuram district, Tamil Nadu, India. Environmental Geosciences, 10(4), 157–166.

Lemière, B., & Négrel, P. (2015). O, H and Sr isotopes tracing the migration distance of mining, ore processing and metallurgical activities end-products in a river basin (Subarnarekha River, India). Procedia Earth and Planetary Science, 13, 223-226.

Lewandowska, A.U., & Falkowska, L.M. (2013). Sea salt in aerosols over the southern Baltic. Part 1. The generation and transportation of marine particles. Oceanologia, 55(2), 279–298.

Marie, A., & Vengosh, A. (2001). Sources of salinity in groundwater from Jericho Area, Jordan Valley. Ground Water, 39(2), 240-248.

Martin, J.-M. & Whitfield, M., 1983. The Significance of the River Input of Chemical Elements to the Ocean. Trace Metals in Sea Water, 9, 265-296.

McDowell, R.W. (2008). Environmental Impacts of Pasture-Based Farming. *CAB International*, Oxford shire.

Meadows, M. E., Baxter, A.J., & Parkington, J. (1996). Late Holocene environments at the Verlorenvlei, Western Cape Province, South Africa. Quaternary International, 33,81-95.

Moore, S. J., Bassett, R. L., Liu, B., Wolf, C. P., & Doremus., D. (2008). Geochemical tracers to evaluate hydrogeological controls on river salinization. Groundwater, 46(3), 489-501.

Monjerezi, M., Vogt, R. D., Aagaard, P., Gebru, A. G., & Saka, J. D. (2011). Using 87 Sr/86 Sr, δ 18 O and δ 2 H isotopes along with major chemical composition to assess groundwater salinization in lower Shire valley, Malawi. Applied Geochemistry, 26(12), 2201-2214.

Murray, K. & Wade, P. (1996). Checking anion-cation charge balance of water quality analysis: Limitations of the non-traditional method for non-potable waters. Water of South Africa, 27-32.

Negrel, P., Petelet-Giraud, E., & Wildory, D. (2004). Strontium isotope geochemistry of alluvial groundwater: a tracer for groundwater resources characterization. Hydrology and Earth System Sciences, 8(5) 959-972.

Nyaga, J. M., Cramer, M. D., & Neff, J. C. (2013). Atmospheric nutrient deposition to the west coast of South Africa. Atmospheric environment, 81, 625-632.

Panno, S.V., Hackley, K.C., Hwang, H.H., Greenberg, S.E., Krapac, I.G., Landsberger, S., & O'Kelly, D.J. (2006). Characterisation and identification of Na-Cl sources in ground water. Ground Water,44, 176-187.

Phillips, F. M. (2013). Chlorine 36 Dating of Old Groundwater. In Isotope Methods for Dating Old Groundwater (pp. 125-152). Vienna: IAEA.

Phillips, F.M., Hogan, J., Mills, S., & Hendricks, J.M.H. (2003). Environmental tracers applied to quantifying causes of salinity in arid-region rivers: Preliminary results from the Rio Grande, Southwestern USA. Developments in water science**,** 50, 327-334.

Pitman, W.V. (2011). Overview of water resources assessment in South Africa: Current state and future challenges. Water of South Africa, 37(5), 659 -664.

Ravikumar, P., & Somashekar, R. K. (2011). Environmental Tritium ($^{3}H$) and hydrochemical investigations to evaluate groundwater in Varahi and Makandeya river basins, Karnataka, India. Journal of Environmental Radioactivity, 102, 153-162.

Richter, B. & Kreitler, C. (1993). Geochemical techniques for identifying groundwater salinisation. Florida, USA: CRC

Rozendaal, A., Gresse, P. G., Scheepers, R. & Le Roux, J. P. (1999). Neoproterozoic to early cambrian crustal evolution of the Pan-African Saldania Belt, South Africa. Precambrian Research, 303-323.

Rozendaal, A., & Scheepers, R. (1995). Magmatic and related mineral deposits of the Pan-African Saldania belt in the Western Cape Province, South Africa. Journal of African Earth Sciences, 107-126.

Saffigna, P. G., & Keeney, D. R. (1977). Nitrate and chloride in ground water under irrigated agriculture in central Wisconsin. Groundwater, 15(2), 170-177.

Salama, R. B., Otto, C. J., & Fitzpatrick, R. W., 1999. Contributions of groundwater conditions to soil and water salinization. *Hydrology Journal,* 46-64.

Sami, K. (1992). Recharge mechanisms and geochemical processes in a semi-arid sedimentary basin, Eastern Cape, South Africa. Journal of Hydrology, 139, 27- 48.

Scanlon, B. R., Healy, R. W., and Cook, P. G. (2002). Choosing appropriate techniques for quantifying groundwater recharge. Hydrogeology Journal, 10, 18-39.

Schulze, R. E. (2005). Setting the scene: the current hydroclimatic “Landscape” in Southern Africa. In: Schulze RE (ed) Climate change and water resources in Southern Africa: studies on scenarios, Climatic Change impacts, vulnerabilities and adaptation. Pretoria, Water Research Commission WRC Report 1430/1/05: 6: 83–94.

Seun, J. P., & Lai H. N. (2013). A salinity projection model for determining impacts of climate change on river ecosystems in Taiwan. Journal of Hydrology, 493, 124-131.

Shand, P., Darbyshire, D. P. F., Love, A. J., & Edmunds, W. M. (2009). Sr isotopes in natural waters: Applications to source characterisation and water–rock interaction in contrasting landscapes. *Applied Geochemistry*, *24*(4), 574-586.

Sheikhy Narany, T., Ramli, M. F., Aris, A. Z., Sulaiman, W. N. A., Juahir, H., & Fakharian, K. (2014). Identification of the hydrogeochemical processes in groundwater using classic integrated geochemical methods and geostatistical techniques, in Amol-Babol plain, Iran.The Scientific World Journal, 2014.

Sinclair, S.A., Lane, S.B., & Grindley, J.R. (1986). Estuaries of the Cape. Part II, Synopses of available information on individual systems. Stellenbosch: CSIR Research Report No 431.

Skrzypek, G., Dogramaci, S., & Grierson, P. F. (2013). Geochemical and hydrological processes controlling groundwater salinity of a large inland wetland of northwest Australia. Chemical Geology, 357, 164-177.

Slinger, D., & Tension, K. (2005). Salinity glove box guide for NSW Murray & Murrumbidgee. NSW Department of Primary Industries: Ourimbah, New South Wales, Australia.

Soderberg, K., & Compton, J.S. (2007). Dust as a Nutrient Source for Fynbos Ecosystems, South Africa. Ecosystems, 10(4), 550–561.

Tiwari, A. K., & Singh A., K. (2014). Hydrogeochemical investigation and groundwater quality assessment of Pratapgarh District, Uttar Pradesh. Journal of Geological society of India, 83, 329-343.

Utom, A. U., Odoh, B. I., & Egboka, B. C. (2013). Assessment of hydrogeochemical characteristics of groundwater quality in the vicinity of Okpara coal and Obwetti fireclay mines, near Enugu town, Nigeria. Applied Water Science, 3(1), 271-283.

Van Weert, F., Van der Gun, J., & Reckman, J. (2009). Global Overview of Saline Groundwater Occurrence and Genesis. International Groundwater Resources Assessment Centre (IGRAC), Utrecht: Report nr. GP2009-1.

Vengosh, A., Gill, J., Lee Davisson, M., & Bryant Hudson, G. (2002). A multi-isotope (B, Sr, O, H, and C) and age dating ($^{3}H$–$^{3}He$ and $^{14}C$) study of groundwater from Salinas Valley, California: Hydrochemistry, dynamics, and contamination processes.Water Resources Research, 38(1).

Vengosh, A., Spivack, A.J., Artzi, Y., & Ayalon, A. (1999). Geochemical and boron, strontium, and oxygen isotopic constraints on the origin of the salinity in groundwater from the Mediterranean coast of Israel. Water Resources Research, 35(6), 1877-1894.

Warner, N., Lgourna, Z., Bouchaou, L., Boutaleb, S., Tagma, T., Hsaissoune, M., Vengosh, A. (2013). Integration of geochemical and isotopic tracers for elucidating water sources and salinization of shallow aquifers in the sub-Saharan Dara Basin, Morocco. Applied Geochemistry, 34, 140-151.

Watson, A., Miller, J., Fleischer, M., & de Clercq, W. (Submitted). Estimation of groundwater recharge via percolation outputs from a rainfall / runoff model for the Verlorenvlei estuarine system, west coast, South Africa. Journal of Hydrology.

Wen, X., Wu, Y., Su, F., Zhang, Y., & Liu F. (2005). Hydrochemical characteristics and salinityof groundwater in the Ejina Basin, Northwestern China. Environmental Geology, 48, 665–675.

Williams, W.D. (1999). Salinisation: A major threat to water resources in the arid and semi-arid regions of the world. Lakes and Reservoirs: Research and Management 4, 58-91.

Williams, R.M., (1982). A model for the dry deposition of particles to natural water surfaces? Atmospheric Environment, 16(8), 1933-1938.

WHO, (2008). Chemical Fact sheet - Guidelines for drinking water quality, Geneva: World Health Organisation.

WHO, (2011). Guidelines for Drinking-water Quality (4th ed.), Geneva: World Health Organisation.

Yechieli, Y., & Wood, W.W. (2002). Hydrogeologic processes in saline systems: playas, sabkhas, and saline lakes. Earth-Science Reviews, 58, 343-365.

Yohannes, H., Elias, E. (2017). Contamination of rivers and water reservoirs in and around Addis Ababa city and actions to combat It. Environment Pollution and Climate Change, 1, 116.

Van Niekerk, H., Silberbauer, M. J., & Hohls, B., C. (2009). Monitoring programme revision highlights long-term salinity changes in selected South African rivers and the value of comprehensive long-term data sets. Environmental Monitoring Assessment ,154, 401-411.

Visser, H.D., & Toerien, D.K. (1971). The geology of the area between Vredendal and Elandsbaai. Pretoria, Department of Mine, Geologigal Survaey Publications No. 62813-1.

Zaidi, F. K., Nazzal, Y., Jafri, M. K., Naeem, M., & Ahmed I. (2015). Reverse ion exchange as major processes controlling groundwater chemistry in an arid environment: a case study from northwestern Saudi Arabia. Environmental Monitoring Assessment, 187(10), 607.

Zhai, S., Yang, L., & Hu. W. (2009). Observations of atmospheric nitrogen and phosphorus deposition during the period of Algal Bloom Formation in Northern Lake Taihu, China. Environmental Management, 44, 542–551.

Zhang, G., Deng, W., Yang, Y. S., & Salama, R. B. (2007). Evolution study of a regional groundwater system using hydrochemistry and stable isotopes in Songnen Plain, northeast China. Hydrological Processes, 21(8), 1055-1065.

Ziervogel, G., New, M., van Garderen, E., A., Midgley, G., Taylor, A., Hamann, R., Stuart-Hill, S., Myers, J., & Warburton M. (2014). Climate change impacts and adaptation in South Africa. WIREs Climate Change, 5, 605-620.

Zhu, B., & Yang, X. (2010). The origin and distribution of soluble salts in the sand seas of northern China. Geomorphology 123 ,232-242.

# APPENDIX 1

1. *Piezometer coordinates for each tributary.*

| Krom Antonies | | | Hol | | | Kruismans | | | Verloren confluence | | | Bergvallei | | |
|---|---|---|---|---|---|---|---|---|---|---|---|---|---|---|
| Piezometer | Lat | Long | Piezometer | Lat | Long | Piezometer | Lat | Long | Piezometer | Lat | Long | Piezometer | Lat | Long |
| KAPZ01 | -32.602 | 18.691 | HOLPZ01 | -32.596 | 18.685 | KRPZ01 | -32.6030 | 18.7471 | VLPZ01 | -32.5922 | 18.6850 | BVPZ01 | -32.718 | 18.7494 |
| KAPZ02 | -32.602 | 18.691 | HOLPZ02 | -32.614 | 18.663 | KRPZ02 | -32.6017 | 18.7495 | VLPZ02 | -32.5958 | 18.6870 | | | |
| KAPZ03 | -32.628 | 18.691 | HOLPZ03 | -32.605 | 18.650 | KRPZ03 | -32.6038 | 18.7286 | | | | | | |
| KAPZ04 | -32.660 | 18.685 | HOLPZ04 | -32.624 | 18.657 | KRPZ04 | -32.5999 | 18.6940 | | | | | | |
| KAPZ05 | -32.675 | 18.691 | HOLPZ05 | -32.653 | 18.635 | KRPZ05 | -32.6005 | 18.6939 | | | | | | |
| KAPZ06 | -32.688 | 18.693 | HOLPZ06 | -32.672 | 18.631 | | | | | | | | | |
| KAPZ07 | -32.706 | 18.703 | | | | | | | | | | | | |

*2. Summary of Saturation Indices for surface water samples determined by PHREEQC.*

| | Sample ID | Calcite | Dolomite | Gypsum | Halite |
|---|---|---|---|---|---|
| **Krom Antonies** | | | | | |
| | TS15VLR010 | -2.403 | -4.848 | -3.416 | -7.883 |
| | TS15VLR011 | -2.911 | -5.736 | -3.798 | -7.997 |
| | TS15VLR012 | -0.529 | -1.291 | -2.567 | -7.246 |
| | TS15VLR013 | -0.366 | -7.296 | -3.696 | -8.258 |
| | TS15VLR032 | -0.484 | -0.750 | -2.323 | -5.952 |
| | TS15VLR042 | -4.289 | -8.282 | -4.598 | -7.642 |
| | TS15VLR044 | -0.335 | -0.448 | -2.222 | -5.799 |
| | TS15VLR051 | | | -4.000 | -7.899 |
| | TS15VLR052 | -3.730 | -7.231 | -4.525 | -7.845 |
| | TS15VLR067 | -1.991 | -3.908 | -3.403 | -7.756 |
| | TS15VLR069 | -1.523 | -2.906 | -2.883 | -6.892 |
| | TS15VLR0110 | 0.524 | 1.321 | -1.905 | -5.297 |
| | TS15VLR0123 | -1.183 | -2.220 | -2.783 | -7.057 |
| **Kruismans** | | | | | |
| | TS15VLR014 | 0.087 | 0.807 | -1.476 | -4.196 |
| | TS15VLR038 | 0.339 | 1.274 | -1.507 | -4.220 |
| | TS15VLR046 | 0.033 | 1.258 | -1.463 | -4.184 |
| | TS15VLR049 | 0.071 | 2.006 | -1.438 | -4.203 |
| | TS15VLR054 | -2.604 | -4.853 | -2.432 | -6.153 |
| | TS15VLR066 | -0.035 | 0.627 | -1.637 | -4.576 |
| **Hol** | | | | | |
| | TS15VLR030 | 0.157 | 0.778 | -1.317 | -4.623 |
| | TS15VLR031 | -1.302 | -2.384 | -2.309 | -5.986 |
| | TS15VLR036 | -0.282 | -0.019 | | -4.445 |
| | TS15VLR060 | -2.820 | -5.196 | -3.057 | -6.622 |
| | TS15VLR063 | 0.035 | 1.122 | -1.448 | -5.113 |
| | TS15VLR099 | 0.006 | 0.009 | -1.344 | -5.200 |
| | TS15VLR0108 | 1.031 | 2.612 | -2.355 | -4.377 |
| | TS15VLR0113 | -2.843 | -5.281 | -2.715 | -6.361 |
| **Bergvallei** | | | | | |
| | TS15VLR015 | -2.061 | -3.567 | | |
| | TS15VLR047 | -1.665 | -2.767 | -2.365 | -5.481 |
| **Verloren Confluence** | | | | | |
| | TS15VLR019 | -1.957 | -3.737 | -2.454 | -6.254 |
| | TS15VLR020 | -4.285 | -7.814 | -3.971 | -6.736 |
| | TS15VLR028 | -0.667 | -0.930 | -1.704 | -5.268 |
| | TS15VLR055 | -0.825 | -1.196 | -1.387 | -4.449 |

*3. Summary of Saturation Indices for surface water samples determined by PHREEQC*

| | Sample ID | Piezometer | Anhydrite | Calcite | Dolomite | Gypsum | Halite |
|---|---|---|---|---|---|---|---|
| Krom Antonies | | | | | | | |
| | TS15VLB0102 | KAPZ07 | -2.721 | -1.591 | -3.833 | -2.501 | -7.358 |
| | TS15VLB0122 | KAPZ07 | -3.542 | -1.618 | -3.820 | -3.322 | -7.610 |
| | TS15VLB068 | KAPZ06 | -1.135 | -2.195 | -5.008 | -0.916 | -5.843 |
| | TS15VLB0124 | KAPZ06 | -0.653 | -1.122 | -3.464 | -0.433 | -5.804 |
| | TS15VLB070 | KAPZ05 | -1.981 | -0.286 | -1.040 | -1.762 | -5.721 |
| | TS15VLB0101 | KAPZ05 | -2.090 | 0.033 | -0.455 | -1.870 | -5.811 |
| | TS15VLB072 | KAPZ04 | -2.653 | -1.254 | -2.963 | -2.433 | -6.168 |
| | TS15VLB0100 | KAPZ04 | -1.575 | -0.510 | -1.578 | -1.355 | -5.625 |
| | TS15VLB0125 | KAPZ04 | -3.133 | -0.736 | -1.986 | -2.913 | -6.535 |
| | TS15VLB071 | KAPZ03 | -2.262 | -1.348 | -2.948 | -2.042 | -5.799 |
| | TS15VLB053 | KAPZ02 | -2.254 | -0.201 | -0.584 | -2.035 | -5.315 |
| | TS15VLB077 | KAPZ02 | -2.186 | -0.554 | -1.318 | -1.966 | -5.431 |
| | TS15VLB088 | KAPZ02 | -2.526 | -0.790 | -1.859 | -2.307 | -5.814 |
| | TS15VLB0109 | KAPZ02 | -3.297 | -0.515 | -1.315 | -3.077 | -6.305 |
| | TS15VLB078 | KAPZ01 | -1.811 | -3.103 | -6.517 | -1.591 | -5.136 |
| | TS15VLB087 | KAPZ01 | -2.920 | -1.880 | -4.158 | -2.700 | -6.584 |
| | TS15VLB0111 | KAPZ01 | -2.846 | -1.350 | -3.020 | -2.626 | -6.355 |
| Kruismans | | | | | | | |
| | TS15VLB045 | KRPZ01 | -1.699 | 0.046 | 0.041 | -1.481 | -4.361 |
| | TS15VLB081 | KRPZ01 | -1.812 | 0.244 | 0.518 | -1.593 | -4.533 |
| | TS15VLB0105 | KRPZ01 | -1.738 | 0.250 | 0.420 | -1.519 | -4.614 |
| | TS15VLB0121 | KRPZ01 | -1.998 | -0.328 | -0.749 | -1.778 | -4.953 |
| | TS15VLB082 | KRPZ02 | -1.671 | -0.306 | -0.553 | -1.453 | -4.216 |
| | TS15VLB0104 | KRPZ02 | -1.749 | -0.105 | -0.222 | -1.531 | -4.312 |
| | TS15VLB0119 | KRPZ02 | -1.886 | -0.308 | -0.627 | -1.668 | -4.278 |
| | TS15VLB065 | KRPZ03 | -1.640 | -0.293 | -0.513 | -1.422 | -4.157 |
| | TS15VLB095 | KRPZ03 | -1.856 | -0.305 | -0.595 | -1.638 | -4.329 |
| | TS15VLB035 | KRPZ04 | -1.817 | 0.147 | 0.294 | -1.599 | -4.132 |
| | TS15VLB048 | KRPZ04 | -1.924 | 0.294 | 0.658 | -1.706 | -4.043 |
| | TS15VLB079 | KRPZ04 | -1.338 | 0.164 | 0.399 | -1.121 | -4.167 |
| | TS15VLB093 | KRPZ04 | -1.784 | 0.652 | 1.309 | -1.567 | -4.043 |
| | TS15VLB0117 | KRPZ04 | -1.806 | 0.235 | 0.502 | -1.588 | -4.095 |
| | TS15VLB050 | KRPZ05 | -1.249 | -0.233 | -0.550 | -1.033 | -3.758 |
| | TS15VLB080 | KRPZ05 | -1.286 | -0.105 | -0.182 | -1.070 | -3.697 |
| | TS15VLB094 | KRPZ05 | -1.130 | 0.201 | 0.349 | -0.915 | -3.496 |
| | TS15VLB0118 | KRPZ05 | -1.114 | 0.028 | 0.030 | -0.901 | -3.276 |

| | Sample ID | Piezometer | Anhydrite | Calcite | Dolomite | Gypsum | Halite |
|---|---|---|---|---|---|---|---|
| Hol | | | | | | | |
| | TS15VLB0115 | HolPZ06 | -1.076 | 0.705 | 1.291 | -0.860 | -3.600 |
| | TS15VLR062 | HolPZ05 | -1.144 | -1.312 | -2.733 | -0.926 | -4.331 |
| | TS15VLR089 | HolPZ05 | -1.083 | -1.959 | -4.055 | -0.866 | -4.188 |
| | TS15VLR061 | HolPZ04 | -2.070 | 0.404 | 0.816 | -1.851 | -4.643 |
| | TS15VLB090 | HolPZ04 | -1.455 | 0.533 | 1.035 | -1.239 | -3.735 |
| | TS15VLB0116 | HolPZ04 | -2.135 | 0.154 | 0.257 | -1.917 | -4.458 |
| | TS15VLR059 | HolPZ03 | -1.269 | -4.129 | -8.309 | -1.050 | -4.999 |
| | TS15VLB091 | HolPZ03 | -1.468 | -3.282 | -6.686 | -1.249 | -4.908 |
| | TS15VLR058 | HolPZ02 | -1.587 | -1.330 | -2.529 | -1.368 | -4.523 |
| | TS15VLB092 | HolPZ02 | -1.569 | -1.094 | -2.126 | -1.351 | -4.549 |
| | TS15VLB0114 | HolPZ02 | -1.611 | -1.543 | -3.024 | -1.393 | -4.513 |
| | TS15VLR075 | HolPZ01 | -1.700 | 0.441 | 1.004 | -1.482 | -4.122 |
| | TS15VLR085 | HolPZ01 | -1.639 | 0.760 | 1.582 | -1.422 | -3.904 |
| | TS15VLB0107 | HolPZ01 | -1.078 | 0.310 | 0.640 | -0.868 | -3.223 |
| | TS15VLB0127 | HolPZ01 | -1.673 | 0.657 | 1.351 | -1.456 | -3.948 |
| Bergvallei | | | | | | | |
| | TS15VLB083 | BVPZ01 | -1.799 | -1.140 | -2.208 | -1.581 | -4.212 |
| | TS15VLB0103 | BVPZ01 | -1.869 | -1.043 | -2.012 | -1.651 | -4.173 |
| | TS15VLB0120 | BVPZ01 | -1.784 | -1.543 | -2.979 | -1.566 | -4.226 |
| Verloren | | | | | | | |
| | TS15VLB018 | VLPZ02 | -2.475 | -1.727 | -3.492 | -2.255 | -5.371 |
| | T15VLSB056 | VLPZ02 | | -0.856 | -1.888 | | -5.369 |
| | TS15VLB074 | VLPZ02 | -2.271 | -0.497 | -1.141 | -2.052 | -5.271 |
| | TS15VLB086 | VLPZ02 | -2.177 | -0.020 | -0.211 | -1.958 | -5.247 |
| | TS15VLB022 | VLPZ01 | -2.187 | -1.844 | -3.978 | -1.967 | -5.612 |
| | TS15VLB024 | VLPZ01 | -2.650 | -3.492 | -7.237 | -2.430 | -6.009 |
| | T15VLSB055 | VLPZ01 | -1.462 | -0.705 | -1.630 | -1.243 | -4.848 |
| | TS15VLB076 | VLPZ01 | -2.716 | -2.538 | -5.303 | -2.497 | -6.069 |
| | TS15VLB084 | VLPZ01 | -2.621 | -3.297 | -6.737 | -2.401 | -5.866 |
| | TS15VLB0106 | VLPZ01 | -2.612 | -3.363 | -6.875 | -2.392 | -5.713 |
| | TS16VLB0126 | VLPZ01 | -2.863 | -3.439 | -7.004 | -2.643 | -6.018 |

*4.Summary of the water levels measured during field sampling using a dip meter and the EC recorded.*

| | | Water level (m) | | | EC (mS/m) | | |
|---|---|---|---|---|---|---|---|
| **Dates** | | 2015-09-09 | 2015-11-24 | 2016-06-17 | 2015-09-09 | 2015-11-24 | 2016-06-17 |
| **Krom Antonies** | Piezometers | | | | | | |
| | KAPZ07 | 0.86 | 1 | 1.243 | 32.8 | 18.18 | 27.9 |
| | KAPZ06 | 1.51 | 1.92 | 0.95 | 212 | 196.3 | 145.7 |
| | KAPZ05 | 1.54 | | 1.16 | 143.3 | | 197.4 |
| | KAPZ04 | 0.54 | | 0.36 | 178.3 | | 87.8 |
| | KAPZ03 | 0.87 | | 0.14 | 46.4 | | 31.1 |
| | KAPZ02 | 1.5 | 1.82 | 1 | 132.9 | 65 | 216 |
| | KAPZ01 | 0.41 | 0.941 | 0.095 | 54.3 | 77 | 26 |
| **Kruismans** | | | | | | | |
| | KRPZ05 | 0.75 | 1.5 | | 1795 | 1988 | |
| | KRPZ04 | 0.9 | 1.66 | 1.531 | 953 | 865 | 102.5 |
| | KRPZ03 | 0.46 | | 0.62 | 738 | | 1031 |
| | KRPZ02 | 1.39 | 1.48 | 1.38 | 713 | 664 | 671 |
| | KRPZ01 | 0.25 | 1.36 | 0.825 | 530 | 354 | 432 |
| **Hol** | | | | | | | |
| | HOLPZ06 | 1.33 | 1.45 | 0.84 | 1260 | 1499 | 1893 |
| | HOLPZ05 | 0.8 | | | 804 | | |
| | HOLPZ04 | 0.82 | 1.72 | 0.55 | 1255 | 583 | 643 |
| | HOLPZ03 | 1.78 | 1.75 | 1.565 | 387 | 353 | 189.4 |
| | HOLPZ02 | 0.66 | 1.25 | | 562 | 566 | |
| | HOLPZ01 | 0.92 | 0.84 | | 997 | 989 | |
| **Bergvallei** | | | | | | | |
| | BVPZ01 | 1.26 | 1.68 | 1.3 | 784 | 741 | 1020 |
| **Verloren confluence** | | | | | | | |
| | VLPZ01 | 0.91 | 1.61 | 2.28 | 116.5 | 135.3 | 92.4 |